National Library of Canada

Acquisitions and Bibliographic Services Branch

395 Wellington Street
Ottawa, Ontario
K1A 0N4

Bibliothèque nationale du Canada

Direction des acquisitions et des services bibliographiques

395, rue Wellington
Ottawa (Ontario)
K1A 0N4

Your file *Votre référence*

Our file *Notre référence*

NOTICE

The quality of this microform is heavily dependent upon the quality of the original thesis submitted for microfilming. Every effort has been made to ensure the highest quality of reproduction possible.

If pages are missing, contact the university which granted the degree.

Some pages may have indistinct print especially if the original pages were typed with a poor typewriter ribbon or if the university sent us an inferior photocopy.

Reproduction in full or in part of this microform is governed by the Canadian Copyright Act, R.S.C. 1970, c. C-30, and subsequent amendments.

AVIS

La qualité de cette microforme dépend grandement de la qualité de la thèse soumise au microfilmage. Nous avons tout fait pour assurer une qualité supérieure de reproduction.

S'il manque des pages, veuillez communiquer avec l'université qui a conféré le grade.

La qualité d'impression de certaines pages peut laisser à désirer, surtout si les pages originales ont été dactylographiées à l'aide d'un ruban usé ou si l'université nous a fait parvenir une photocopie de qualité inférieure.

La reproduction, même partielle, de cette microforme est soumise à la Loi canadienne sur le droit d'auteur, SRC 1970, c. C-30, et ses amendements subséquents.

Canada

UNIVERSITY OF ALBERTA

APPLICATIONS OF PROGRESSIVE FAILURE ANALYSIS

BY

© MICHAEL MATHIOUDAKIS

A THESIS

SUBMITTED TO THE FACULTY OF GRADUATE STUDIES AND RESEARCH IN

PARTIAL FULFILMENT OF THE REQUIREMENTS FOR THE DEGREE OF

DOCTOR OF PHILOSOPHY

DEPARTMENT OF CIVIL ENGINEERING

EDMONTON, ALBERTA

SPRING, 1993

National Library of Canada
Acquisitions and Bibliographic Services Branch
395 Wellington Street
Ottawa, Ontario
K1A 0N4

Bibliothèque nationale du Canada
Direction des acquisitions et des services bibliographiques
395, rue Wellington
Ottawa (Ontario)
K1A 0N4

Your file Votre référence

Our file Notre référence

The author has granted an irrevocable non-exclusive licence allowing the National Library of Canada to reproduce, loan, distribute or sell copies of his/her thesis by any means and in any form or format, making this thesis available to interested persons.

L'auteur a accordé une licence irrévocable et non exclusive permettant à la Bibliothèque nationale du Canada de reproduire, prêter, distribuer ou vendre des copies de sa thèse de quelque manière et sous quelque forme que ce soit pour mettre des exemplaires de cette thèse à la disposition des personnes intéressées.

The author retains ownership of the copyright in his/her thesis. Neither the thesis nor substantial extracts from it may be printed or otherwise reproduced without his/her permission.

L'auteur conserve la propriété du droit d'auteur qui protège sa thèse. Ni la thèse ni des extraits substantiels de celle-ci ne doivent être imprimés ou autrement reproduits sans son autorisation.

ISBN 0-315-82082-9

Canada

UNIVERSITY OF ALBERTA

RELEASE FORM

NAME OF AUTHOR : MICHAEL MATHIOUDAKIS

TITLE OF THESIS : APPLICATIONS OF PROGRESSIVE FAILURE ANALYSIS

DEGREE : DOCTOR OF PHILOSOPHY

YEAR THIS DEGREE GRANTED : 1993

PERMISSION IS HEREBY GRANTED TO THE UNIVERSITY OF ALBERTA LIBRARY TO REPRODUCE SINGLE COPIES OF THIS THESIS AND TO LEND OR SELL SUCH COPIES FOR PRIVATE, SCHOLARLY OR SCIENTIFIC RESEARCH PURPOSES ONLY.

THE AUTHOR RESERVES OTHER PUBLICATION RIGHTS, AND NEITHER THE THESIS NOR EXTENSIVE EXTRACTS FROM IT MAY BE PRINTED OR OTHERWISE REPRODUCED WITHOUT THE AUTHOR'S WRITTEN PERMISSION.

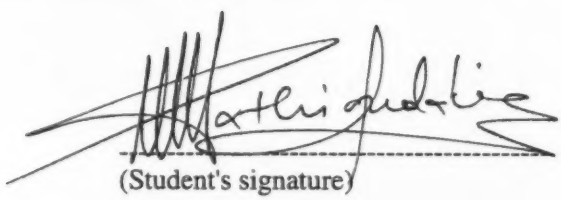

(Student's signature)

54 PONTOU STREET,
ATHENS 11527
GREECE

(Permanent address)

Date : February 19th, 1993

UNIVERSITY OF ALBERTA

FACULTY OF GRADUATE STUDIES AND RESEARCH

THE UNDERSIGNED CERTIFY THAT THEY HAVE READ AND RECOMMEND TO THE FACULTY OF GRADUATE STUDIES AND RESEARCH FOR ACCEPTANCE, A THESIS ENTITLED **APPLICATIONS OF PROGRESSIVE FAILURE ANALYSIS** SUBMITTED BY **MICHAEL MATHIOUDAKIS** IN PARTIAL FULFILMENT OF THE REQUIREMENTS FOR THE DEGREE OF **DOCTOR OF PHILOSOPHY**.

Dr. N. R. Morgenstern (Thesis supervisor)

Dr. D. H. Chan

Dr. J. D. Scott

Dr. P. K. Robertson

Dr. T. M. Hrudey

Dr. K. Barron

Dr. D. H. Shields (External Examiner)

Date : February 19, 1993

DEDICATION

TO SUSAN,

TO IOANNIS AND MARIA,

TO GEORGE

FOR BEING THERE...

ABSTRACT

The mechanism of progressive failure has been extensively studied and well understood as one which involves nonuniform straining of a strain weakening material. The ability to study and model the behaviour of a strain weakening material is a prerequisite for any progressive failure study. The observation method, i.e. interpretation of field measurements, refining the engineering calculation and making predictions of the subsequent response of the earth structure, could be very useful in order to advert problems of this nature. Collapse due to progressive failure may be sudden and reliance on instrumentation alone might not allow enough time for remedial measures to be taken or modification of the design to suit actual conditions. On the other hand, numerical models combined with local experience and engineering judgement can be used to aid in the forecast process in an earlier stage. The ability to fine tune models by means of history matching and utilizing these models to cope with the most probable scenario in the next stage of the construction relies heavily on experience and familiarity with the various modeling techniques.

The main thrust of this thesis is to reveal the effectiveness of combining the finite element with the observational method in order to evaluate the potential for progressive failure of an earth structure. To meet this objective, the case study approach is chosen and three cases are analyzed. Although all three cases are superficially different (excavation, embankment, offshore structure), they all have an inherent similarity that can pose a threat to their structural integrity. The existence of brittle layer(s) in their foundation subsoil has

been confirmed by the findings of the site investigation and the potential for progressive failure has to be evaluated.

The results of the sensitivity analysis provide an insight to the various parameters that control the onset as well as the degree of spreading of progressive failure. They also illustrate the importance of a comprehensive site investigation and the need to identify weak and brittle layers embedded in otherwise competent strata.

ACKNOWLEDGEMENTS

The author wishes to express his gratitude to his supervisor Dr. N.R. Morgenstern for his continuous interest and intense enthusiasm in the subject, and his guidance and support for this research. His ideas, time and invaluable discussions throughout the course of this research in making it a success will be forever appreciated.

Many thanks to Dr. Dave Chan for his critical comments and our long discussions on numerical modeling aspects of this research.

Dr. Ronnie Borja provided an invaluable amount of information on the concepts of the consistent tangent operator and the return mapping algorithms during our meetings at Stanford University as well as through the E-mail. His valuable suggestions and kind help are very much appreciated.

Dr. Richard G. Wan of CANMET, besides being a great friend and an office-mate, has been my mentor in the field of computational mechanics for the last five years. Our endless discussions and sleepless nights in front of a computer terminal have contributed tremendously in the developments of this study.

Many thanks to Prof. John Hadjigeorgiou of Laval University for his friendship, encouragement and support in my life since 1985. John triggered my interest in Soil Mechanics from our years at McGill and he recommended the University of Alberta for my doctoral studies - probably one of the wisest decisions in my life so far!

Geotechnical research at the University of Alberta takes place in an exceptional environment. Technical and social interactions with fellow students and staff have been a

major part of my life for many years and no individual details will ever justly record the value of these relationships. My friends know who they are.

I am very grateful to all my Greek friends in Edmonton for their constant support, encouragement and brotherhood throughout my stay here. We have shared many unforgettable moments together over the last 5 years, but the surprise graduation party in my honor will be forever cherished. I can only say that they made my life here enjoyable and memorable and my departure very difficult.

The love and support of my parents Ioannis and Maria, my brother George, my Aunt Cleanthi and my Uncles Simon and Nicholas have always been an essential source of strength at all stages of my life, especially through graduate school. Despite the difficulties of the intercontinental communications they always managed to track me down and provided constant encouragement every time I needed. To them I will always be grateful.

Finally, I would like to acknowledge the importance of the love and support of my wife Susan E. Gorman during the difficult periods of the "thesis years". Without her in my life this work would have been considerably more difficult to accomplish.

TABLE OF CONTENTS

Chapter Page

1. INTRODUCTION....1

1.1 The problem of progressive failure....1

1.2 Observational approach and the role of numerical methods....8

1.3 Purpose of the research....9

1.4 Thesis organization....11

2. EXCAVATION MODELING....14

2.1 Introduction....14

2.2 Review of previous work....15

2.2.1 Simulation of Excavation....15

2.2.1 Constitutive modeling : Background....19

2.2.2.1 Von Mises model....20

2.2.2.2 Drucker - Prager model....21

2.3 Excavation Analysis Algorithm....22

3. FINITE ELEMENT FORMULATION....29

3.1 Introduction....29

3.2 Governing equations....29

3.3 Iterative algorithm....31

3.4 Stress Integration algorithms....33

3.4.1 Introduction....33

3.4.2 Overview....34

3.5 Excavation in elastic soil....36

3.6 Excavation in elastoplastic soil....38
3.6.1 Von Mises criterion with linear strain hardening or softening....38
3.6.2 Drucker - Prager criterion with J_2 plastic flow....40
3.7 Implementation and verification of the modeling techniques....41
3.7.1 Introduction....41
3.7.2 Model verification....42
3.7.3 Simulation of excavation and fill in elastic soil....43
3.7.4 Simulation of excavation in a dry elastoplastic soil....45
3.7.4.1 Plane strain excavation....45
3.7.4.2 Axisymmetric excavation....47
4. THE SAXON CLAY PIT....59
4.1 Introduction....59
4.2 Geological conditions....59
4.3 Oxford clay structure and fabric....60
4.4 Geotechnical properties....61
4.5 Instrumentation....62
4.5.1 Observed horizontal movements....64
4.5.2 Observed vertical movements....65
4.5.3 Overall displacement pattern....65
4.5.4 Inferred shear zone propagation....65
4.6 Finite element analysis procedures....66
4.6.1 Simulation of excavation procedures....67
4.6.2 Selection of material models and parameters....68
4.6.3 Selection of shearband thickness....68
4.6.4 Mesh detailing near the notch....69
4.6.5 Mesh summary....69

4.7 Simulation of excavation behaviour....69
4.7.1 Material properties....70
4.7.2 Elastoplastic analysis I....71
4.7.3 Elastoplastic analysis II....72
5. PROGRESSIVE FAILURE ANALYSIS OF WINDROW INDUCED SLOPE MOVEMENTS AT THE SYNCRUDE MINE SITE....88
5.1 Introduction....88
5.2 Geology of the Marine sediments....90
5.3 Geotechnical parameters of Marine sediments....90
5.4 Impact of Marine sediments on dragline operations....92
5.4.1 Operation foundation pad problems....92
5.4.2 Highwall failures near operating draglines....93
5.5 Statement of the problem....94
5.6 Finite element analysis....98
5.7 Discussion of the results....100
5.7.1 In-situ stress field generation....100
5.7.2 Open-pit excavation....101
5.7.3 Windrow construction step....101
5.8 Sensitivity analysis....103
5.8.1 Stiffness of the surrounding oilsand material....103
5.8.2 Strength parameters of the clay layer....104
5.8.3 Pore water pressure parameters....105
5.8.4 Depth of embedment of the clay layer....106
5.8.5 In-situ stress field....106
5.8.6 Construction method....107
5.9 Conclusions....108

6. PROGRESSIVE FAILURE ANALYSIS OF GRAVITY BASE STRUCTURES....123
6.1 Introduction....123
6.2 Statement of the problem....125
6.3 Geological profile....126
6.4 In-situ stress profile....128
6.5 Finite element analysis....129
6.6 Discussion of the results....132
6.6.1 Switch on gravity step....132
6.6.2 Full GBS pressure....132
6.6.3 Critical storm load....133
6.7 Sensitivity analysis....134
6.7.1 Embedment depth of the clay layer....134
6.7.2 Stiffness of the granular material....135
6.7.3 Stiffness of the upper most granular material....136
6.7.4 Undrained stiffness of the clay layer....136
6.7.5 Undrained shear strength of the clay layer....136
6.9 Conclusions....137
7. CONCLUSIONS AND RECOMMENDATIONS....148
7.1 Introduction....148
7.2 General conclusions....149
7.3 Recommendations for future research....152
REFERENCES....154

LIST OF TABLES

Table		Page
T.5.1	Geotechnical parameters of the Marine Sediments	122

LIST OF FIGURES

Figure		Page
2.1	Schematic Illustration of Excavation Problem	27
2.2	Results from One- and Three Step Analyses	28
2.3	Computed Stresses and Displacements for Different Meshes	28
3.1	Schematic Illustration of Time-Varying Problem Domain and Boundaries	49
3.2	Schematical representation of the radial and closest return mapping algorithms	50
3.3	Finite element mesh used for excavation in elastic soil	51
3.4	Final Deformed Wall-Floor system after excavation of elements 1 to 4	52
3.5	Displacement History of node A and B during excavation	53
3.6	Finite element mesh used for excavation in plane strain and axisymmetric excavation in elastoplastic soil	54
3.7	Plane strain excavation in elastoplastic soil. Final excavation induced displacements on the excavation boundary	55
3.8	Plane strain excavation of elastoplastic soil : Displacement History of node A obtained from one-, two-, four and eight step analyses	56
3.9	Axisymmetric excavation in elastoplastic soil : Final excavation-induced displacements along the final excavation boundary	57
3.10	Axisymmetric excavation of elastoplastic soil : Displacement history of node A obtained from one-, two-, four- and eight step analyses	58
4.1	Plan view of the excavation face, Saxon Clay Pit	75
4.2	Geology and excavation cross-section	76

4.3 Summary geotechnical properties....77
4.4 Direct shear test summary data....78
4.5 Typical overthrust gauge movements....79
4.6 Vertical compression pattern variation....80
4.7 Summary surface displacements....81
4.8 Inferred surface displacement trajectories....82
4.9 Inferred shear band yielding mechanism....83
4.10 Idealized slope for finite element analysis....84
4.11 Finite element discretization of the idealized domain....85
4.12 Horizontal displacements of the shear band vs. distance from the advancing excavation face....86
4.13 Settlements of surface points on the center line with advancing face....87
5.1 Schematic of Syncrude Mining Operation....110
5.2 Location Map....111
5.3 Syncrude Dragline Mining Scheme....112
5.4 Typical Marine Sediments Geology....113
5.5 Highwall Failure Modes....114
5.6 Finite Element Idealization....115
5.7 Influence of the stiffness of the oilsand on the length of the yielded portion of the clay layer....116
5.8 Influence of the value of the peak cohesion on the extend of yielding....117
5.9 Influence of the depth of embedment on the length of the yielded portion of the clay layer....118
5.10 Influence of Ko on the length of the yielded portion of the clay layer....119
5.11 CLM (Center Line Method) of construction....120

5.12 DPM (Double Pyramid Method) of construction....121

6.1 Assumed foundation profile for the GBS....139

6.2 K_o versus depth profile....140

6.3 Finite element idealization....141

6.4 Variation of undrained shear strength along the clay layer after GBS set down....142

6.5 Variation of the OCR from the GBS centerline along the clay layer after the full tank pressure....143

6.6 Displacement field under full GBS pressure....144

6.7 Plot of the maximum shear stress τ_{max} under full GBS pressure....145

6.8 Displacement field of the foundation under full wave load....146

6.9 Influence of the depth of embedment on the length of the yielded portion of the clay layer....147

CHAPTER 1

INTRODUCTION

1.1 THE PROBLEM OF PROGRESSIVE FAILURE

In soil mechanics, we often encounter problems where some externally applied loads cause plastic deformation or failure in only part of the soil mass which may or may not result in the development of a collapsible mechanism. Since the maximum available strength is not fully mobilized throughout the soil mass, the assumption of limiting equilibrium is not valid because part of the soil body is still experiencing stresses below the peak strength of the material. On the other hand, the assumption of linear elastic behaviour is not appropriate because of failure in localized regions. Therefore, both the deformation and the strength properties of the soil must be considered in this type of analysis, i.e., a stress analysis is necessary. (Chan, 1985)

The earliest clear statement of the progressive failure problem was made by Taylor (1948) who discussed the necessary conditions for progressive failure to arise as well as the degree to which such action arises. He states that "...if a soil mass in nature is gradually brought to failure, the conditions will seldom be uniform over an entire incipient rupture surface and failure will not be reached at all points at the same time. The shearing strains that will occur will not be uniform, and concentrations of shearing stress

will tend to take place at points of maximum strain, causing rupture to start at these points." He also pinpoints that, "...the most important factors that control the degree to which progressive action occurs are the difference between the true peak-point strength and the ultimate strength as well as the shape of the true stress-strain curve". Taylor (1948) also observed that "progressive action exists during all shear failures, both in nature and laboratory tests" and "only by the merest of chances, will the degree to which progressive action occurs in nature be the same as that in any given type of testing apparatus". He also warned that "any assumption to the effect that progressive effects need not be considered because they occur both in nature and in the laboratory tests is definitely unsound".

As field evidence from slope failures accumulated in the 50's, it became apparent in most field situations that full peak strength was not being mobilized at failure. Some early observations attributed the loss of the cohesive peak strength component to weathering and softening. Skempton (1964) pointed out the importance of nonuniform mobilization of shear strength along slip surfaces and raised the concept of the residual factor to describe the reduction of strength (cohesive and frictional components) due to strain softening.

Bjerrum in his Terzaghi Lecture (1966), outlined the basic mechanism of progressive failure due to strain softening. He listed three conditions:

(1). Non-homogeneous strain development with localized straining sufficient to strain the soil beyond the failure;

(2). Distinct strain softening behaviour characterized by rapid decrease in strength after peak;

(3). Shear stresses have reached the peak along a continuous slip surface.

Time effects are not a necessary condition for progressive failure. This distinguishes progressive failure defined above from delayed failure, in which pore pressure redistribution, softening or bond degradation with time may cause failure. No doubt, time effects can also create conditions favorable for progressive failure.

Bishop (1967) defined the brittleness index to measure the amount of strain softening and recognized the importance of localized deformations caused by strain softening during the development of progressive failure. Morgenstern and Tchalenko (1967) observed real shear bands by means of microscopic techniques. It has been observed from the failure of heavily overconsolidated clays that a distinct failure or shear plane is formed and the deformation of this shear zone subsequently governs the overall behaviour of the soil mass. Although shear band deformation is not a necessary condition in progressive failure, it is definitely an important aspect of it.

Searching through the case histories available at his time, James (1970) examined more than 50 slope failures and could not find evidence for progressive failure (i.e first time slides). His studies demonstrated that:

(1) Delayed failure processes result in the loss of any cohesive strength component in the field, while peak frictional strength is maintained.

(2) Very large displacements in the first-time slides are required to develop residual strength by the progressive failure mechanism.

(3) Delayed failure processes and activation of presheared surfaces are sufficient to explain the range of slope behaviour observed.

Progressive failure in overconsolidated clays and clay shale slopes has been substantiated by limited field experience to date [Chan and Morgenstern (1987), Chen et al (1992), etc.]. Delayed failures, particularly softening of the cohesive strength component and pore pressure equilibration, have been quite well documented. Morgenstern (1977) discussed the state-of-the-art for these failure conditions at some length and drew attention to three basic concerns for futher research work.

Firstly, geological conditions in such materials control failure geometry. Residual strength is attained much more rapidly by shear along bedding than across it. Geological factors associated with the stress history of many materials virtually assure the development of in-situ preshearing along bedding planes irrespective of whether any overall slip failures develop.

Secondly, delayed failure processes are difficult to separate from the progressive failure mechanism. This means that exceptionally careful, and complete investigation is required of any field record which suggests progressive failure of a first time slide.

Thirdly, residual strength in the field is only obtained after sufficient straining has developed along thin, localized shear zones. Analytical treatment of the progressive failure problem thus requires careful attention to the geometrical constraints of shear zones as well as correct treatment of representative constitutive behaviour.

The above discussion is specific to slope behaviour in overconsolidated clays or clay shales, where indeed most of the engineering concerns regarding progressive failure are centered. However, progressive failure mechanisms may develop in any material which exhibits strain softening behaviour. Laboratory tests, dams, embankments, bearing

capacity problems, underground excavations are other areas where progressive failure can be expected to develop if strength parameters, stress paths and drainage conditions are suitable.

In order to gain some insight into the driving mechanisms that give rise to a softening response in geotechnical materials, it has to be seen what happens in granular and cohesive materials during shearing. In granular materials, during the evolution of the deviatoric loading, the microstructure undergoes damage in the form of dilation and grain crushing. That results in fewer contacts between the particles and hence lower sustainable strength. In cohesive materials, the driving mechanism is particle reorientation and the restructuring in the microfabric. Energy release is occuring as interparticle bonds break during dilation, which gives rise to the softening response.(Wan, 1990)

From laboratory results, it is seen that a progressive failure mechanism does not in general lead to a diffused type of plastic deformation but rather leads to localized deformation into rupture surfaces or shear bands. Chan (1985) divides the study of shear bands into two class of problems. In the first class the location and the direction of the propagation of the shear band is pre-determined by existing geological conditions such as a weak layer embedded in more competent strata, which is very common in Western Canada. Since the direction of the shear band is predefined, the objective is to calculate the extent of the softening zone along the shear band due to some external disturbance. In the second class of problems, where the location and the direction of the shear band are unknown, the initiation of localized failure and the formation of the shear band have to be detected first and then a search must be made for the direction and the extent of shear band propagation.

Although theoretical studies as well as the development of one dimensional models (Christian and Whitman, 1969) provide in depth understanding of the mechanism and effect of various factors causing progressive failure, they cannot be used to obtain solutions to realistic engineering problems. Numerical methods can follow the development of a non-homogeneous strain field and have been proved to be the most effective means for addressing complicated problems.

The first attempt to numerically model progressive failure in soils was probably made by Lo and Lee (1973) who succesfully modified conventional finite element analysis to predict stress levels in slopes cut in clays. Once failure had occurred, the elastic modulus was made to become negative and stresses were redistributed iteratively to surrounding zones in an attempt to simulate strain softening behaviour. The arbitrary assignment of a negative elastic modulus, once failure occurs, does not necessarily portray the actual mechanism, i.e plastic flow of the material. The simplest model used to model progressive failure is the elastic brittle perfectly plastic model, where the peak strength is allowed to drop to residual in a brittle fashion. Concern must be expressed that this sudden drop in strength might cause a release of energy which might lead to numerical instability. Also, the way the stresses are redistributed is still obscure, although perfect plasticity is used at residual strength. (Wan, 1990)

Models with a negative hardening modulus, as proposed by Nayak and Zienkiewicz (1972), Hoeg (1972), Prevost and Hoeg (1975), are classical but may lead to problems with respect to uniqueness and the convergence of the solution. That arises from the fact that the tangent stiffness matrix may become non positive definite for a strain softening material and the validity of the obtained solutions may be questionable. General

numerical instability reflected in difficulty of convergence becomes more prominent with strain softening.

Sture (1976) observed a variety of fracturing patterns during post-peak testing of coal, while Sture and Ko (1978) studied the stability of the machine-specimen system and derived conditions for strain softening as a localization process. They proved that the shear band mode could not be modelled as an overall homogeneous deformation problem.

An analysis of progressive failure in rock slopes was carried out by Kawamoto and Takeda (1978), but the constitutive models employed did not account for realistic strain softening. Cramer et al (1979) analysed direct shear tests on rock joints, but unfortunately using models which did not realistically match strength-loss and dilatancy characteristics. Cleary and Bathe (1979) discussed some of the difficulties which arise when trying to adapt classical finite element solutions and associated elastoplastic laws to progressive failure problems. Dong (1980) obtained some solutions for shear band development during flow of granular material in a hopper.

Looking into the physics of progressive failure, Chan (1985) studied the possibility of simulating localized deformations by using elastoplastic models and reported the effectiveness of finite element analyses in tackling real engineering problems. De Alencar (1988) studied the behaviour of fills built on presheared foundations and introduced a cracking model to simulate cracking failure. Chen (1990) investigated the progressive failure of the Carsington Dam via elastoplastic finite element analyses and captured the failure mechanism and the mode of failure.Wan (1990) developed a realistic and rational model that captures localized deformation using bifurcation theory. Discontinuous shape or interpolation functions were also developed for the discretization of his finite element

equations. Although this procedure is theoreticaly very sound, occasionally arising mesh locking can pose serious problems and its use is intended for the experienced finite element user.

1.2 OBSERVATIONAL APPROACH AND THE ROLE OF NUMERICAL METHODS

One of the outstanding contributions of Terzaghi to the art of geotechnical engineering is the observational method (Peck, 1973). By appropriate observations in the early stages of construction, reliable information can be obtained concerning the real geotechnical conditions, as opposed to those that previously could only be deduced or assumed. Whenever construction has already started and some unexpected development has occurred, or whenever a failure or accident threatens or has already taken place, an observational procedure may offer a satisfactory way out of difficulties. The method involves interpretating the field observations, refining the engineering calculations and making modifications to design and predictions of the subsequent behaviour of the structure. Under these circumstances perhaps most engineers would instinctively adopt such a procedure. The mere observation of events, such as the measurements of settlements, lateral movements or pore pressures, often suggests remedial measures that prove to be successful.

With the rapid developments in the field of constitutive modeling of geomaterials, advanced deformation analyses of geotechnical structures can be used to aid the forecast process. Chen et al (1992) view that the major role of such analyses lies not so much in

the prediction as part of the design process but more as an adjunct to the observational method by means of history matching.

Almost every geotechnical job, large or small, calls for some degree of instrumentation primarily during the construction phase. The results of the field observation are a powerful and indispensable tool in applied soil mechanics as they provide the best way to fine tune the numerical models. This enhances the ability to utilize these models in marching forward in real time as construction progresses and unveil the future of the structure in terms of its recent observed and backanalysed past. This is by no means an easy task, since a great amount of experience in the methodology of history matching and engineering judgement is usually required in making predictions of the behaviour of the structure. Successful applications of this methodology builds confidence in relying on those tools in practise. This acquired confidence can be very useful in cases where collapse may be sudden and reliance on the instrumentation could be dangerous, as it is often the case when progressive failure occurs.

1.3 PURPOSE OF THE RESEARCH

From the amount of research related to progressive failure problems undertaken by the Geotechnical Group of the University of Alberta, a great deal of understanding of the fundamental elements governing the phenomenon has been achieved. As a result of this effort, some powerful analytical and computational tools have been developed. The paramount importance of being able to utilize these tools in making forward projection of history matching models in cases where progressive failure is a possibility has been stated by Chen et al (1992). This ability stems from the familiarity of the user with the

methodology as well as from the user's confidence in the predictions of the model and can only be acquired by successfully analysing well documented case studies.

The difficulties in predicting soil response have long been recognized. Peck (1969) realizing that the art of geotechnical engineering is to deal with a limited amount of information and numerous uncertainties, emphasized the merits of the observational method in geotechnical design. A large amount of research effort has been devoted by the Geotechnical Group of the University of Alberta in exploring the applications of finite element analysis in backanalysis and the coupling of numerical simulation with the observational approach to construction problems. The objectives of this effort are usually well balanced between analytical developments and backanalysis of well documented cases [Chan (1985), de Alencar (1989), Chen (1990)]. The present thesis is an integral part of this effort but its main thrust lies in proving the applicability of the finite element analysis to aid in the forecast process based on the interpretation of field observations. To achieve this objective, three well documented cases were chosen to be analysed in the course of this study. These are, the classic case of "progressive" failure of the Oxford Clay pit reported by Burland et al (1977), the windrow induced highwall movements in the Syncrude open pit mine and the behaviour of the foundation of a gravity base structure.

One of the benefits of analysing complex case studies, is the opportunity to evaluate the capability and the computational efficiency of the numerical tools to tackle real life progressive failure problems. Almost from the beginning of the elastoplastic analysis using the finite element program PISA (Program for Incremental Stress Analysis) [Chan, (1986)], problems related to the convergence of the solution appeared, as the rate of convergence after a few steps was either extremely low or the solution was not

converging. It is essential to possess a powerful, reliable and computationally efficient finite element code that can tackle problems of this nature. Therefore, during the course of this research study, an effort to enhance the applicability and computational efficiency of PISA to solve problems of progressive failure due to strain softening in realistic engineering problems was undertaken. To achieve these goals, the following steps are necessary:

1. Analyse a class of progressive failure problems using the program PISA as it was originally developed by Chan (1986).

2. Assess, if any, the numerical difficulties in the solution process using the above code.

3. Locate the probable source(s) of the problem(s) and modify or add any algorithms in PISA to enhance its ability to solve progressive failure problems efficiently.

4. Solve the same cases with the modified version of the code and show the robustness of the new algorithm(s).

5. Repeat steps 1 to 4 for other types of progressive failure problems and show again the computational superiority of the modified version.

1.4 THESIS ORGANIZATION

Chapter 1 : Introduction - Purpose of the research - Thesis organization.

Chapter 2 : Since two out of three cases analyzed in this study are related to problems involving a geometrically altering domain, it was thought that a review and a historical development of various excavation/fill algorithms from the literature was

appropriate. Special emphasis was given to the general excavation fill algorithm adopted in this study, as it was proposed by Ghaboussi and Pecknold (1984).

Chapter 3: The finite element formulation of the algorithm proposed by Ghaboussi and Pecknold (1984) is presented. Also, the stress integration algorithm adopted in this study as proposed by Simo and Taylor (1985) is briefly reviewed. The derivation of "consistent stress-strain tensors" for the elastoplastic models used in the case studies as presented by Lee (1989) is also reviewed. Finally some simple examples are solved to verify the effectiveness of the adopted numerical techniques.

Chapter 4 : The response of the Saxon Clay pit wall to full face excavation was carefully monitored by Burland et al (1977). This was the best documented available case study for which Burland et al (1977) postulated that true progressive failure developed, causing propagation of a shear zone behind the toe of the wall. The prime objective of the deformation analyses undertaken in this chapter is to evaluate whether progressive failure could have occurred in the field as a result of the excavation induced displacements. Further deformation analyses combined with field measurements are intended to evaluate the hypothesis that only residual strength was mobilized in the field.

Chapter 5 : Several windrow induced highwall failures have been recorded on the Syncrude Canada Ltd. open pit mine in Ft. McMurray, Alberta. Geotechnical investigation has indicated that the failure surface is predominantly within a flat lying brittle clay layer. Due to the threat that these failures pose to the dragline safety as well as due to their significant economic impact on the mine productivity it was decided to study a typical windrow induced failure. Deformation analyses carried out to evaluate whether the windrow loading can induce progressive failure along the brittle clay layer, as well as the influence of various parameters control the extent of the propagation of yielding

Chapter 6 : In this chapter the potential for progressive failure of a Gravity Base Structure (GBS) founded on a hypothetical soil profile is evaluated. A provision in the

Commentary to the Canadian Code for the Design, Construction and Installation of Fixed Offshore Structures advises the undertaking of such an analysis under certain foundation and loading conditions. The influence of the strength and stiffness parameters of various layers and the depth of embedment of a hypothetical weak layer on the potential for progressive failure are evaluated.

Chapter 7 : Conclusions and recommendations for further study.

CHAPTER 2

EXCAVATION MODELLING

2.1. INTRODUCTION

A finite element code, PISA, developed by Chan (1986) is to be used to analyze excavation case histories and to predict excavation-induced movements. The finite element solution proposed here is based on a variational formulation which explicitly treats excavation as a process whereby the contributions of the external and internal forces acting on the excavated elements are removed directly from the global matrix equations. The resulting equations are solved by Newton-Raphson iterations for both linear and non linear applications.

For linear excavation problems, the global equations are solved directly. For non-linear excavation problems, the roots are solved iteratively by Newton's method using the notion of consistent tangent operator for rate-independent elastoplasticity proposed by Simo and Taylor (1985). The use of this tangent operator results in an iterative solution scheme which preserves the asymptotic rate of quadratic convergence of Newton's method.

The Von Mises and Drucker-Prager plasticity models with non-associated flow rule were tested in numerical examples to validate the proposed excavation analysis algorithm.

2.2. REVIEW OF PREVIOUS WORK

2.2.1 Simulation of Excavation

Numerical simulation of construction processes is important in determining stresses and deformations in many geotechnical structures. The construction process may involve fill-placement and/or excavation which, when simulated using the finite element method necessitates the addition and/or subtraction of finite elements from the original mesh.

A widely used technique for simulating the process of incremental excavation using the finite element method is based on an indirect procedure as illustrated schematically in Figure 2.1. In this Figure, it is desired to simulate the removal of a subdomain represented by region A from the initial domain, thus leaving in place a complementary subdomain represented by region B in the solution. The indirect method of excavation simulation entails the replacement of subdomain A by a consistent set of tractions, τ_i, applied on the stress free excavated boundaries of the remaining region B (Fig. 2.1.b). These applied surface tractions, τ_i, should ideally represent the tractions along the boundary between regions A and B which existed prior to the removal of region A. The effects of excavation (removal) of region A on the remaining region B are then modelled by applying tractions equal to τ_i in magnitude and opposite in sign (Fig. 2.1.c). The resulting increments of displacement, strain and stress are then added to the

original quantities in Fig. 2.1.a and the solution is then repeated for the next time step or the next increment of excavation.

In summary, this method of excavation simulation involves the following steps:

i. Establish initial displacements, strains and stresses within region B prior to excavation of region A (the "initial" conditions).

ii. Find the tractions τ_i transmitted from A to B.

iii. Remove the stiffness of A, leaving only portion B.

iv. Apply to B tractions equal to τ_i, in magnitude and opposite in sign.

v. Add the incremental displacements, strains and stresses of step 4 to the total displacements, strains and stresses of the previous step.

A major problem in the implementation of the above method involves the calculation of the consistent tractions τ_i, which must be applied to the resulting excavated boundary to satisfy a stress free surface. Although almost all excavation procedures reported so far in the literature [e.g. Dunlop et al.(1968), Duncan and Dunlop (1969), Chang (1969), Clough (1969), Clough and Duncan (1969), Dunlop and Duncan (1970), Wong (1971), Christian and Wong (1973), Chadrasekaran and King (1974), Clough and Mana (1976) and Mana (1978)] incorporate this conventional computation sequence, the technique used for correctly determining the consistent tractions is still a problem to be resolved.

Dunlop et al (1968), proposed a method to estimate the equivalent nodal forces by simple interpolation of the stresses between pairs of adjacent elements across the excavation boundary. Chang (1969) proposed a different technique for calculating the required nodal forces by considering only stresses within elements directly above the

excavation boundary with appropriate corrections for an assumed gravity stress gradient within the elements. Clough (1969), Clough and Duncan (1969), Wong (1971) and Christian and Wong (1973) proposed the use of interpolating polynomials to predict stresses on the excavation boundary. Wong (1971) extrapolated the stresses along a horizontal row of elements to be excavated using one-dimensional least square polynomials fitted to stresses at the element centers. Christian and Wong (1973) used higher order extrapolation to get better estimated tractions from the stresses in the elements around the excavated boundary, and showed that the resulting errors are reduced in their solution.

Chandrasekaran and King (1974) proposed a different method of computing the required equivalent nodal forces. In their method, equivalent nodal forces due to initial geostatic stresses are computed at all potential (eventual) excavation boundaries. These equivalent nodal forces are then updated during each increment of excavation by adding to them the calculated changes resulting from the incremental excavation. These incremental changes in nodal forces on any potential excavation boundary were obtained from the product of the stiffness matrices of the elements located just below that boundary and the corresponding incremental excavation-induced displacements due to the previous stage of excavation.

Clough and Mana (1976) proposed that the equivalent nodal forces be evaluated from local equilibrium at the excavation boundary as

$$\{F\} = \sum_{i=1}^{M} \int_{\Omega} B^T \sigma \, d\Omega \tag{2.1}$$

where $\{\mathbf{F}\}$ is a vector of nodal forces exerted by the elements to be excavated on the nodes of the remaining elements along the excavation surface, M is the number of elements which have common boundary with unexcavated elements, $\mathbf{B}$ is the strain - displacement matrix for all common boundary elements, and σ is the corresponding vector of current stresses.

A major drawback of the above procedures is that the solutions thus obtained are using their formulation to evaluate the equivalent nodal forces for an excavation problem was independent of the number of excavation steps (Fig. 2.2), Desai and Sargand (1974) demonstrated the non-uniqueness of Clough and Mana's solution by using one-dimensional eight-node elements. The calculated stresses and displacements were sensitive to the number of elements to be excavated and employed in the finite element mesh (Fig. 2.3). Thus, these solutions are unable to pass the test for elastic materials requiring that excavation induced deformations be functions solely of the final stage configuration and not of the construction history tracked in getting to this final stage. (Ishihara, 1970). It should be noted, however, that this non-uniqueness of the elastic case can be minimized by using a large number of excavation increments or stages, and that, partly as a result of this, the Clough and Mana solution methodology is currently the most widely one used for modelling excavations in both elastic and elastoplastic soils.

Desai and Sargand (1984) proposed an algorithm based on a hybrid formulation in which stresses were calculated directly at element boundaries, rather than at the internal Gauss points. Accordingly, it appears that the element boundary forces can be directly and correctly evaluated, and thus the correct "excavation face tractions" can be applied to model each successive stage of excavation. Unfortunately, this solution strategy

suffers from extreme complexity and unconventional formulation which is responsible, in large part, for the lack of widespread use in general geotechnical practice. (Lee, 1989).

In the finite element framework, Ghaboussi and Pecknold (1984), and Brown and Booker (1986) demonstrated that a unique solution for a linear material can be obtained by employing a virtual work formulation over the remaining post-excavation domain. Based on the total equilibrium concept, they presented a theoretically correct method of excavation simulation in linear elastic structures subjected to gravity loads and pointed out the source of gross numerical errors reported by investigators who employed the indirect procedures. Their technique will form the basis for the elastoplastic excavation analysis algorithm proposed in this research.

2.2.2 Constitutive modelling : Background

A realistic mathematical description of material response to applied load is essential if one is to make accurate predictions of the short- and long- term performance of geotechnical structures. The use of an appropriate constitutive model for soils is especially important in the analysis of earth structures since geomaterials exhibit a response which is highly nonlinear, irreversible and time dependent. In the following, some of the most commonly used plasticity models for characterizing the nonlinear response and irreversible deformation behaviour of engineering materials, and their suitability to soils will be discussed.

2.2.2.1. Von - Mises model

According to the Von - Mises theory, yielding is initiated when the second invariant of the deviatoric stress tensor reaches a certain value. Only rate-independent plasticity with linear strain hardening or softening conditions is considered. The yield criterion is given by :

$$F=F(\xi,\bar{\varepsilon}^p) = \| \xi \| - \sqrt{\frac{2}{3}}(\bar{\sigma}_o + H' \bar{\varepsilon}^p) = 0 \qquad (2.2)$$

where σ is the Cauchy stress tensor, $\xi = \sigma - \frac{1}{3}\,\mathrm{tr}\,(\sigma)\mathbf{1}$ is the deviatoric part of σ with $\mathbf{1}_{ij} = \delta_{ij}$, the Kronecker delta, tr(.) is the trace operator , $\bar{\sigma}_o$ is the uniaxial yield stress, $\bar{\varepsilon}^p$ is the effective plastic strain, H' is the hardening/softening parameter (assumed constant) and $\| \, . \, \|$ denotes a tensor norm. The evolution equations are given as:

$$\mathbf{p} = \frac{1}{3}\,\mathrm{tr}\,\sigma = K\,\mathrm{tr}\,\varepsilon \quad , \quad \xi = 2\mu(\mathbf{e}-\mathbf{e}^p) \qquad (2.3)$$

where p is the volumetric effective stress, K is the elastic bulk modulus , ε is the Cauchy strain tensor, μ is the elastic shear modulus, **e** is the deviatoric strain tensor, $\mathbf{e}^p$ is the plastic part of the deviatoric tensor, and a dot (.) denotes the partial of the variable with respect to time (the rate). By applying the asssociated flow rule

$$\mathbf{e}^p = \phi \frac{\partial F}{\partial \xi} \equiv \phi\, \hat{\mathbf{n}} \qquad (2.4)$$

where ϕ is the scalar consistency parameter and $\hat{\eta} = \frac{\xi}{\|\xi\|}$ .By enforcing the consistency condition, we get a rate-independent constitutive equation as follows:

$$\dot{\sigma} = \dot{\mathbf{C}}^{ep} : \dot{\varepsilon} \qquad (2.5)$$

where $\dot{C}^{ep}$ is a fourth-order tensor which has the explicit expression

$$\dot{C}^{ep} = K\,\mathbf{1}\otimes\mathbf{1} + 2\mu(\mathbf{I} - \frac{1}{3}\,\mathbf{1}\otimes\mathbf{1}) - 2\mu\gamma_{n+1}\,\hat{\mathbf{n}}\otimes\hat{\mathbf{n}} \qquad (2.6)$$

where $\mathbf{I}$ is the identity tensor defined such that $\mathbf{I}_{ijkl}=\frac{1}{2}(\delta_{ik}\delta_{jl}+\delta_{il}\delta_{jk})$ the symbol $\otimes$ denotes a tensor product in the sense that $(\mathbf{a}\otimes\mathbf{b})_{ijkl}=(a)_{ij}(b)_{kl}$ for any second order tensors **a** and **b**, and

$$\gamma = \frac{1}{1+\frac{H'}{3\mu}} - 1 \qquad (2.7)$$

is the flow rule factor obtained by applying the consistency condition on F.

This yield criterion was developed for metals, and assumed that yielding begins when the distortional energy reaches a value that is equal to the distortional energy at yield in simple tension. This is typically not strictly valid for soils, but it is very easy to deal with mathematically, and so provides an attractive simplification for evaluating the undrained behaviour of saturated clays in total stress analysis.

2.2.2.2. Drucker - Prager model

This is a generalized criterion accounting for the effects of all principal stresses and was suggested by Drucker and Prager (1952). The yield criterion is given by :

$$F = \sqrt{J_{2D}} + a\,J_1 - k \qquad (2.8)$$

where a and k are positive material parameters, J_1 is the first invariant of the stress tensor as

$$J_1 = \sigma_{11} + \sigma_{22} + \sigma_{33} \qquad (2.9)$$

and J_{2D} is the second invariant of the deviatoric stress tensor as

$$J_{2D}=\frac{1}{2}[(\sigma_{11}-\sigma_{22})^2+(\sigma_{22}-\sigma_{33})^2+(\sigma_{11}-\sigma_{33})^2] +\sigma_{12}^2 +\sigma_{23}^2+ \sigma_{13}^2 \qquad (2.10)$$

The two material parameters a and k can be determined from laboratory tests such as the conventional triaxial compression tests. In the triaxial stress conditions, the values of a and k can be expressed in terms of the angle of internal friction ϕ and the cohesion intercept c as follows :

$$a = \frac{2\sin\phi}{\sqrt{3}(3-\sin\phi)} \quad (2.11a) \qquad \text{and} \qquad k = \frac{6c\cos\phi}{\sqrt{3}(3-\sin\phi)} \quad (2.11b)$$

With this yield function, we get a rate-independent constitutive equation of the form :

$$\dot{\sigma} = \dot{C}^{ep} : \dot{\varepsilon} \qquad (2.12)$$

where $\dot{C}^{ep}$ is a fourth-order tensor which depends on the flow rule employed in conjunction with the Drucker - Prager model.

The use of this yield criterion with the associated flow rule implies very large extensional volumetric plastic strains. This type of deformation is not observed experimentally, even for very dense sands, for which high dilation is observed. Some problems can be solved using a non-associated flow rule in conjunction with the Drucker - Prager model. For example, stresses may be forced to satisfy the Drucker - Prager yield criterion, while the strain states are forced to satisfy certain conditions such as no volume change. The limitations of the Drucker - Prager model have been discussed further by Christian and Desai (1977).

2.3. EXCAVATION ANALYSIS ALGORITHM

This algorithm follows naturally and directly from placing the geometric alteration problem into the context of the Newton-Raphson family of solution techniques which are widely used in non-linear analysis. The major source of non-linearity is the change of geometry of the system due to addition or removal of material. Material property nonlinearities or path-dependent loadings can also be recognized in the analysis.

A residual load vector R is defined as

$$R = P - I \tag{2.13}$$

in which P is the nodal external vector and I is the nodal internal resisting force vector computed from element stresses s as

$$I = \sum_k L_k^T \int_{V_k} B_k^T \ \sigma_k \ dV_k \tag{2.14}$$

In equation (2.14) the subscript k is an element label and the summation is over the relevant group of elements. The usual notations for Boolean incidence matrix L_k, element strain-nodal displacement matrix B_k and element stress vector σ_k are used. Eq. (2.14) will be evaluated by Gaussian integration. It is also noted that eq. (2.14) provides a consistent relation between nodal forces and element stresses, derived from virtual work arguments.

In a standard incremental formulation for nonlinear analysis, the incremental equilibrium equations for increment n are

$$K_n \Delta U_n = \Delta P_n + R_n \tag{2.15}$$

in which K_n=tangent stiffness, ΔU_n=displacement increment, ΔP_n=load increment=P_n-P_{n-1} , and the residual R_n=P_{n-1}-I_{n-1}. For a system which is exactly in equilibrium

R_n=0. In nonlinear analysis, iterations are usually carried out until $\|R_n\|$ is zero to within a small tolerance.

Displacements, stresses and strains are then updated as follows:

$$U_n = U_{n-1} + \Delta U_n$$

$$\varepsilon_n=\varepsilon_{n-1}+\Delta\varepsilon_n \qquad (2.16)$$

$$\sigma_n=\sigma_{n-1}+\Delta\sigma_n$$

The load vector on the right - hand side of the equation (2.15) can be expressed in the alternative form (P_n-I_{n-1}) using the definitions of ΔP_n and R_n given following eq. (2.15). Eq. (2.15) can therefore be written in the equivalent form

$$K_n.\Delta U_n=P_n-I_{n-1} \qquad (2.17)$$

When elements and their associated external loads and internal stresses are added to or removed from the structure at the beginning of increment n, the standard nonlinear formulation can be used as long as the load vectors are modified appropriately to take account for the initial disturbance in equilibrium caused by altering the structure. Denote the modified residual load vector as R_n^*, where:

$$R_n^* = P_{n-1} - I_{n-1}^* \qquad (2.18)$$

Whereas R_n is quite small, R_n^* may be large. Effects of external loads such as gravity loads are reflected in P_{n-1}. Effects of internal stresses are reflected in I_{n-1} and I_{n-1}^*. I_{n-1}^* can differ from I_{n-1} due to two distinct effects : First, elements which are removed from the structure no longer contribute to the internal resisting force vector and are therefore not included in I_{n-1}^*; second, if prestressed elements are added to the structure, I_{n-1}^* contains these additional load effects while I_{n-1} does not.

For convenience, the applied load vector P_{n-1} at increment n-1 is regarded as unchanged when structural alterations are made at the beginning of increment n, since all changes in external loads such as gravity loads are then taken into account in the load

vector P_n. Thus, R_n^* reflects only part of the initial disturbance in equilibrium due to removal or addition of element internal stresses. The portion of the initial disturbance in equilibrium due to removal or addition of external loads is reflected in ΔP_n.

As a result, R_n^* is near zero when elements are added, unless the newly activated elements are prestressed. When elements are removed, both ΔP_n and R_n^* are non-zero, ΔP_n reflecting changes in the external load vector and R_n^* changes in the internal resisting force vector.

Understanding how the physical changes in the structure are reflected in ΔP_n and R_n^* helps in understanding the algorithm. However, it is more convenient for application of the method to express the incremental equilibrium equations in the form given by eq. (2.17). With the modifications needed to account for structural alterations, the incremental equilibrium equations are written as

$$K_n \cdot \Delta U_n = P_n - I_{n-1}^* \qquad (2.19)$$

In eq. (2.19), P_n simply represents all external loads acting on the structure as it currently exists. I_{n-1}^* simply represents the effects of internal stresses in those elements which are currently active. Note that PISA is using P_{n-1} instead of P_n in eq. (2.19), i.e the external loads that were acting on the structure as it was in the previous step.

The implementation of equation (2.19) is straightforward. The only new requirement imposed on a general nonlinear analysis system is the ability to "activate" and deactivate elements so that the stiffness assembly, the generation of external loads and the internal resisting load vector reflect the appropriate geometry changes of the system. The size of the stiffness matrix and the load and displacement vectors is kept the same throughout the analysis. Degrees of freedom which are currently not active because

no active elements connect to them are simply constrained to zero in the usual manner. The following simple procedure for activating and deactivating elements is used.

Activating elements Assume that a number of elements are to be added at the n^{th} step. All elements are actually treated as being present in the finite element mesh at all times, but until the element group is activated, its contributions to the stiffness matrix, element load vector (self weight) and internal resisting force vector are simply not assembled in eq. (2.19). At the n^{th} step and for all subsequent steps until it is again deactivated, the element group contributions are assembled. Newly activated elements are usually stress free and their initial contribution to the internal resisting force vector is then zero.

Deactivating elements Removal of a group of elements from the structure at the n^{th} step involves a procedure exactly opposite to that described. At step n and for all subsequent steps the group of elements to be deactivated is ommited from the assembly of eq. (2.19).

This approach can easily be incorporated in any existing finite element computer program. It treats the simulation of construction and excavation processes within the same general framework. Complicated multi-stage sequences of events can be simulated in a routine manner and inelastic material behaviour can easily be handled. Note in particular that the computation of equivalent nodal forces corresponding to reversed tractions acting on newly excavated surfaces requires only standard operations which are carried out as a matter of course in nonlinear analysis programs. Some examples illustrating the applicability of this procedure are presented in chapter 3.

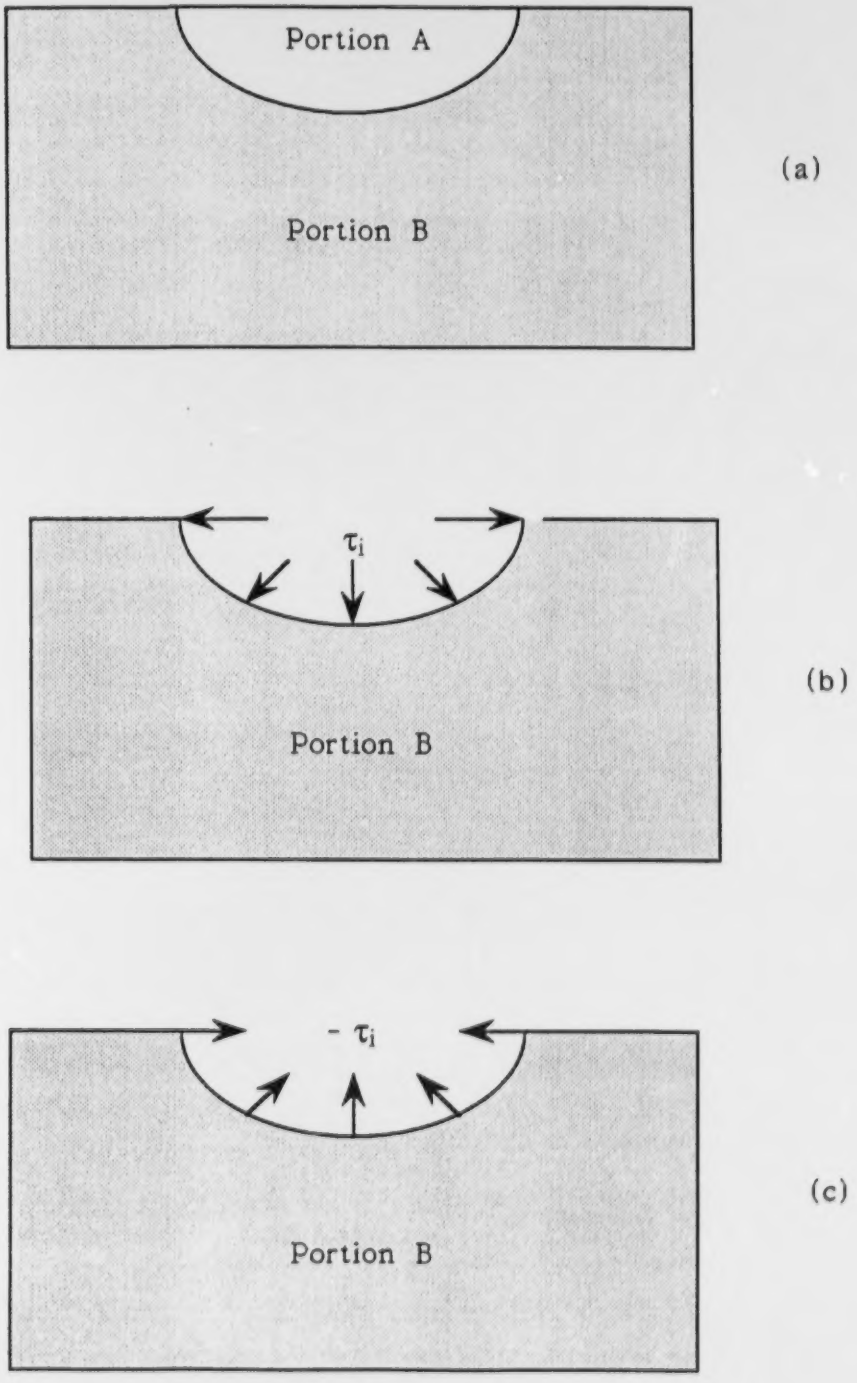

Fig. 2.1 Schematic Illustration of Excavation Problem (modified after Ghabousi and Pecknold, 1984).

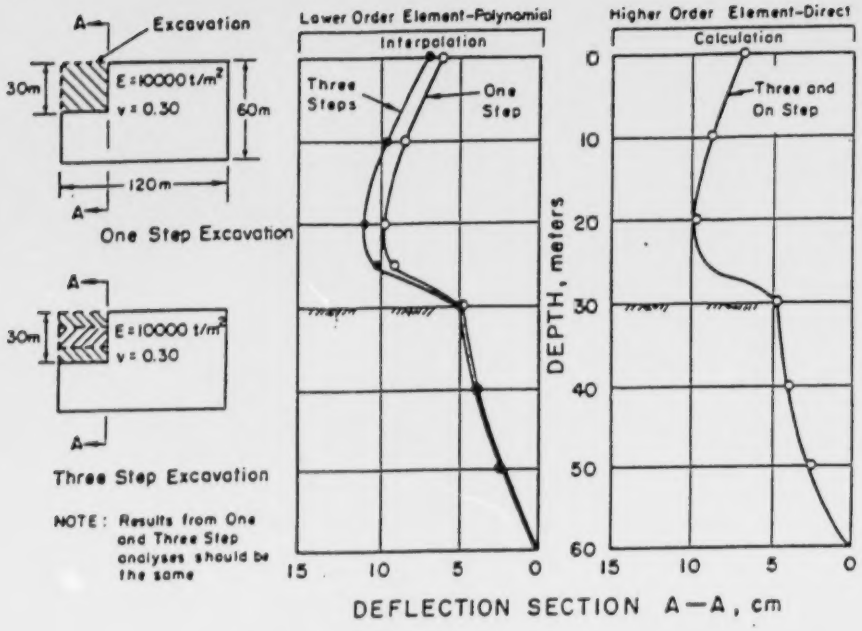

Fig. 2.2 Results from One- and Three- Step Analyses (modified after Clough and Mana (1976)).

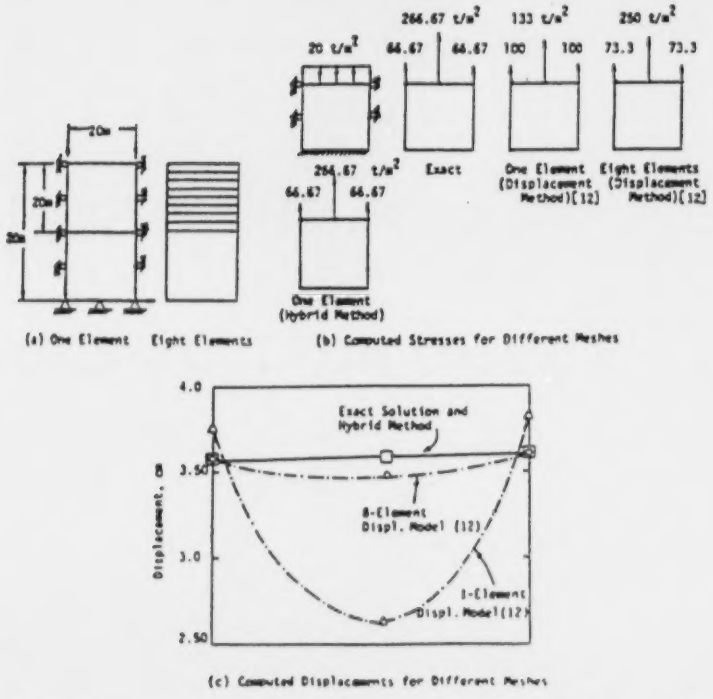

Fig. 2.3 Computed Stresses and Displacements for Different Meshes (modified after Desai and Sargand (1984)).

CHAPTER 3

FINITE ELEMENT FORMULATION

3.1 INTRODUCTION

The excavation algorithm described in the previous chapter, produces a unique solution for the strictly linear elastic case that is independent of the number of excavation stages. It was motivated by Ishihara's (1970) postulate that there exists a unique solution independent of the sequence of excavation or "cutting" for a linear, time-independent and elastic material. Also, subsequent work of the ADINA group (1981) and Brown and Booker (1986) demonstrated that by employing a virtual work formulation over the post-excavation domain, a unique solution for a linear elastic material can indeed be achieved.

3.2 GOVERNING EQUATIONS

Consider the following non-linear boundary value problem, stated in its strong form :

Given the unit body force vector $\mathbf{f}=\mathbf{f}(\mathbf{x})$ and surface traction $\mathbf{h}=\mathbf{h}(\mathbf{x})$, where $\mathbf{x}$ is the position vector, find the displacement vector $\mathbf{u}=\mathbf{u}(\mathbf{x})$ such that :

$$\nabla.\sigma(\mathbf{u}) - \mathbf{f} = 0 \quad \text{in } \Omega \qquad (3.1)$$

subject to the boundary conditions :

$$\mathbf{u} = \mathbf{u_g} \quad \text{on } \Gamma_g \tag{3.2}$$

$$\mathbf{n}.\sigma = \mathbf{h} \quad \text{on } \Gamma_h \tag{3.3}$$

where ∇ is the vector gradient operator, σ is the effective Cauchy stress tensor, $\mathbf{u_g}$ is the prescribed displacement vector, $\mathbf{h}$ is the prescribed surface traction vector, $\mathbf{n}$ is the surface unit normal, Ω is the geometrically altering problem domain and $\Gamma_g \cup \Gamma_h = \Gamma$ are the geometrically altering problem boundaries, see Fig. 3.1 i.e :

$$\Omega=\Omega(t), \quad \Gamma_g=\Gamma_g(t), \quad \Gamma_h=\Gamma_h(t) \tag{3.4}$$

Within this formulation, the problem domain and boundaries may vary due to excavation (removal of material) or fill placement (addition of material). Derivation of the matrix equations equivalent to eqs. (3.1)-(3.3) in a geometrically altering domain may be carried out along the lines presented by Borja et al. (1989).

If the "residual" generated by eq. (3.1) is weighted in accordance with a vector function $\mathbf{w}$ such that :

$$\int_{\Omega(t)} \mathbf{w}.(\nabla.\sigma(\mathbf{u}) - \mathbf{f})\, d\Omega = 0 \tag{3.5}$$

then by integrating equation (3.5) by parts, one obtains :

$$W_{INT}(t) = W_{EXT}(t) \tag{3.6}$$

where

$$W_{INT}(t) = \int_{\Omega(t)} \nabla \mathbf{w}:\sigma \, d\Omega \tag{3.7}$$

represents the internal virtual work and

$$W_{EXT}(t) = \int_{\Omega(t)} \mathbf{w}.\mathbf{f}\, d\Omega + \int_{\Gamma_h(t)} \mathbf{w}.\mathbf{h}\, d\Gamma \tag{3.8}$$

represents the external virtual work.

Eq. (3.6) can be transformed into a global - force equilibrium equation by numerically simulating staged construction as a piecewise constant function in the time domain. Physically, this is equivalent to considering fill placement and excavation as instanteneous events which can be modelled discretely by the addition or subtraction of nodes or elements from the original finite element mesh. Therefore, if $\Omega(t_{n+1})=\Omega_{n+1}$ and $\Gamma(t_{n+1})=\Gamma_{n+1}$ at time t_{n+1}, then the non-linear boundary value problem requires the determination of the roots $\mathbf{d}^*=\mathbf{d_{n+1}}$ representing the (global) nodal displacement vector $\mathbf{d}$ at time t_{n+1} such that :

$$(\mathbf{F_{INT}})_{n+1} - (\mathbf{F_{EXT}})_{n+1} = 0 \qquad (3.9)$$

where $(\mathbf{F_{INT}})_{n+1}= \mathbf{F_{INT}}(\mathbf{d_{n+1}})$ is the internal nodal force vector and $(\mathbf{F_{EXT}})_{n+1}= \mathbf{F_{EXT}}(\Omega_{n+1},\Gamma_{n+1})$ is the external nodal force vector representing the integration of all body forces and surface tractions acting on Ω_{n+1} and Γ_{n+1} respectively. As an illustration, let $\mathbf{B_{n+1}}$ denote the (global) strain-displacement transformation matrix and $\mathbf{N_{n+1}}$ the (global) shape function matrix at time $t=t_{n+1}$. This internal force vector from equation (3.9) is computed as:

$$(\mathbf{F_{INT}})_{n+1} = \int_{\Omega_{n+1}} \mathbf{B}_{n+1}^{T} \{\sigma\}_{n+1} \, d\Omega \qquad (3.10)$$

while the external nodal force vector is evaluated from the integral expression :

$$(\mathbf{F_{EXT}})_{n+1} = \int_{\Omega_{n+1}} \mathbf{N}_{n+1}^{T} \mathbf{f} \, d\Omega + \int_{(\Gamma h)_{n+1}} \mathbf{N}_{n+1}^{T} \mathbf{h} \, d\Gamma \qquad (3.11)$$

where $\{\sigma\}_{n+1}$ is the vector of stress components whose elements are derived from the stress tensor σ_{n+1}.

3.3 ITERATIVE ALGORITHM

To solve eq. (3.9) for the unknown nodal displacement vector **d**, an iterative scheme based on the linearization of eq. (3.9) must be employed:

$$\mathbf{F_{INT}}(\mathbf{d}^{k}_{n+1}) = \mathbf{F_{EXT}}(\mathbf{d}_{n+1}) \Rightarrow \mathbf{F_{INT}}(\mathbf{d}^{k}_{n} + \Delta\mathbf{d}^{k}_{n}) = \mathbf{F_{EXT}}(\mathbf{d}_{n+1})$$

But,

$$\mathbf{F_{INT}}(\mathbf{d}^{k}_{n} + \Delta\mathbf{d}^{k}_{n}) = \mathbf{F_{INT}}(\mathbf{d}^{k}_{n}) + \left(\frac{\partial \mathbf{F}^{(d)}_{INT}}{\partial \mathbf{d}}\right)_{\mathbf{d}_n}^{k} \Delta\mathbf{d}^{k}_{n} \Rightarrow$$

$$\Rightarrow \mathbf{F_{INT}}(\mathbf{d}^{k}_{n+1}) = \mathbf{F_{INT}}(\mathbf{d}^{k}_{n}) + \left(\frac{\partial \mathbf{F}^{(d)}_{INT}}{\partial \mathbf{d}}\right)_{\mathbf{d}_{n+1}}^{k} \Delta\mathbf{d}^{k}_{n} \Rightarrow$$

$$\Rightarrow \mathbf{F_{INT}}(\mathbf{d}^{k}_{n+1}) = \mathbf{F_{INT}}(\mathbf{d}^{k}_{n}) + \mathbf{F'_{INT}}(\mathbf{d}^{k}_{n+1})\Delta\mathbf{d}^{k}_{n} \qquad (3.12)$$

Performing the linearization of eq. (3.9) about the configuration $\mathbf{d}^{k}_{n+1}$ of the k^{th} iteration and using eq. (3.12) leads to the iterative solution scheme

$$\mathbf{F'_{INT}}(\mathbf{d}^{k}_{n+1})\Delta\mathbf{d}^{k}_{n} = (\mathbf{F_{EXT}})_{n+1} - \mathbf{F_{INT}}(\mathbf{d}^{k}_{n+1}) \qquad (3.13)$$

where $\mathbf{d}^{k+1}_{n+1} = \mathbf{d}^{k}_{n+1} + \Delta\mathbf{d}^{k}$ and $\mathbf{F'_{INT}}(\mathbf{d}^{k}_{n+1}) = \left(\frac{\partial \mathbf{F}^{(d)}_{INT}}{\partial \mathbf{d}}\right)_{\mathbf{d}_{n+1}}^{k}$ (3.14)

The second one of equations (3.14) is the Jacobian matrix. which can be evaluated from eq. (3.10) as :

$$\mathbf{F'_{INT}}(\mathbf{d}^{k}_{n+1}) = \int_{\Omega_{n+1}} \mathbf{B}^{T}_{n+1}\mathbf{C}^{k}_{n+1}\mathbf{B}_{n+1}\,d\Omega \qquad (3.15)$$

where $\mathbf{C}^{k}_{n+1} = \dfrac{\partial\{\sigma\}^{k}_{n+1}}{\partial\{\varepsilon\}^{k}_{n+1}}$ (3.16)

is the consistent matrix of tangential moduli obtained by evaluating the variation of $\{\sigma\}^{k}_{n+1}$ with respect to the strain vector $\{\varepsilon\}^{k}_{n+1}$.

By Newton's method, the next estimate of $\mathbf{d}^{*}$ is obtained from the iterative expression

$$\mathbf{d}^{k+1}_{n+1} = \mathbf{d}^{k}_{n+1} + [\mathbf{F}'_{INT}(\mathbf{d}^{k}_{n+1})]^{-1} [(\mathbf{F}_{EXT})_{n+1} - \mathbf{F}_{INT}(\mathbf{d}^{k}_{n+1})] \tag{3.17}$$

Theoretically, the convergence rate of Newton's method is asymptotically quadratic (Ortega and Rheinbold, 1970). In practice, this (optimal) rate of convergence can be achieved in elastoplastic analysis if the matrix of tangential moduli, $\mathbf{C}^{k}_{n+1}$, is derived not from the rate constitutive equation, but from a consistent linearization of the integrated constitutive equation (Simo and Taylor, 1985).

3.4 STRESS INTEGRATION ALGORITHMS

3.4.1 INTRODUCTION

In the context of finite element plasticity analysis, the solution of boundary value problems requires the use of numerical integration procedures for describing the evolution of stresses and hardening parameters.

In general, one seeks a numerical integration algorithm which is both accurate and stable over a range of physically reasonable step size. By accuracy, we mean that the algorithm converges to a prescribed tolerance level and produces nearly identical stress solutions when the step size is divided into sub-increments; by stability we mean that even

with a reasonably large step size, convergent solutions may still be achieved. In addition, an efficient algorithm that converges rapidly is desirable, in view of the large number of loading steps that are used to simulate sequential excavation or fill, with each loading step requiring an iterative algorithmic treatment for accurate solution.

3.4.2 OVERVIEW

Several explicit and implicit integration schemes are being used for elastoplastic computations. Explicit integration schemes usually require the evaluation of the elastoplastic transition through the calculation of a contact stress on the yield surface and a scale factor for the plastic multiplier. This procedure often breaks down in cases of complex stress and loading conditions since it can produce undesirable phenomena such as negative plastic flow (when the plastic multiplier numerically becomes negative) (Deng and Rosakis, 1990). They are also computationally inefficient especially for complex yield surfaces that require an iterative procedure for finding the scaling factor and contact stresses. Further refinements of these algorithms can be achieved by subdividing the step size into increments (Owen and Hinton, 1980), however, the algorithm is only first-order accurate and conditionally stable (Prevost, 1987).

For rate-independent plasticity the so called "return mapping algorithms" provide an efficient and robust integration scheme of the rate constitutive equations. This procedure amounts to a "discrete" enforcement of the consistency condition and appears to have been suggested first by Wilkins (1964) for the Von-Mises yield criterion. Krieg and Krieg (1976) extended the radial return algorithm to the case of linear isotropic and kinematic

hardening rules, and Simo and Taylor (1985) further extended it to nonlinear hardening rules in conjunction with a formulation for development of consistent tangent moduli.

The closest point projection algorithm was proposed as a generalization of the radial return algorithm to arbitrary convex surfaces [Ortiz and Pinsky (1981), Pinsky, Ortiz and Pister (1983), Ortiz and Popov (1985)]. It is an implicit procedure and thus unconditionally stable since the constraint is linearized and normality is enforced about the final unknown iteration. This requires evaluation of the gradients of the plastic flow direction, the normal to the yield surface, the plastic moduli and the elastic tensor. This can be a very laborious task for complicated plasticity models. Geometrically, the return mapping algorithms amounts to finding the closest distance of a point (trial stress state) to a convex set (yield surface).

It has to be mentioned that radial or closest point return algorithms have been often employed in conjunction with the so-called "elastoplastic tangent". The elastoplastic moduli are obtained from the "continuum" rate constitutive equation by enforcement of the consistency condition. Such procedure, however, results in loss of the quadratic rate of asymptotic convergence of the Newton's method, particularly important for large loading steps. This fact was recognized by Nagtegaal (1982) in the context of linear isotropic hardening rule. Simo and Taylor (1985) have shown that the use of a "consistent" tangent operator derived from the "integrated constitutive equation" corresponding to the linearized incremental problem results in an iterative solution scheme which preserves the asymptotic rate of quadratic convergence of Newton's method.

The radial and the closest point return algorithms are depicted schematically in Fig. 3.2 for a perfectly plastic model. A stress predictor is represented by the vector 1-2, which

is subsequently corrected to satisfy the consistency condition by returning the stress point back to the yield surface via either a non-associative (radial return) stress path (e.g. stress path 2-3 in Fig. 3.2) or an associative (closest point projection) stress path (e.g. stress path 2-4 in Fig. 3.2). The "return" stress path is thus dependent of the applied flow rule with the yield surface.

3.5 EXCAVATION IN ELASTIC SOIL

For an elastic soil with bulk modulus K and shear modulus μ, the integrated constitutive equation is :

$$\boldsymbol{\sigma}_{n+1} = \boldsymbol{\sigma}_n + \mathbf{C}^e : (\boldsymbol{\varepsilon}_{n+1} - \boldsymbol{\varepsilon}_n) \tag{3.18}$$

where $\boldsymbol{\sigma}_n$ and $\boldsymbol{\varepsilon}_n$ are the converged stress and strain tensors of the previous excavation stage, respectively, and $\mathbf{C}^e$ is the fourth - order tensor of elastic moduli given explicitly by

$$\mathbf{c}^e \equiv \frac{\partial \boldsymbol{\sigma}_{n+1}}{\partial \boldsymbol{\varepsilon}_{n+1}} \equiv K\,\mathbf{1}\otimes\mathbf{1} + 2\mu\,(\mathbf{I} - \frac{1}{3}\mathbf{1}\otimes\mathbf{1}) \tag{3.19}$$

in which $\mathbf{1}$ is the second order unit tensor with components $\mathbf{1}_{ij}=\delta_{ij}$ where δ_{ij} is the Kronecker delta, $\mathbf{I}$ is the fourth - order symmetric unit tensor with components $\mathbf{I}_{ijkl} = \frac{1}{2}(\delta_{ik}\delta_{jl}+\delta_{il}\delta_{jk})$ and $\otimes$ denotes a tensor product in the sense that $(\mathbf{a}\otimes\mathbf{b})_{ijkl}=a_{ij}b_{kl}$ for any tensors $\mathbf{a}$ and $\mathbf{b}$ of order of two.

Let $\mathbf{C}^e$ be assembled from the elements of the tensor $\mathbf{c}^e$. The Jacobian matrix is then computed as

$$\mathbf{F'_{INT}} \equiv \mathbf{K} = \int_{\Omega_{n+1}} \mathbf{B}_{n+1}^T \mathbf{C}^e \mathbf{B}_{n+1} d\Omega \tag{3.20}$$

Since **K** in elastic analysis is constant for a given mesh, iteration need not progress more than once in this case. Thus, for the elastic case, Eq. (3.17) reduces to :

$$\mathbf{d_{n+1}} = \mathbf{d_n} + \mathbf{K^{-1}}[(\mathbf{F_{EXT}})_{n+1} - \mathbf{F_{INT}}(\mathbf{d_n})] \qquad (3.21)$$

where $\mathbf{d}^{o}_{n+1} \equiv \mathbf{d_n}$, the converged displacement vector of the previous time step.

Eq. (3.21), as presented by Lee (1989), coincides with the finite elements formulations presented by Ghaboussi and Pecknold (1984) and Brown and Booker (1986) for the elastic case. In elastic analysis, use of eq. (3.21) results in a unique and superposable solution independent of the number of excavation stages. A crucial difference between the nonlinear solution presented by Ghaboussi and Pecknold (1984) and Lee (1989) lies in the algorithmic treatment of the resulting nonlinear finite element equations. Ghaboussi and Pecknold (1984) employed an explicit incremental solution strategy, whereas Lee 's (1989) approach is based on combined implicit stress integration and consistent linearization .

Because of the superposability of the solution obtained with Eq. (3.21) for the elastic case, the solution vector **d** can be based upon an "initially undeformed configuration" (Ω_o, Γ_o) for which $\mathbf{d_o} \equiv 0$, and the total displacement vector **d** at any excavation stage (n+1) can then be computed as

$$\mathbf{d_{n+1}} = \mathbf{K^{-1}}[(\mathbf{F_{EXT}})_{n+1} - \mathbf{F_{INT}}(\sigma_o)] \qquad (3.22)$$

where σ_o is the tensor of initial stresses corresponding to the initial configuration (Ω_o, Γ_o).

3.6. EXCAVATION IN ELASTOPLASTIC SOIL

In contrast to elastic analyses, the evolution of stresses in elastoplastic analyses requires the numerical integration of the rate constitutive equations over a finite time increment. Integrating the rate constitutive equation corresponding to a given yield criterion results in

$$\sigma^{k}_{n+1} = \sigma_n + \delta^k(\varepsilon^{k}_{n+1}, \varepsilon_n) \tag{3.23}$$

where σ_n and ε_n are the converged stress and strain tensors of the previous time step, and δ^k is the incremental stress function consistent with a given stress integration algorithm. Simo and Taylor (1985), showed that the tensor of elastoplastic moduli obtained by taking the variation

$$c^{k}_{n+1} \equiv \frac{\partial \sigma^{k}_{n+1}}{\partial \varepsilon^{k}_{n+1}} = \frac{\partial \delta^k(\varepsilon^{k}_{n+1}, \varepsilon_n)}{\partial \varepsilon^{k}_{n+1}} \tag{3.24}$$

is consistent with the linearization of equation (3.9) and results in an iterative solution scheme which preserves the asymptotic rate of convergence of Newton's method. To illustrate the application of Eq. (3.24) to various yield criteria, the Von - Mises and Drucker - Prager criteria will be considered.

3.6.1 Von - Mises criterion with linear strain hardening or softening

The yield criterion is given by :

$$F=F(\xi,\bar{\varepsilon}^p) = \| \xi \| - \sqrt{\frac{2}{3}}(\bar{\sigma}_o + H' \bar{\varepsilon}^p)= 0 \tag{3.25}$$

where $\xi = \sigma - \frac{1}{3}\,\mathrm{tr}\,(\sigma)\mathbf{1}$ is the deviatoric part of σ, $\bar{\sigma}_o$ is the uniaxial yield stress, $\bar{\varepsilon}^p$ is the effective plastic strain, H' is the hardening/softening parameter (assumed constant), $\| \ \|$ denotes a tensor norm and tr( ) is the trace operator. Use of this (non-kinematic) yield criterion in conjunction with the radial return algorithm on the trial stress σ^{tr}_{n+1} for integrating stresses results in an incremental stress function for the Von-Mises plasticity model of the form:

$$\delta^{k}_{VM}(\varepsilon^{k}_{n+1},\varepsilon_n)=K\,\mathrm{tr}(\varepsilon^{k}_{n+1}-\varepsilon_n)\mathbf{1} + \sqrt{\frac{2}{3}}(\bar{\sigma}_o + H' \bar{\varepsilon}^{p}_{n+1})\hat{\mathbf{n}} - \xi_n \tag{3.26}$$

where $\hat{\mathbf{n}}= \dfrac{\xi^{tr}_{n+1}}{\|\xi^{tr}_{n+1}\|}$ is the unit normal to F in the radial direction, $\xi^{tr}_{n+1}= \sigma^{tr}_{n+1} - \frac{1}{3}\,\mathrm{tr}\,(\sigma^{tr}_{n+1})\mathbf{1}$ is the deviatoric part of the trial stress σ^{tr}_{n+1}, and ξ_n is the deviatoric part of the converged tensor σ_n of the previous time step. From eq. (3.24), the symmetric consistent tangential tensor of moduli is obtained as :

$$\mathbf{c}^{k}_{n+1} = K\,\mathbf{1}\otimes\mathbf{1} + 2\mu\beta_{n+1}(\mathbf{I} - \tfrac{1}{3}\,\mathbf{1}\otimes\mathbf{1}) - 2\mu\gamma_{n+1}\,\hat{\mathbf{n}}\otimes\hat{\mathbf{n}} \tag{3.27}$$

$$\text{where} \quad \beta_{n+1}= \frac{\sqrt{\frac{2}{3}}(\bar{\sigma}_o + H' \bar{\varepsilon}^{p}_{n+1})}{\|\xi^{tr}_{n+1}\|} \tag{3.28a}$$

$$\text{and} \quad \gamma_{n+1}= \frac{1}{1+\frac{H'}{3\mu}} - (1-\beta) \tag{3.28b}$$

Note that (3.28b) differs from the elastoplastic stress - strain tensor derived from the rate constitutive equation given by :

$$\mathbf{c}^{k}_{n+1} = K\,\mathbf{1}\otimes\mathbf{1} + 2\mu(\mathbf{I} - \tfrac{1}{3}\,\mathbf{1}\otimes\mathbf{1}) - 2\mu\gamma_{n+1}\,\hat{\mathbf{n}}\otimes\hat{\mathbf{n}} \qquad (3.29)$$

where $\gamma_{n+1} = \dfrac{1}{1+\dfrac{H'}{3\mu}} - 1$ (3.30)

is the flow rule factor obtained by applying the consistency condition to F. This is true since β as given by equation (3.28a) is generally not equal to unity. Use of eq. (3.27), rather than eq. (3.29), results in a tangent operator that preserves the quadratic convergence of Newton's method.

3.6.2 Drucker - Prager criterion with J_2 plastic flow

Let $p = \frac{1}{3}\,\mathrm{tr}\,(\sigma)$ be the mean normal (volumetric) stress, $\xi = \sigma - p\mathbf{1}$ be the deviatoric part of σ, c the soil's cohesion and ϕ the soil's friction angle, and assume that H'=0. The Drucker - Prager yield criterion is formulated as:

$$G = G(\xi,p) = \|\xi\| - \sqrt{\tfrac{2}{3}}\,k(p) \qquad (3.31)$$

where $k(p) = \dfrac{6}{3-\sin\phi}\,(c\cos\phi + p\sin\phi)$ (3.32)

Note that $\sqrt{\frac{2}{3}}\,k(p)$ is the radius of the cone responding to the mean stress p. By applying the (non-associative) radial return algorithm as shown schematically in Fig. (3.2), one obtains the incremental stress function for the Drucker - Prager yield criterion as

$$\delta^{k}_{DP}(\varepsilon^{k}_{n+1},\varepsilon_n) = K\,\mathrm{tr}(\varepsilon^{k}_{n+1} - \varepsilon_n)\mathbf{1} - \sqrt{\tfrac{2}{3}}\,k(p_{n+1})\,\hat{\mathbf{n}} - \xi_n \qquad (3.33)$$

Substituting eq. (3.33) into eq. (3.34) results in the non symmetric tangential tensor

$$\mathbf{c}^{k}_{n+1} = K\,\mathbf{1}\otimes\mathbf{1} + 2\mu\beta_{n+1}(\mathbf{I} - \tfrac{1}{3}\,\mathbf{1}\otimes\mathbf{1}) - 2\mu\beta_{n+1}\,\hat{\mathbf{n}}\otimes\hat{\mathbf{n}} - \sqrt{\tfrac{2}{3}}\,K\,\frac{6\sin\phi}{3-\sin\phi}\,\hat{\mathbf{n}}\otimes\mathbf{1}$$

(3.34)

where $\beta_{n+1} = \dfrac{\sqrt{\frac{2}{3}}\,k(p_{n+1})}{\|\xi^{tr}_{n+1}\|}$ (3.35)

Again, eq. (3.34) differs from the corresponding elastoplastic stress - strain tensor given by

$$\mathbf{c}^{ep}_{n+1} = K\,\mathbf{1}\otimes\mathbf{1} + 2\mu\,(\mathbf{I} - \tfrac{1}{3}\,\mathbf{1}\otimes\mathbf{1}) - 2\mu\,\hat{\mathbf{n}}\otimes\hat{\mathbf{n}} - \sqrt{\tfrac{2}{3}}\,K\,\frac{6\sin\phi}{3-\sin\phi}\,\hat{\mathbf{n}}\otimes\mathbf{1} \qquad (3.36)$$

since β_{n+1} in eq.(3.35) is generally not equal to unity. Use of eq. (3.34) to define the consistent tangent operator again results in formulation with an iterative scheme which preserves the quadratic rate of convergence of Newton's method.

Similar expressions can be derived for any other convex yield surfaces, by applying the consistent linearization principle to the corresponding integrated constitutive equation rather than to the rate constitutive one.

3.7 IMPLEMENTATION AND VERIFICATION OF THE MODELLING TECHNIQUES

3.7.1. INTRODUCTION

In this section some numerical examples involving applications of the proposed analysis and modelling techniques will be presented. The accuracy and stability of the

proposed excavation modelling scheme will be examined, using linear elastic modelling first and then the plasticity models described in the previous chapter.

Using some simple "model" examples, the theoretical validity of the excavation modelling technique and the validation of the computer program will be demonstrated. It will be shown that in elastic analyses, the solutions to problems involving time-varying domain and boundaries are superposable and do not depend on the number of construction (excavation) stages, therefore satisfying Ishihara's (1970) uniqueness postulate for the elastic case. It will be also demonstrated that in elastoplastic analyses, an "asymptotically unique" solution can be achieved with this modelling technique which converges with increased number of excavation steps used in the analysis.

3.7.2. MODEL VERIFICATION

A major concern in estimating excavation-induced displacements, is the degree of sensitivity of the solution to the number of excavation increments to get to the final stage. By definition, the true final stage solution is one which entails the removal of infinitesimally thin layers of elements sequentially, until the full final depth of the excavation is reached. The accuracy of a stress integration algorithm can then be assessed by looking at the "error" generated as a result of removing these layers in finite increments. Thus, a solution is asymptotically unique if excavation-induced deformations are functions solely of the final stage configuration and not of the construction sequence (number of increments) employed to get to this final stage.(Lee, 1989).

In the original version of the program PISA two convergence criteria were being implemented and enforced :

1. Residual Force criterion

$$\|\mathbf{r}^k\| \leq \varepsilon_R \|\mathbf{r}^o\|$$

2. Displacement criterion

$$\|\Delta\mathbf{d}^k\| \leq \varepsilon_d \|\Delta\mathbf{d}^o\|$$

where $\mathbf{r}^k=(\mathbf{FEXT})_{n+1}-(\mathbf{FINT}(\sigma^k_{n+1}))$ is the residual force vector of the k^{th} iteration, $\Delta\mathbf{d}^k$ is the increment of displacement at iteration k and $\|\ \|$ denotes a vector norm. The parameters ε_R and ε_d represent the residual force and displacement thresholds, respectively and their magnitudes are specified by the user, depending on the problem being analyzed.

A third convergence criterion that incorporates both the displacements and forces is the energy criterion, which is defined as:

$$|\Delta\mathbf{d}^k \cdot \mathbf{r}^k| \leq \varepsilon_E |\Delta\mathbf{d}^o \cdot \mathbf{r}^o|$$

This is not implemented in the original version of PISA. In the above equation ε_E is the energy threshold.

Because the reference residual was chosen as $\mathbf{r}^o$ in the above equations, convergence in the solution is achievable after only one iteration in elastic analyses provided that one does not under-integrate the internal nodal force vector. (Borja, 1988).

3.7.3 SIMULATION OF EXCAVATION AND FILL IN ELASTIC SOIL

In this section, the modified finite element code is tested to verify that it satisfies the uniqueness principle for elastic materials postulated by Ishihara (1970). Simple

numerical examples are used to demonstrate that the solutions to problems involving a shrinking (excavation) or expanding (fill) domain are superposable and do not depend on the number of construction stages or increments modelled. For the sake of comparison, the simple numerical examples presented by Borja et al (1989) and Lee (1989) will be used.

Consider the mesh composed of 20, four-noded isoparametric soil elements shown in Fig 3.3 and assume a condition of plane strain. In this example, it is desired to excavate the four elements labelled 3, 4, 7 and 8. Nodes along the right-hand, base, and left-hand boundaries of the global mesh may translate freely along the boundaries, but are fixed against displacements normal to these mesh boundaries. Assume that the soil's Young's modulus is $E = 10^3$ kN/m^2 Poisson's ratio $\nu = 0.40$ and the unit weight of the elastic material $\gamma = 20.0$ kN/m^3 In evaluating the internal nodal force vector, $\mathbf{F}_{INT}$, the standard 2*2 Gauss quadrature rule was employed. Only one iteration per excavation stage was then required in the elastic solution. For purposes of definition, consider the "initially undeformed configuration" (Ω_0,Γ_0) as the configuration right after switching the gravity loads on. Thus, $\mathbf{d}_0 = 0$ when $\sigma=\sigma_0$ where σ_0 are the stresses due to the elastic soil's self-weight.

One - step Excavation

In this case, elements 1-4 were removed simultaneously. The resulting displacement profile at the end of the excavation stage is denoted as configuration (Ω_2,Γ_2) in Fig. 3.4. The horizontal and vertical movements of two reference corner nodes labeled A and B in Fig. 3.4 are shown as solid $0\rightarrow2$ in the displacement history profiles of Fig. 3.5. These final displacements are to be compared with those computed using different excavation or fill increments (sequences).

Two - step Excavation

Taking the same initial configuration (Ω_o,Γ_o), the same four elements shown in Fig. 3.3 were excavated in two stages: elements 1 and 2 in the first stage, and elements 3 and 4 in the second. The resulting deformed mesh at the end of the second excavation stage is identical to the one - step solution, as shown previously in Fig. 3.4. The displacement profiles of the same corner nodes A and B are shown as solid lines $0 \rightarrow 1 \rightarrow 2$ in Fig. 3.5. As shown in Figs. 3.4 and 3.5 , the final displacements are independent of the number of excavation steps, thus demonstrating the superposability of the solution for this elastic case, and the satisfaction of Ishihara's (1970) uniqueness postulate.

3.7.4. SIMULATION OF EXCAVATION IN A DRY ELASTOPLASTIC SOIL

In the previous sections, the implemented technique showed the uniqueness of solutions to problems involving excavation in elastic soils. This section presents analyses of numerical examples involving excavation in dry elastoplastic soils. The plasticity models employed in the examples are Von - Mises and Drucker - Prager in conjunction with return mapping algorithms.

3.7.4.1 PLANE STRAIN EXCAVATION

Consider the mesh made up of 80, four-noded elements shown in Fig 3.6 and assume a homogeneous, elastoplastic material which yields according to the Von-Mises criterion. Let E = 10^4 kN/m^2, ν = 0.40, H'= 1.0, and assume the same unit weight of γ= 20.0 kN/m^3 for the soil. A low value of$\bar{\sigma}_o$=2 kN/m^2 is selected to ensure that all Gauss

points yield from the initial to the final stage of excavation (with this value of $\bar{\sigma}_o$, the gravity loads alone already caused all Gauss points to plastify).

In the analysis performed, sixteen elements in the upper left-hand corner of the original mesh shown in Fig. 3.6 were removed in :
(a) one step, (b) two steps, (c) four steps and (d) eight steps. These excavation schemes are equivalent to removing 16, 8, 4 and 2 row-elements at a time, respectively. Excavation of these sixteen elements resulted in plastification of all Gauss points in the mesh. The sensitivity of the elastoplastic solution to the number of excavation stages was then investigated.

Fig. 3.7 shows the calculated incremental excavation - induced nodal point displacement vectors for all nodes along the final excavation boundary resulting from the excavation of the sixteen elements as predicted by the one-, two-, four- and eight- step analyses (these incremental displacements are the total displacements minus the initial displacements that occured directly due to imposition of initial gravity loads). The calculated excavation-induced displacements were identical for the one-, two-, four- and eight-step excavation analyses, showing that the solution thus obtained is unique, and does not depend on the number of excavation stages.

To further illustrate the insensitivity of the elastoplastic solution to the number of excavation stages, the displacement history profile of node A, located in the upper left-hand corner of the final mesh shown in Fig. 3.6, is plotted in Fig. 3.8 for each of the one-, two-, four- and eight-step schemes. From Fig. 3.8, it can be seen that the displacement history profile of this node is uniquely defined.

3.7.4.2 AXISYMMETRIC EXCAVATION

Consider the same mesh shown in Fig. 3.6 and assume an axisymmetric condition. Assume further that the material comprising this mesh is homogeneous and elastoplastic and yields according to the non-associative Drucker-Prager model. The stiffness matrix defining the linearized finite element equations is non-symmetric in this case. Let E = 10^2 kN/m^2 (note that this value of E is 100 times smaller than the one used in the plane strain excavation analysis since the deformations induced in axisymmetric excavation problems are many times smaller than those that develop under a plane strain condition), ν=0.40, γ=20 kN/m^3, and assume a non-hardening Drucker-Prager soil model with cohesion c= 0.1 kN/m^2 and friction angle ϕ= 20^o. This friction angle was so chosen to guarantee that the K_o line crosses the Drucker-Prager cone. Thus, the initial gravity load already caused the soil to plastify in one-dimensional compression.

The same sixteen elements shown in Fig. 3.6 were again removed in one-, two-, four- and eight-step schemes. Fig 3.9 shows the resulting calculated final excavation-induced nodal point displacements, which were again identical for the one-, two-, four- and eight-step analyses. The displacements of the exposed excavation boundaries are thus again unique, and independent of the number of excavation stages. Comparing Fig. 3.9 with 3.7 for the plane strain case, it is seen that (a) the displacements that develop in axisymmetric excavation are generally smaller than those that develop in plane strain; (b) basal heaving is proportionally more prominent than lateral deflections in axisymmetric than in plane strain excavation, and (c) vertical movements on the vertical face of the pit are proportionally less significant in axisymmetric than in plane strain excavation.

Fig. 3.10 shows the displacement history profile of the same corner node A considered in plane excavation. All excavation schemes yielded a unique solution as shown in this figure. Note that at some point of the excavation process, node A heaved significantly. This has to do with the axisymmetry of the problem and is not due to the characteristics of the constitutive model used.

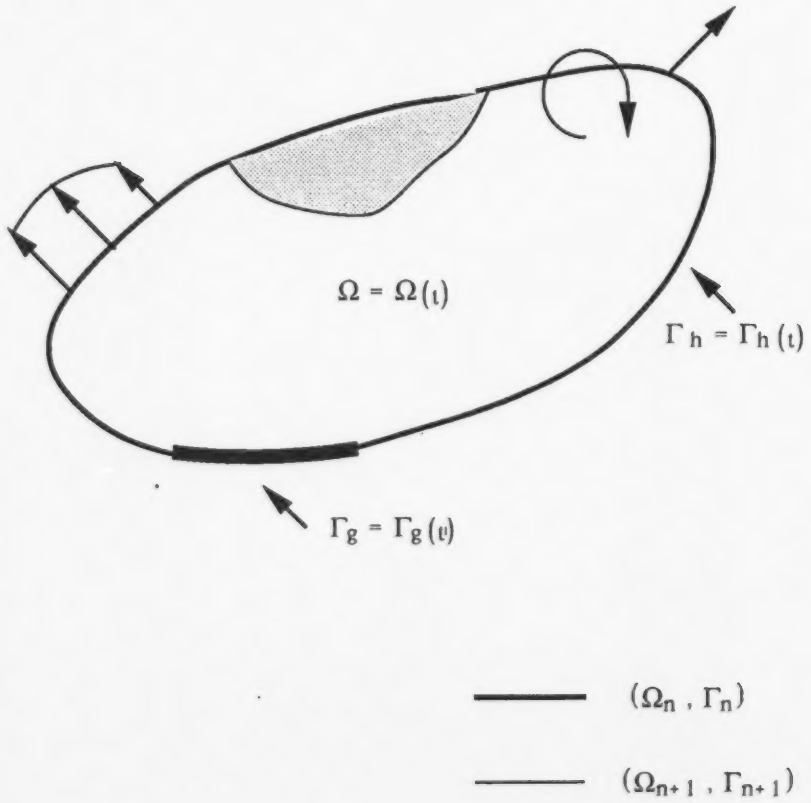

Fig. 3.1 Schematic Illustration of Time - Varying Problem Domain and Boundaries (modified after Lee, 1989).

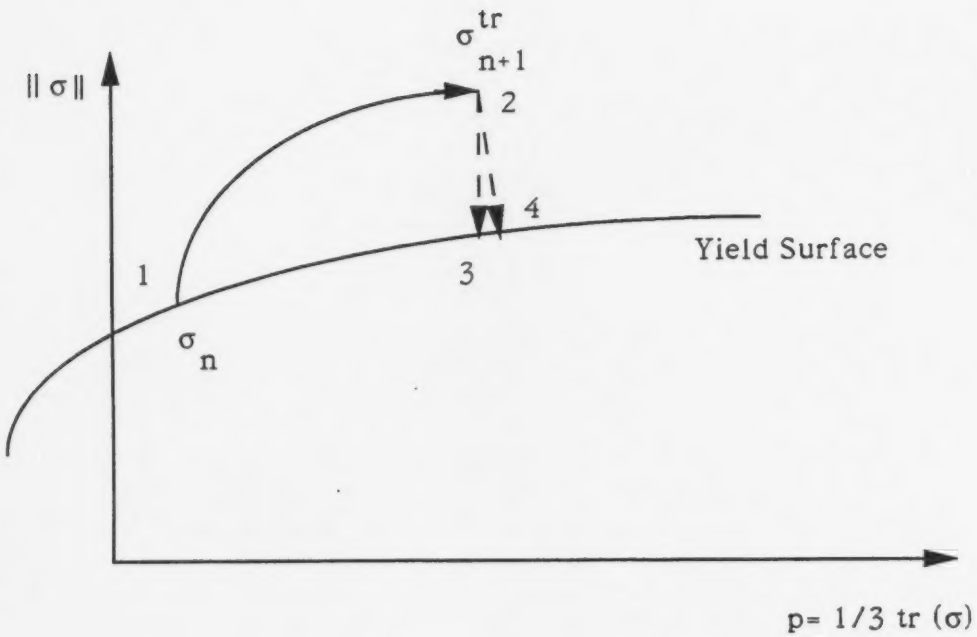

Fig. 3.2 Schematical representation of the radial and closest return mapping algorithms (modified after Borja et al., 1989)

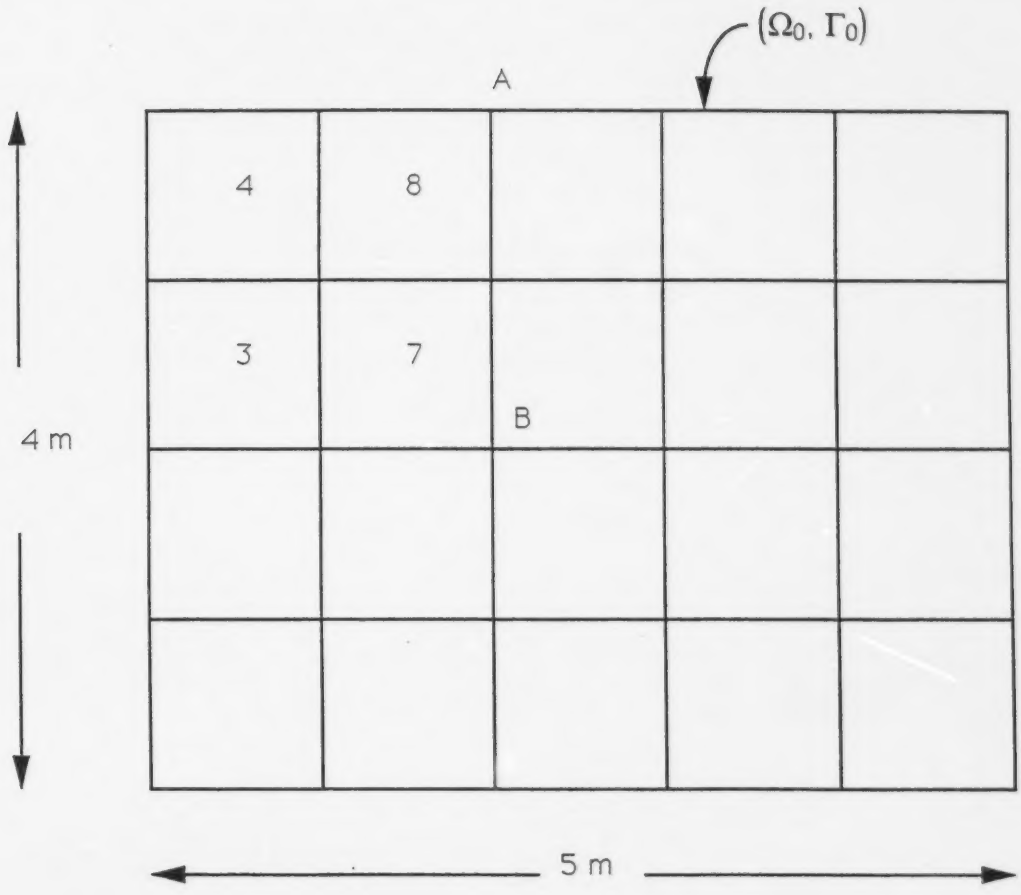

Fig. 3.3 Finite element mesh used for excavation in elastic soil

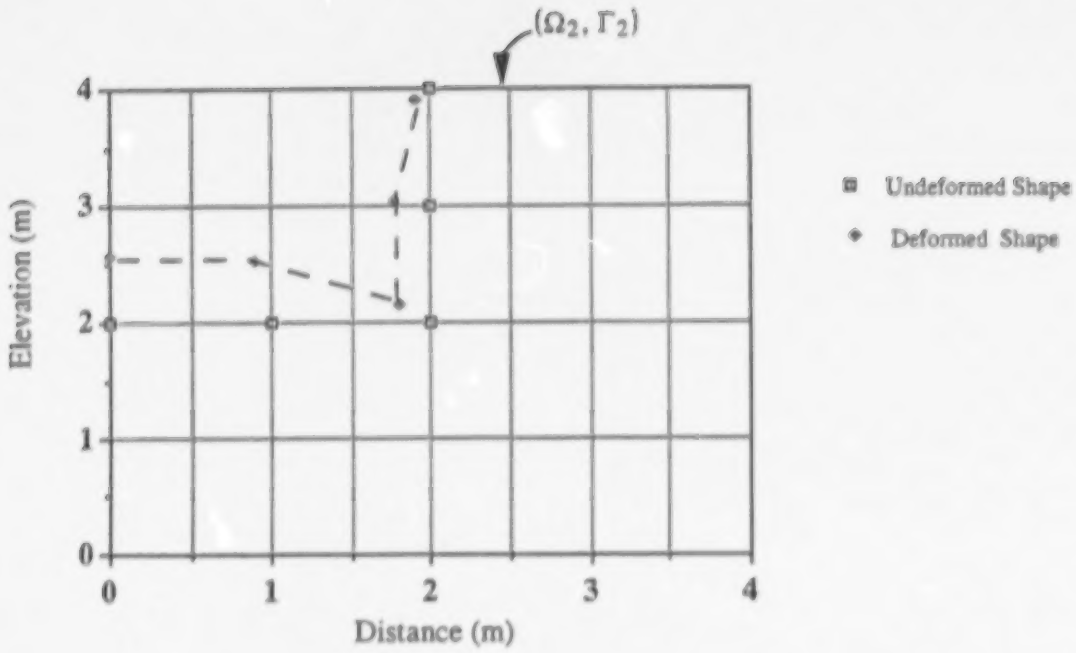

Fig. 3.4 Final Deformed Wall - Floor system after excavation of elements 1 to 4

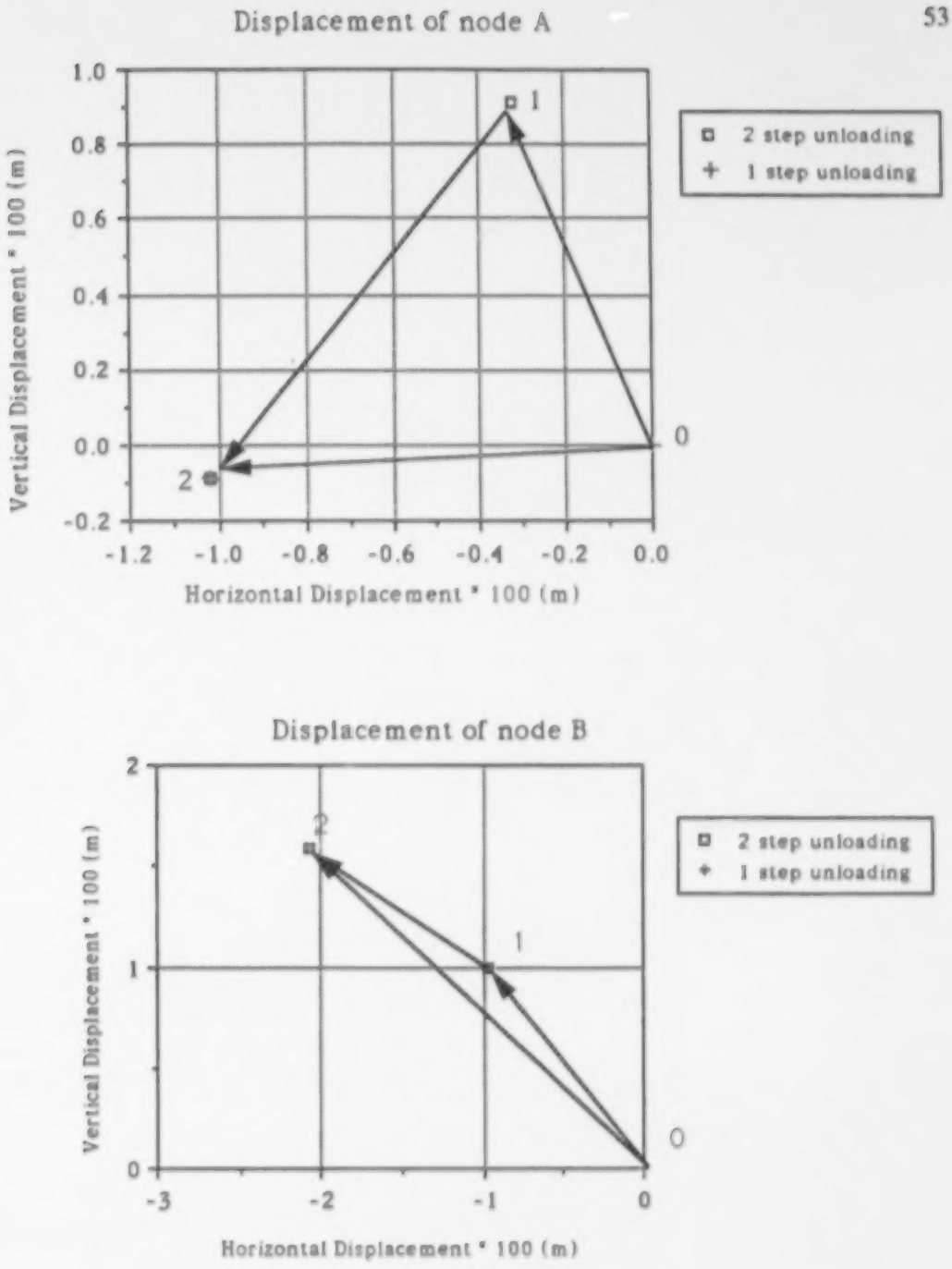

Fig. 3.5 Displacement History of node A and B during excavation

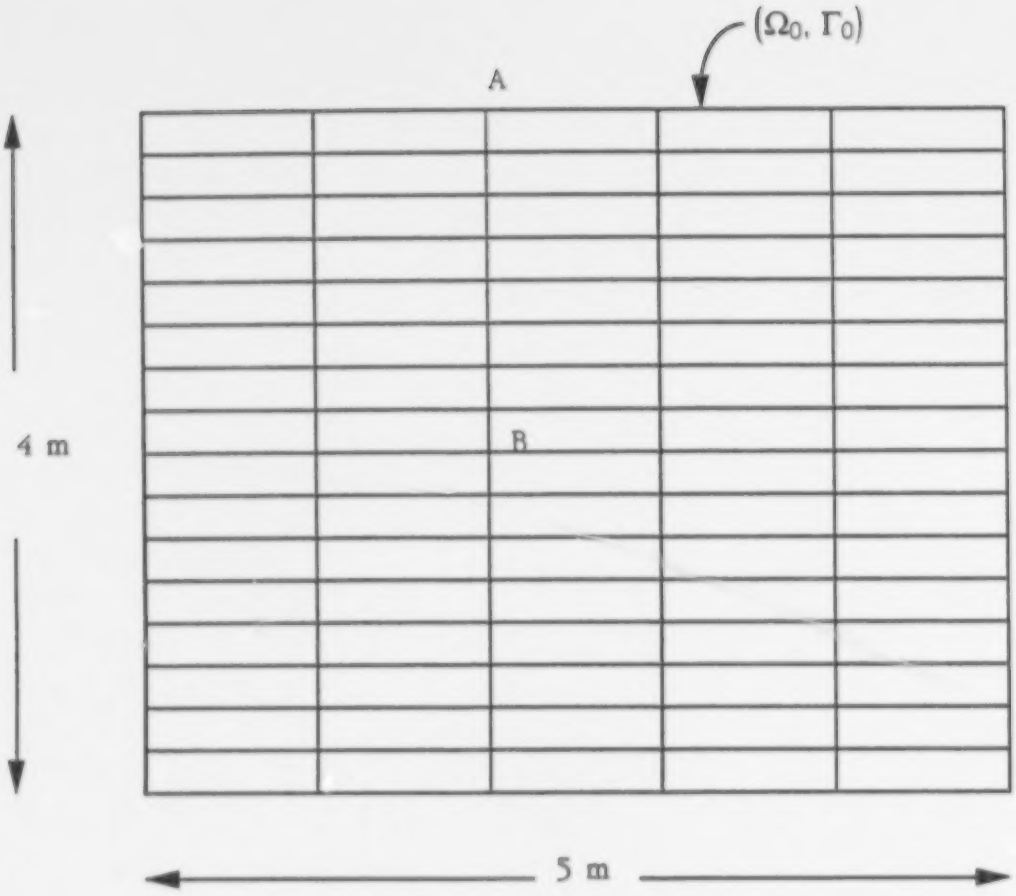

Fig. 3.6 Finite element mesh used for excavation in plane strain and axisymmetric excavation in elastoplastic soil

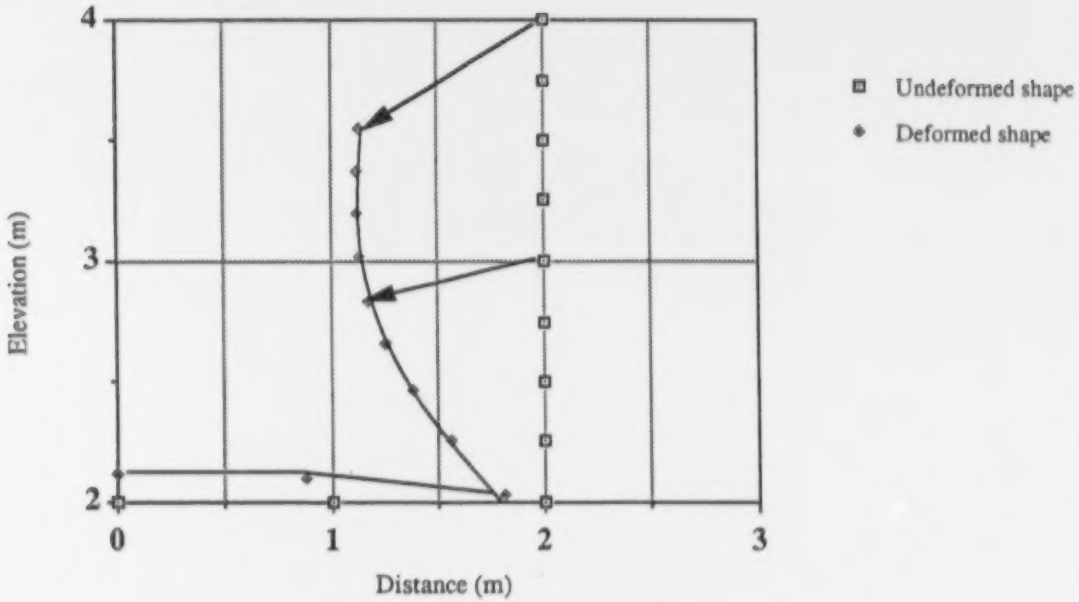

Fig. 3.7 Plane strain excavation in elastoplastic soil. Final excavation induced displacements on the excavation boundary.

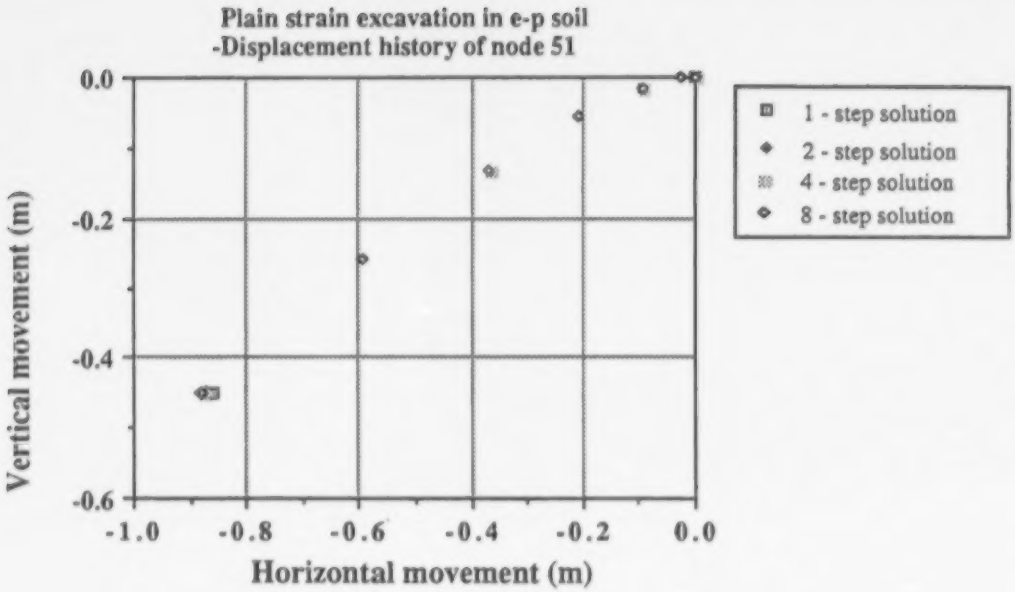

Fig. 3.8 Plane Strain Excavation of Elastoplastic Soil: Displacement History of node A obtained from One-, two-, four- and eight- step analyses.

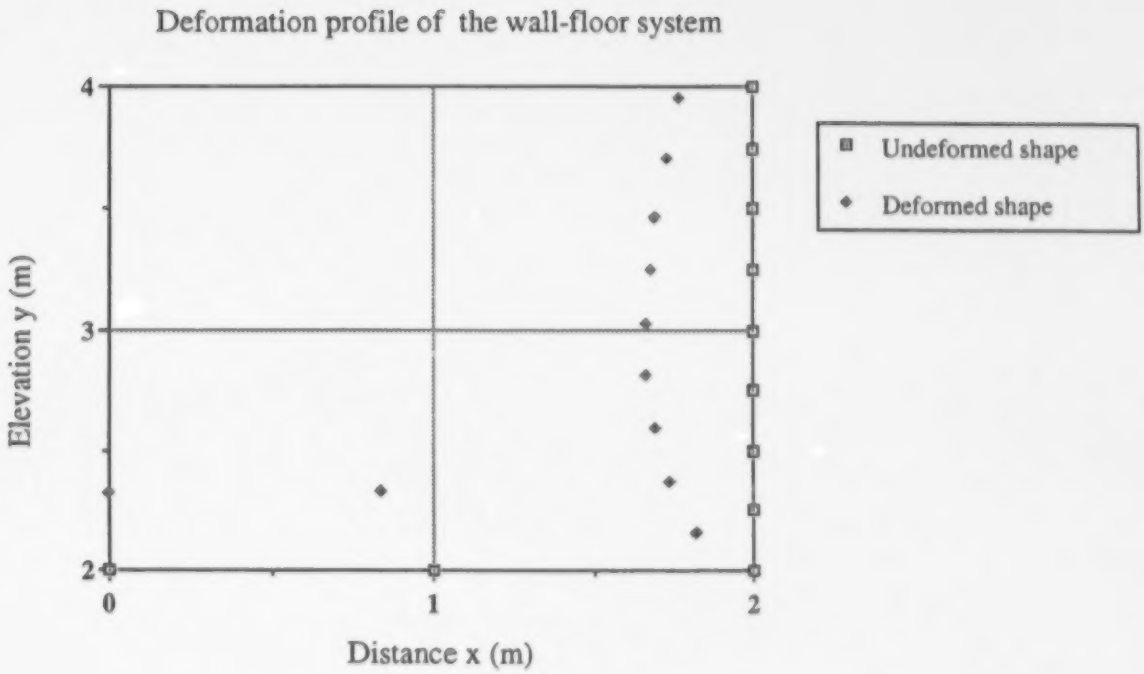

Fig. 3.9 Axisymmetric Excavation in Elastoplastic Soil : Final Excavation - induced Displacements along the final excavation boundary.

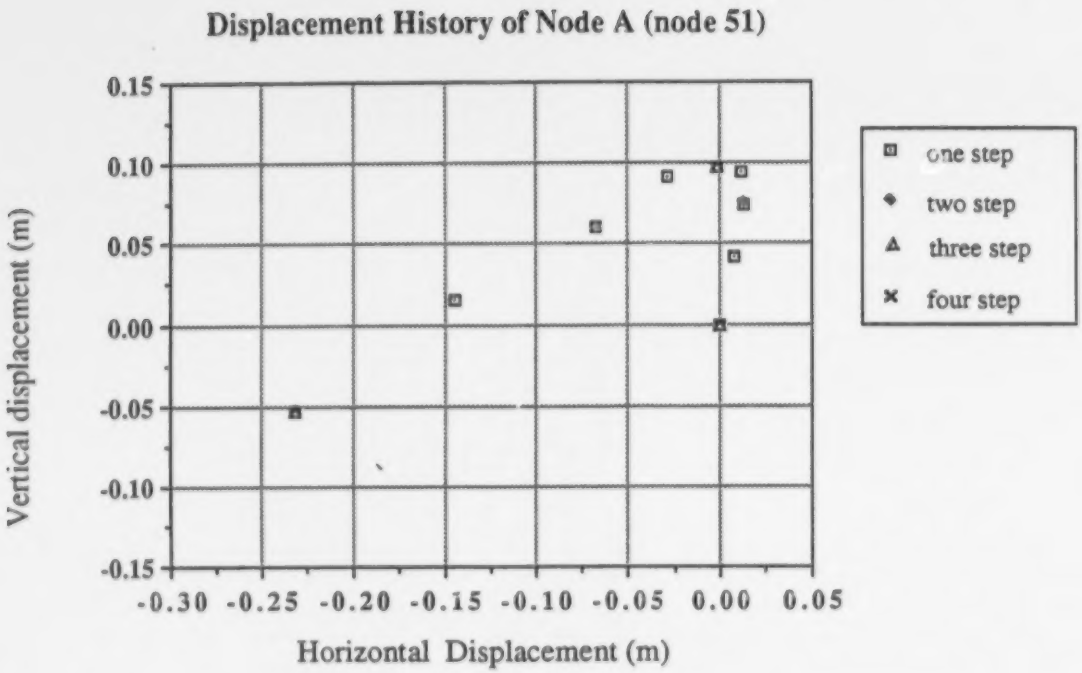

Fig. 3.10 Axisymmetric Excavation of Elastoplastic Soil : Displacement History of node A obtained from One-, two-, four- and eight- step analyses.

CHAPTER 4

THE SAXON CLAY PIT

4.1 INTRODUCTION

The behaviour of the ground surrounding a 29 m deep open-pit in overconsolidated Oxford Clay has been extensively studied by Burland et al. (1977) as it was progressively excavated. The Saxon Clay Pit is operated by the London Brick Company at Whittlesey near Peterborough, UK. The excavation process is carried out by a mobile continuous-face planer, that excavates the overconsolidated clay shale in a 25 meter high face at a slope of 72^{o}. The planer moved parallel to the wall, removing 10m to 15m from the face, completing a full transverse of the face in 3 to 6 months. Fig. 4. 1 is a plan view of the studied pit wall, showing successive faces of excavation.

4.2. GEOLOGICAL CONDITIONS

Fig. 4. 2 is a cross section of the working face, and also shows a geological profile. The mineable clay shale is overlain by 3 to 6 meters of surficial deposits, collectively termed "callow". The callow consists of peat, sandy gravel, and completely

weathered clay shale (Oxford clay), and was periodically stripped for some distance away from the pit wall.

Underneath the callow the Oxford Clay consists of 8 to 10 m of Middle Oxford Clay overlying 17 m of Lower Oxford Clay. The Middle Oxford Clay is moderately weathered at the top, with frequent brown stained fissures, and a homogeneous mass appearance. Lower down, however, it is much less fissured and weathered and more blocky in appearance. According to Fig. 4. 2 (Burland et al., 1977), the Middle Oxford Clay is characterized as a grey-green, calcareous plastic clay. The Lower Oxford Clay consists of two distinct lithological types: dark brown-grey highly bituminous strongly laminated shale predominates near the base of the face and interbeds of paler green-grey blocky clay.

The underlying strata, as revealed in excavated drainage trenches in the base of the pit, are comprised of 3.2 m. of green-grey dense clayey silt and fine sand, locally cemented for the top 0.6 m., termed the Kellaways Sand (and "Rock"); 2.1 m. of dark blue-grey plastic Kellaways Clay; 2.5 m. of massive biolithic limestone; and then alternating clays, limestones and sands in a thick sequence. The minimum estimated depth of burial of the Oxford Clay is about 330 meters.

4.3. OXFORD CLAY STRUCTURE AND FABRIC

An extensive study of the spacing and orientation of the structural discontinuities revealed the following: The most obvious structural features at Saxon pit are near-vertical major joints, often extending laterally for hundreds of meters, which are seen to intersect the Oxford Clay face in inclined lines and curves. There are two orthogonal sets

of joints, of 100 meters or more lateral extent, forming near-parallel 5 to 20 meters spacings. One set is approximately parallel to the face and the other approximately perpendicular to the face as indicated in Fig. 4. 1. The second set of joints tend to remain closed, whereas joints in the first set intersect the working face at low angles and are preferentialy opened up by stress release, thus appearing more prominent. Both sets are best seen in the shaley Lower Oxford Clay and they appear to die out upwards in the Middle Oxford Clay.

On a smaller scale the Oxford Clay has a fissured fabric typical of most over-consolidated clays: a blocky fissure fabric ranging from 10 to 300 millimeters in spacing is displayed.

4.4. GEOTECHNICAL PROPERTIES

The unit weight of the clay was approximately constant with depth, averaging 19.9 kN/m ^{3}. Average Liquid and Plastic Limits were 55% and 24% respectively, while the clay content is typically greater than 55%, denoting a highly plastic clay and clay shale. The Middle Oxford Clay may be further classified as a "stiff" clay on the grounds of strength (Skempton and Hutchinson, 1969), while the more strongly laminated Lower Oxford Clay is termed a "clay-shale" from consideration of both strength and soil fabric. The average calcium carbonate content was 10% to 20%, which is high and which probably caused local cementing. The variation with depth of the geotechnical properties of the Oxford Clay and Kellaways Beds is shown in Fig. 4. 3. With depth, moisture contents plot consistently below the Plastic Limits, implying that brittle behaviour could be expected.

The laboratory undrained shear strength values range from 50 kPa to more than 1200 kPa with depth. The strengths were found to be strongly anisotropic, typically having a ratio of 1.7 between horizontally and vertically oriented specimens. The ratio E_u / C_u shows no net increase with depth and averages about 100. Lab tests gave vertical Young's moduli averaging about 100 MPa, and the horizontal Young's modulus were generally higher by a factor of two. Therefore, a value of 200 MPa was thought to be representative for the horizontal Young's modulus.

The effective strength parameters determined from triaxial tests are very scattered and no consistent trend is evident. Average peak parameters are $\phi' = 28^o$ and $c' = 80$ kN/m^2. Shear box tests on intact specimens of Lower Oxford Clay from near the base of the face, sheared parallel to the bedding, gave peak parameters of $c_p' = 172$ kN/m^2 and $\phi'_p = 27.5^o$ and residual shear parameters of $c'_r = 3.5$ kN/m^2 and $\phi'_r = 13^0$. Fig. 4.4 illustrates that typical shear stress / displacement curves were very sharp and strengths dropped to near residual after only 3 to 4 mm of shearing displacement. Tests carried out on specimens containing a prominent bedding plane on which shearing was known to have occurred in the field indicate that the shear strength on the in situ plane is near and possibly identical to residual. (Burland et al, 1977)

Sampling of the Kellaways beds proved difficult and testing indicated substantial disturbance. Therefore, little reliable data was available for these materials.

4.5. INSTRUMENTATION

A variety of instrumentation and measurement techniques were employed to measure ground movement and groundwater pressure.

Piezometers: Casagrande-type standpipes were installed. Groundwater pressures dropped as the excavated face approached the piezometers. Significantly, the lower piezometers recorded the lowest water levels. This could have been due to pressure drops associated with dilatant shearing in the basal shearzone. However, it may also have been due to downward flow into the more permeable basal Kellaways Sand, which was exposed in drainage ditches in the floor of the pit. Interpolation of the piezometric measurements was difficult because of the highly anisotropic initial fabric, and subsequent stress relief and drainage.

Precise surveying: This was used to control surface movement points, mapping, and photogrammetry. A grid of surface movement points was monitored throughout the study. Reference pillars were installed in the base of the pit, and were affected by sudden, uncontrolled basal heaving due to groundwater pressure in the underlying aquifer. Wherever possible, subsequent measurements were corrected for this occurrence.

Photogrammetry: The positions of the face, and of major joints, were recorded by a series of eight photogrammetric surveys.

Horizontal Extensometers: A horizontal multiple point extensometer was installed on the upper surface of the clay behind the wall, to measure surface strains and to indicate the influence of the major joints on the surface displacements.

Inclinometers: Five vertical inclinometers were installed to measure lateral movements with depth. An overall accuracy of less than 10 mm in 30 meters was achieved. The surface collars were surveyed using the precise survey grid.

Vertical Extensometers: Following early site experience, it was found necessary to measure the distribution of vertical displacements with depth throughout the height of

the face and to a certain depth below it. Two multipoint magnet extensometers with accuracies better than 1 millimeter were installed.

4.5.1 OBSERVED HORIZONTAL MOVEMENTS

The first instruments installed were the horizontal extensometers. Little or no horizontal strain was measured beyond 30 meters from the face, even though significant horizontal displacements were measured. This suggested block movement towards the pit, and some discrete overthrusts were found near the base of the wall, particularly one located 1.6 meters above the base. Micrometer slip gauge measurement points were mounted at eight locations along the overthrust. A typical slip episode (from immediately after passage of the planer until its imminent return) is shown in Fig. 4. 5. Note that the slip movement accelerated when the planer was close to the gauge location. These early measurements indicated that the ground within the region of 1.0 to 1.5 times the wall height was sliding as a block on a horizontal shearzone formed by a series of bedding planes near the pit base. More instrumentation was then installed to study ground behaviour during propagation of the shearzone.

Horizontal movements with depth, as measured by inclinometers, showed that displacement at the base of the excavation was always at least 70% of the surface movement. Some horizontal movement was observed down to 3 meters below pit base level. The inclinometer tubes were kinked near pit base level as the face advanced. Examination of a tube, recovered after the planer had passed, showed kinking to have also developed just below pit base level. After the planer was moved to a new location significant time - dependent movements continued to be observed.

4.5.2. OBSERVED VERTICAL MOVEMENTS

Significant consolidation of the callow was observed as a result of the drawdown of the originally perched upper water table. Time - dependent settlements were observed generally. These appeared to be somewhat of an acceleration of the settlement rate when the planer passed close to a measurement point.

Movements recorded by a vertical extensometer are summarized as a function of the time in Fig. 4. 6. Settlements are seen to decrease with depth until by mid - height of the face they give way to heaving. Thus the entire sliding block underwent increased compression as horizontal movements developed. Base heave amounted to just over 100 millimeters in two years, during which the face was cut back 60 meters.

4.5.3 OVERALL DISPLACEMENT PATTERN

Summary surface displacements at points on the top of the moving block are shown in Fig. 4. 7. Typical displacement trajectories as a function of distance from the face are shown in Fig. 4. 8. Some influence of the callow was noted from the measurements. When the current excavated face was located close to the callow (that is, prior to another cycle of stripping) extra movement was noted, presumably as a result of the extra wall height.

4.5.4 INFERRED SHEAR ZONE PROPAGATION

By understanding the excavation to be a quasi - continuously advancing face, a model for the observed behaviour was developed as shown in Fig. 4. 9. As the face

approached a given surface point, the tensile strain at first increased slowly. A sudden increase in tensile strain, with the face between 20 and 30 meters away, was inferred to mark the *end - region* of the shearzone. Following this, nonextensional block glide occured.

In conclusion, some stick - slip shearzone movements were also interpreted. Although the overall mechanism of movement was clearly identified, the propagation of the shearzone was inferred to be sensitive to such matters as local variations in strength, drainage conditions, presence of major joints, and rate of face excavation.

4.6 FINITE ELEMENT ANALYSIS PROCEDURES

In principle, the objectives of the simulation of excavation behaviour was to examine the displacement, strain and stress pattern in order to evaluate the hypothesis that only residual sliding occurred. During the original site investigation, the possibility that only residual strength was mobilized in the field was not precluded. The very high estimated OCR for the Oxford Clay deposit at the site (Burland et al, 1977), suggests that insitu preshearing could have developed by flexural slip during stress relief. (Morgenstern, 1991). Detailed deformation analysis is required to address the question of progressive failure, since the deformation pattern must yield parameters compatible with field deformation measurements.

A number of non-routine matters had to be considered in designing and carrying out the finite element analysis.

These included :

1. Overall dimensions of mesh
2. Simulation of excavation procedures
3. Selection of material models and parameters
4. Selection of shearband thickness
5. Mesh detailing in the critically stressed and deforming notch region

Overall dimensions of the mesh

The idealized 72° sloping wall shown in Fig. 4. 10 was adopted for the finite element analysis. With a 27 meters high face, and a shearband with stress concentrations possibly extending 40 to 60 meters behind the face, lateral and bottom mesh boundaries had to be chosen to minimize any effects of boundary constraints. Distances from the face to the left (excavated) and right boundaries of 200 m and 400 m respectively and a depth of 194 m from the bottom of the pit were chosen. These dimensions satisfy the requirements proposed by Lee et al. 1978, as minimum dimensions to avoid boundary effects.

4.6.1 SIMULATION OF EXCAVATION PROCEDURES

It is standard practice in simulation of excavations to simulate an initial Ko stress distribution before the excavated material is removed. This is simply done by selecting an appropriate value of the Poisson's ratio in the switch on gravity step of the analysis. The simulation of removing the excavated elements was performed by adopting the algorithm proposed by Ghaboussi and Pecknold (1985). The simulation of the floor-wall system, before the incremental excavation of the wall, was performed in 12 steps. This created a pit wall isolated from boundary effects, and subjected to an appropriate stress

field corresponding to a history of erosion and small excavation steps. In the following six steps, a 10 meter section of the wall was removed in each step using the same procedure, in order to study the incremental and final displacement and stress fields resulting from a typical pass of the planner. Selection of these stages had an important influence on the mesh discretization close to the wall.

4.6.2 SELECTION OF MATERIAL MODELS AND PARAMETERS

A reliably convergent elastoplastic analysis could be carried out for a strain weakening, strain hardening or perfectly plastic material. Prior to performing the elastoplastic analyses, a series of elastic analyses had to be undertaken to study the nature and extent of the stress concentration at the notch, the deformation pattern of the floor-wall system as well as the possible extent of any tensile zone. To realistically simulate base stiffness without introducing noticeable material-contrast effects into the results, the shearband and overlying Oxford Clay were assigned elastic stiffnesses three times less than the basal material.

4.6.3 SELECTION OF SHEARBAND THICKNESS

The observed shearzone consisted of a series of discrete sliding surfaces, extending from 0.5 to 1.5 meter above the pit base. Discrete sliding surfaces possibly also developed in the hard Kellaway clay (below the pit base level), but this is not very well documented from the field measurements. The finite element shearband consisted of a single layer of 8-node isoparametric quadrilateral elements whose lower surface

coincided with pit base level. A uniform thickness of 1.0 meter was selected for this layer, as an average value from the field observation.

4.6.4 MESH DETAILING NEAR THE NOTCH

Due to the unloading process, intense stress concentration is expected in the vicinity of the current wall face and along the shear band. Therefore that part of the mesh was finely discretized to capture details of the stress, strain and displacement response of the soil mass resulting from each excavation step.

4.6.5 MESH SUMMARY

The final mesh design is shown in Fig. 4. 11. A total of 1877 nodes and 588 elements were used to represent the whole domain, while 1508 nodes and 471 elements remain after the simulation of the floor- wall system before the first pass of the planer. After each pass of the planer (10 meter cut of the wall), 18 elements and 54 nodes were removed. At the final stage of the simulation, i.e after cutting 60 m of the wall, 363 elements and 1202 nodes were present. The elements below the pit base level have elastic stiffnesses three times that of the shearband and wall elements.

4.7 SIMULATION OF EXCAVATION BEHAVIOUR

To obtain solutions for each of the excavation stages proved to be very costly in terms of computation time, when it was first attempted. The implementation of the excavation algorithm proposed by Ghaboussi and Pecknold (1985) but mostly the adoption of the return family of algorithms to evaluate stresses, reduced the computation time by up to ten times in the latest steps of the analysis. Also, a convergent solution

was always possible to obtain and that was a breakthrough in the modelling effort, in the light of the difficulties encountered in the late steps of the analysis, when the excavation was attempted in a high Ko environment.

The sensitivity of the solution to initial ground stress conditions was investigated. Therefore, the analysis was carried out for Ko values of 0.666, 0.987, 1.25, 1.5, 1.75 and 2.0 and for a range of stress parameters from peak to residual.

A general remark, common to every analysis is that even when yielding commenced, the convergence rate of the solution was exponentially asymptotic. This is a major improvement from the technique used by Simmons (1981), i.e reducing the stiffness parameters of the yielded elements in order to obtain a convergent solution.

4.7.1 MATERIAL PROPERTIES

The domain to be analyzed was divided into four material zones. It can be deduced from the field data that minimal movement was observed below the pit level and therefore this material can be assumed to behave in a linear elastic manner (Zone 1, elev. +0.0 to +193.0 m.). The shearband material (Zone 2-elev. +193.0 to +194.0 m.), was assumed to behave as a strain softening material, according to the results of a series of direct shear tests from intact samples close to the face of the wall and just above the base level. It was also assumed that the Drucker-Prager failure criterion with a non associated flow rule can describe the constitutive behaviour of this layer. The Lower Oxford Clay (Zone 3- elev. +194.0 to +212.0 m) as well as the Middle Oxford Clay (Zone 4-elev. +212.0 to +220.0 m.), were assumed to behave as a strain softening material with the same shear strength parameters as the Zone 2 material. The Lower

Oxford Clay was assigned a Young's modulus of 120 MPa, twice as much of the Middle Oxford Clay (60 MPa), as a result of the Young's modulus profile with depth reported by Burland et al (1977). A series of elastoplastic analyses were carried out and the sensitivity of the solution to the insitu stress field (K_o) and to the shear strength parameters of the shearband material as well as the ability to match the observed field behaviour was investigated. Note that through all the above runs, the material properties of Zones 1, 3 and 4 were assumed constant.

4.7.2 ELASTOPLASTIC ANALYSIS I

In this group of runs, the hypothesis that peak shear strength was mobilized along Zone 2 was tested. Therefore, the properties assigned to the shear band material were:

Peak strength $f'_p = 27.5^o$ and $c'_p = 172$ kN/m^2

Residual strength $f'_r = 13^o$ and $c'_r = 3.5$ kN/m^2

Since the insitu horizontal stresses were high, the analyses were run for values of K_o of 1.5 and 2.0. In run IA, the above strength parameters were assigned to Zone 2 with an insitu stress field corresponding to a value of Ko=1.5 and in run IB, the insitu stress field was corresponding to a value of Ko=2.0.

Surprisingly enough, after excavation of 60 m from the face of the wall, no yielding along Zone 2 occurred. Only some minor tensile yielding was observed in Zone 4, 5 to 10 m behind the face on top of the slope. Also, the deformation of the wall - floor system was much less than what was observed in the field (~45 to 30% depending on the value of Ko). These two runs showed that if the material properties reported by Burland et al (1977) are correct, no yielding resulting from stress relief due to excavation can occur along the Zone 2 material (base of the pit). Therefore, since in these cases only peak shear strength was mobilized, progressive failure could not have occurred.

4.7.3 ELASTOPLASTIC ANALYSIS II

In this phase of the analysis, a number of runs were carried out for various combinations of Ko and material properties for Zone 2. Ko values of 1.0, 1.5, 1.75, 2.0, 2.25 and 2.5 were tested in combination with values of f'_r from 13° to 16° and values of c'_r from 3.5 to 20 kPa. For combinations of Ko=2.25 and 2.5 and values of the residual strength parameters in the lower range of the spectrum, general failure occurred after excavating only 10 to 20 m from the face of the wall. For combinations that general-premature failure was not occurring, the yielding was extending only along part of the weak clay layer. Some of those runs were characterized as unsuccesful either because the length of the yielded part of the Zone 2 material was too short (less than 30 m) or too long (more than 70 m), or because the magnitude of the deformation of the wall-floor system was either smaller or larger than that observed in the field or because a combination of the above was occurring. Obviously, short lengths of the yielded part of the clay layer were associated with low values of Ko (usually less than 1.50) and values of the residual strength parameters in the higher range of the investigating spectrum. Long lengths of the yielded part of the clay layer were associated with high values of Ko (usually greater than 2.0) and values of the residual strength parameters in the lower range of the investigating spectrum.

After numerous runs, the set of parameters that gave the best fit to the observed displacements and in the observed yielded part of the material along Zone 2 was:

$$c'_r=15 \text{ kPa}, \quad f'_r = 15^{\circ} \quad \text{and} \quad Ko=2.0.$$

In Fig. 4. 12, the horizontal displacements along the clay layer versus the distance from the advancing excavation face is plotted. Superimposed are the results of the finite element analysis for values of E for the Lower Oxford Clay of 120 and 150 MPa. Very

good overall matching was achieved between the calculated displacements for E=150 MPa and the recorded movements by inclinometers I3 and I4. The agreement is especially remarkable for the tip- and the tail-end displacements of the shearband as recorded by inclinometer I3. The calculated displacements along the middle portion of the shearband are higher than the recorded ones by an average of 15%. This can be attributed to some "slip-and-stick" action that occurred in the field, which could not be captured by the numerical model. It has to be mentioned though, that the displacements reported as "recorded" from inclinometer I4 from 0 to 15 m distance from the face, are extrapolated values by Burland et al. (1977) of what I4 would have recorded, had the slope-cutting continued to this distance from I4. The analysis also indicated that the lower the value of E for the Lower Oxford Clay (softer material), the higher the calculated horizontal displacements along the shearband.

In Fig. 4. 13, the observed settlement history of some surface points with advanced excavation face were plotted. Superimposed are the results of the finite element analysis for a value of E=120 MPa. The predicted settlement follow the same trend as the observed one, but they are consistently lower than the observed ones by approximately 35%. This is hardly surprising, since the Young's modulus used in the analysis is representative of the horizontal in-situ modulus rather than the vertical one and the material is strongly anisotropic, as reported by Burland et al (1977), with a ratio of $E_h / E_v = 2$ (approximately). Therefore, a value of E lower than 120 MPa would have been representative of the material in the vertical direction and they would have matched better the observed settlement history of the surface points. Results of finite element analyses carried out where E=150 MPa, predicted an even stiffer settlement curve response for the surface points as expected. These results are not superimposed on the observed settlement history curves, just for the clarity of Fig. 4. 13.

This second group of runs showed that in order to match the observed field behaviour, residual strength parameters or values very close to the residual had to be assigned to the Zone 2 material. In other words, the mobilized shear strength in the field along this layer was either residual or reduced close to residual before excavation commenced. That means, that the material along this layer was either presheared or greatly disturbed to a state close to preshearing from an event during the geological history of the area. Considering the glacial geology of the area, such a disturbance can be attributed to glacial drag and rebound that may have occurred 10000 years ago. The hypothesis that the Oxford Clay pit is a classic case of progressive failure was proven unrealistic from the above analysis.

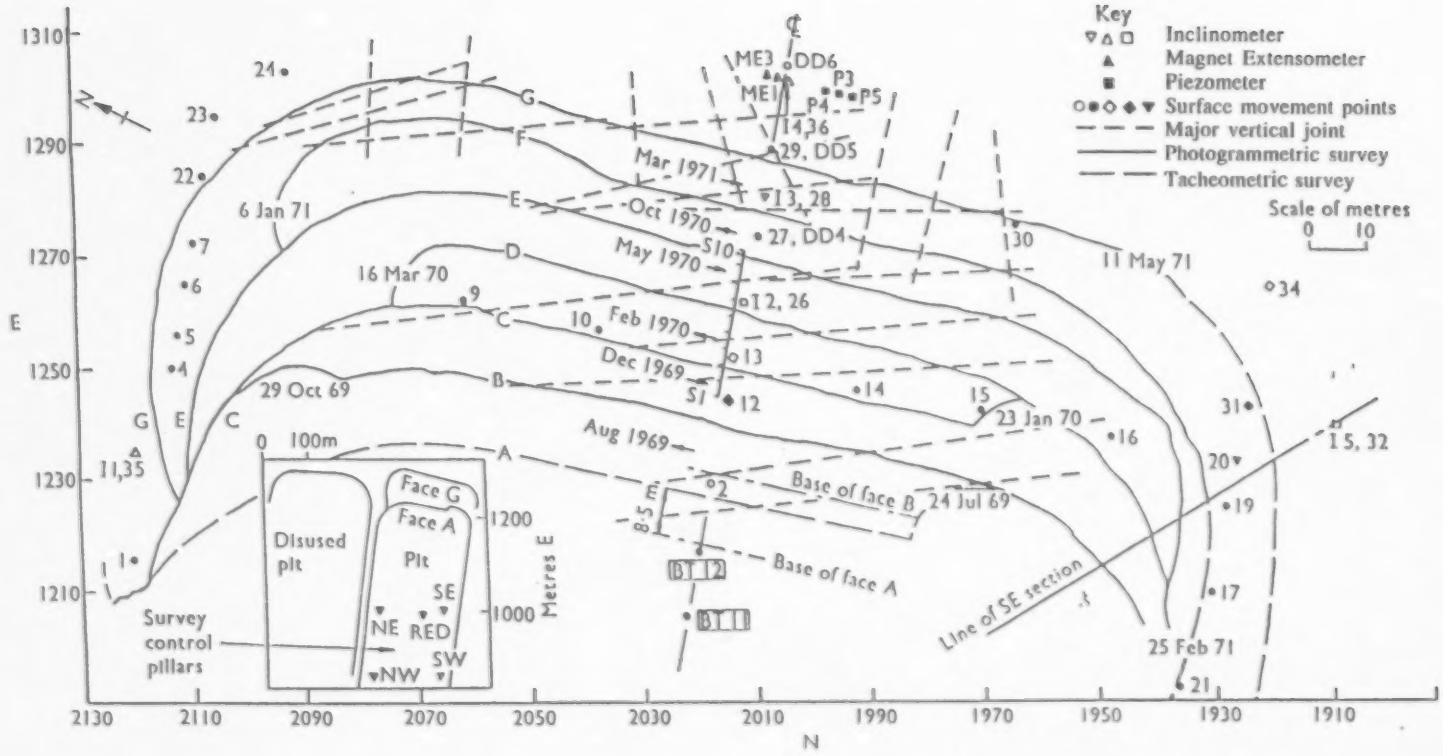

Fig. 4.1 Plan view of the excavation face, Saxon Clay Pit (modified after Burland et al., 1977)

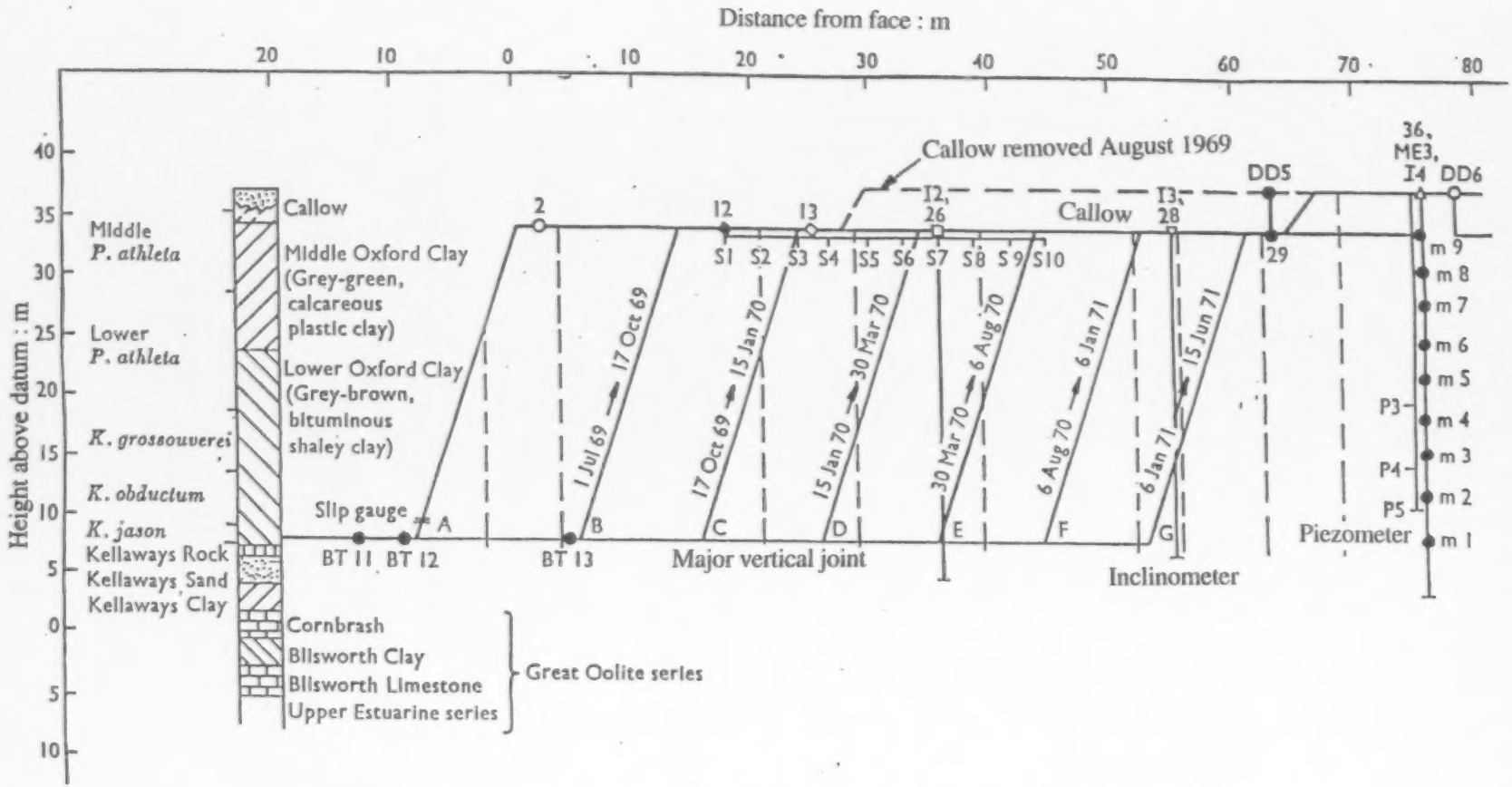

Fig. 4.2 Geology and excavation cross-section (modified after Burland et al., 1977)

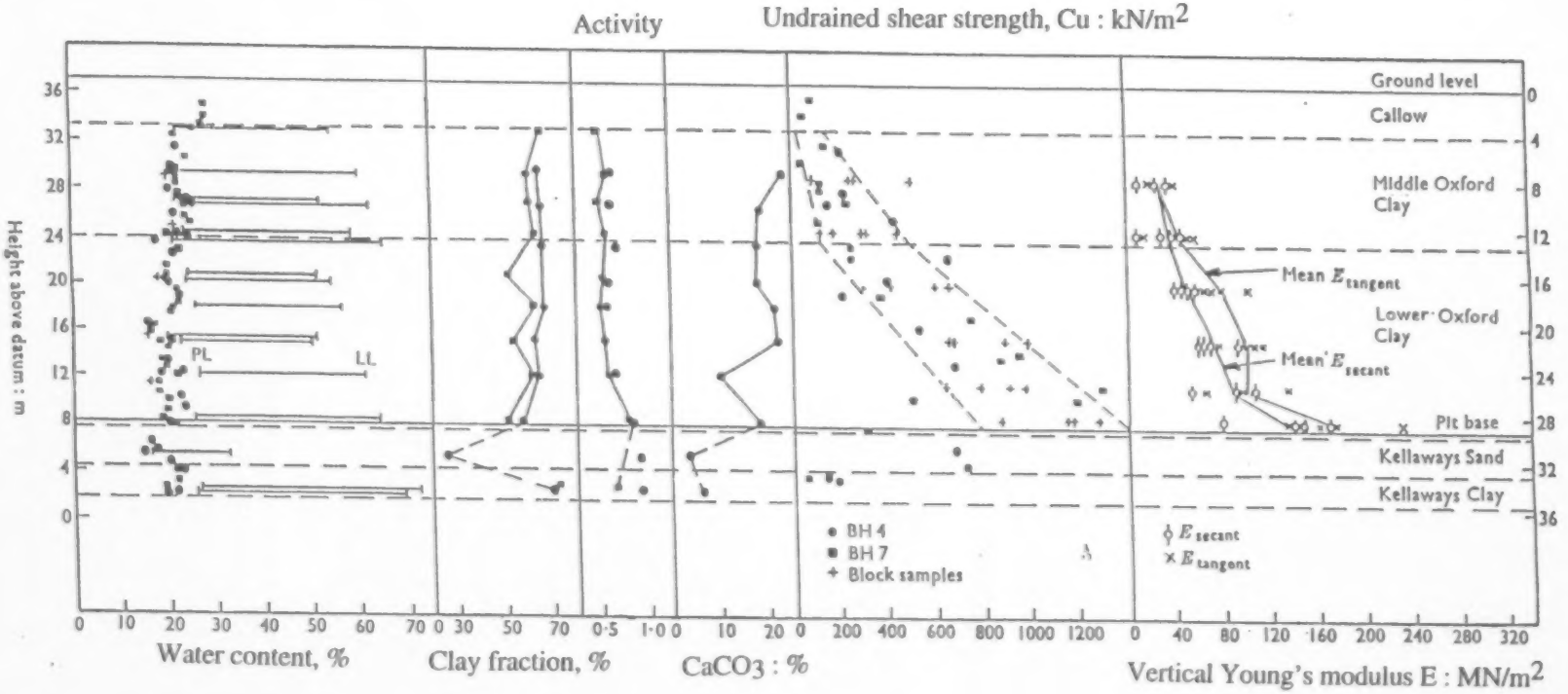

Figure 4.3 Summary of the geotechnical properties (modified after Burland et al., 1977)

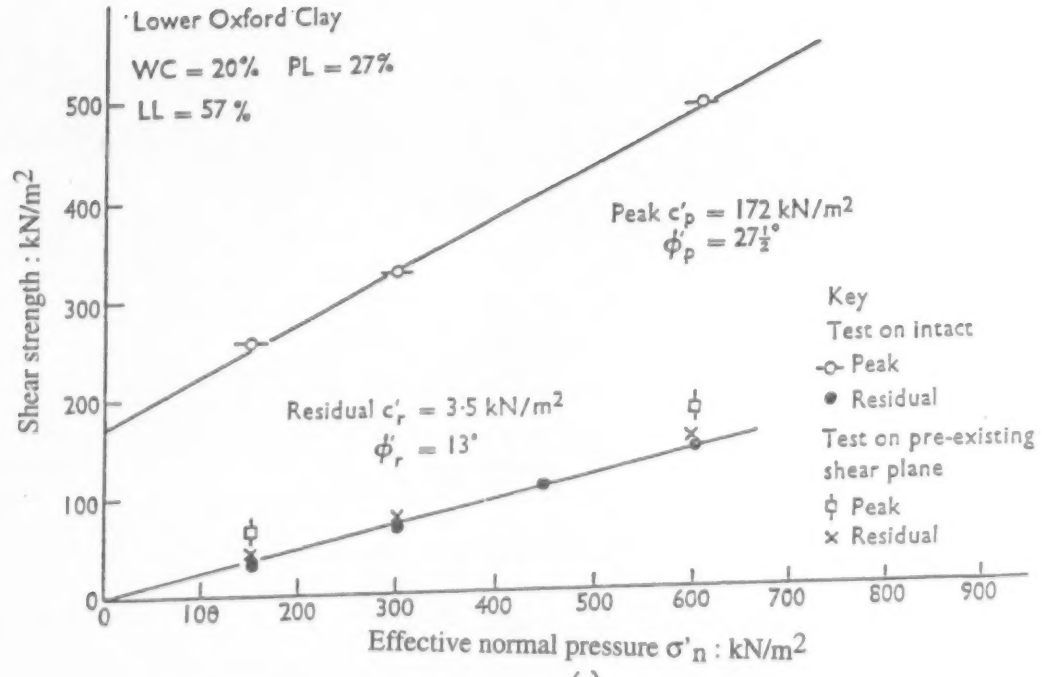

(a)

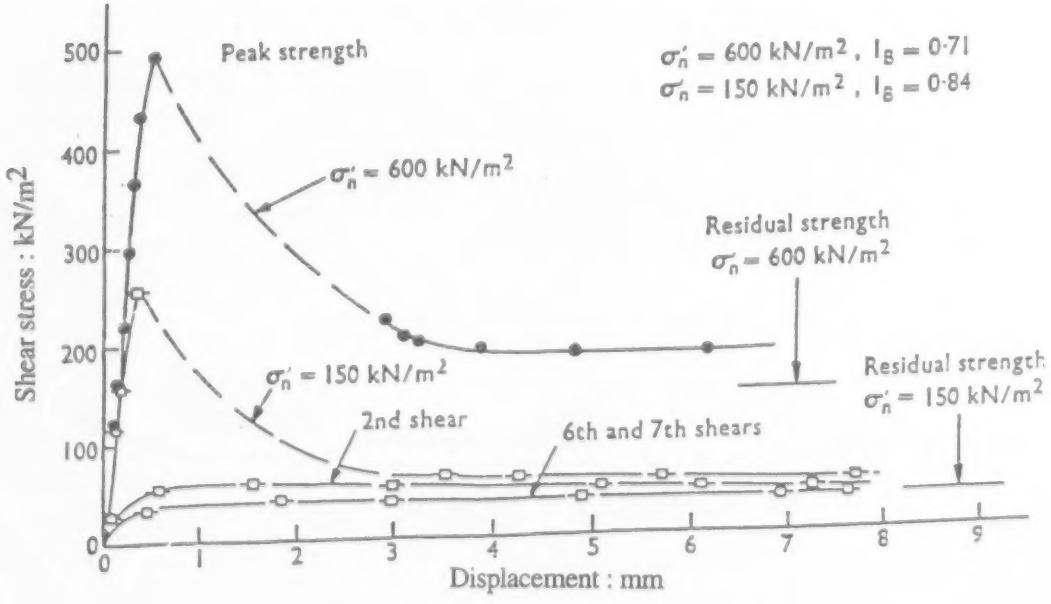

Fig. 4.4 Direct shear test summary data (modified after Burland et al., 1977)

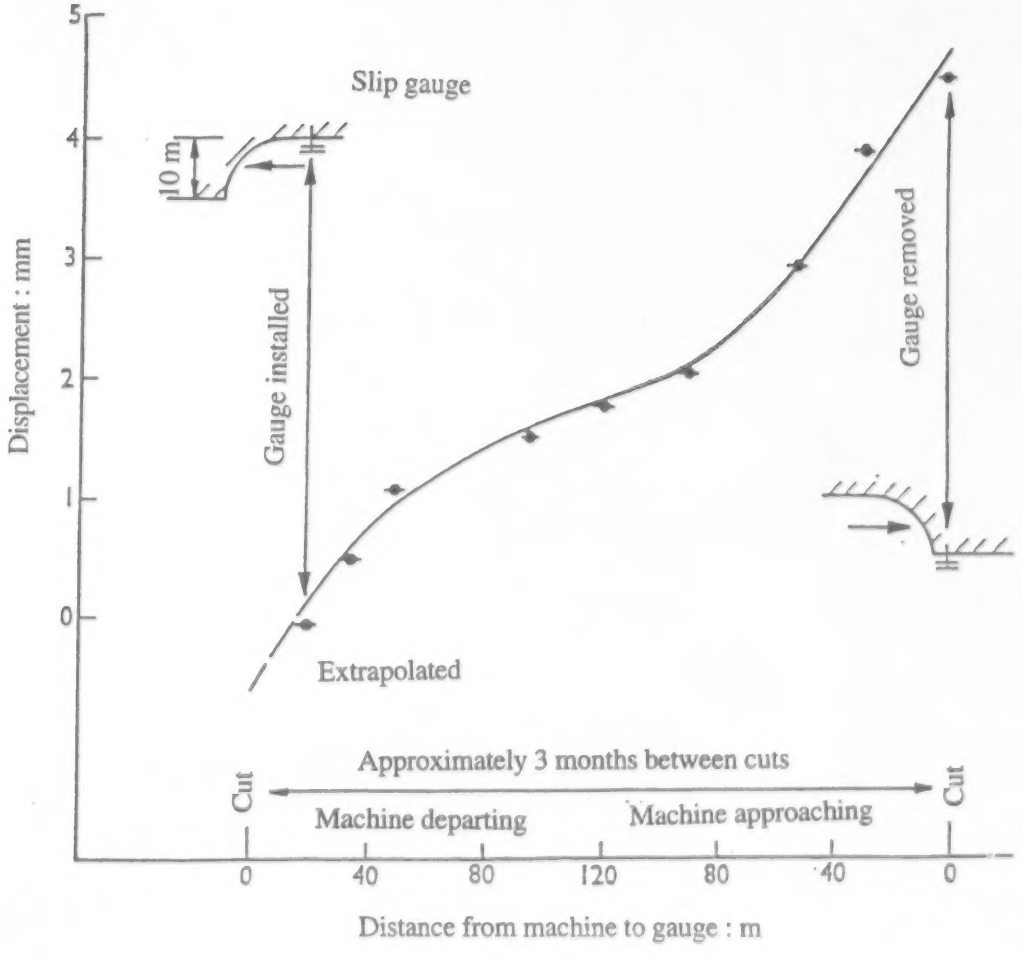

Fig. 4.5 Typical overthrust gauge movements (modified after Burland et al., 1977)

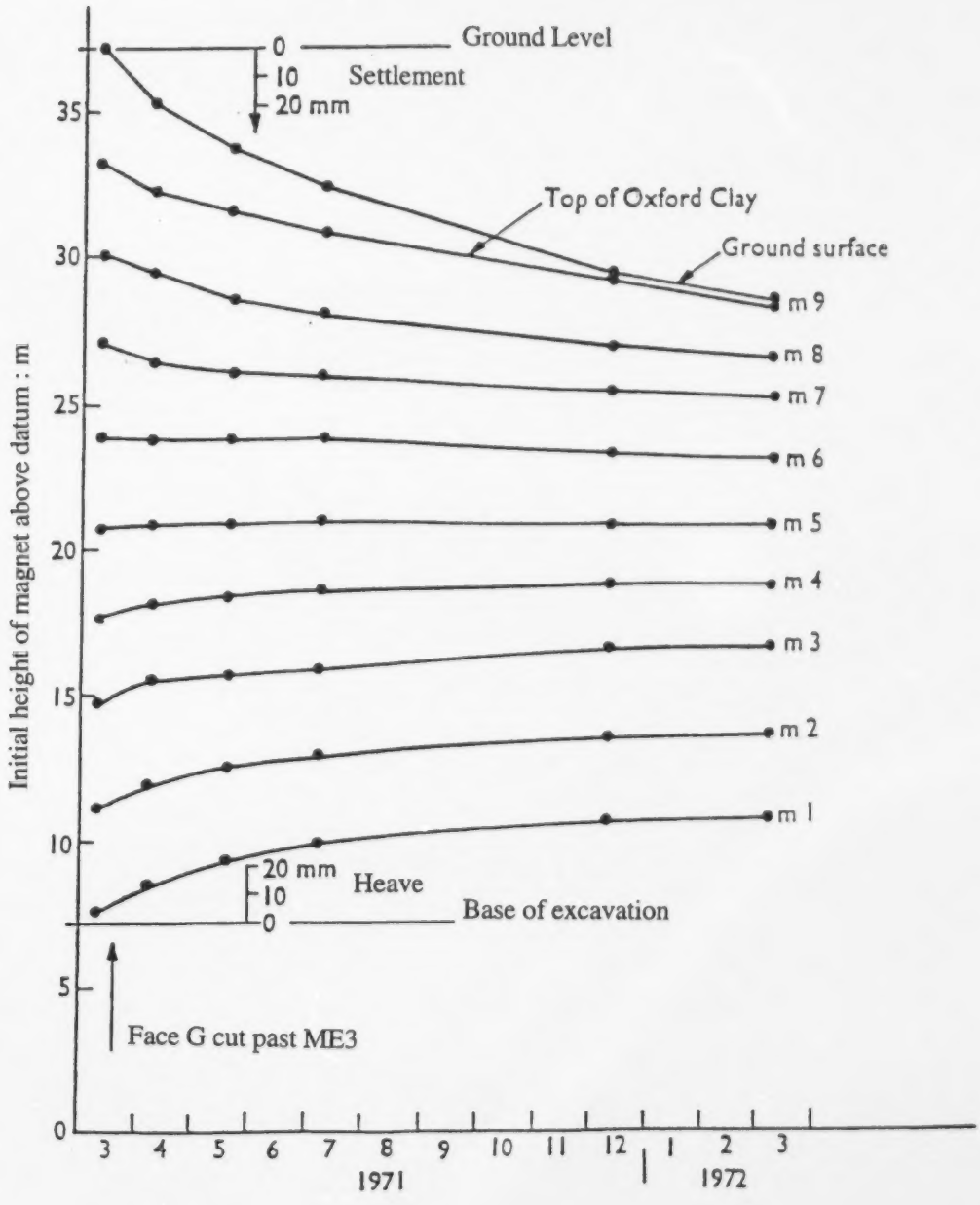

Fig 4.6 Vertical compression pattern variation (modified after Burland et al., 1977)

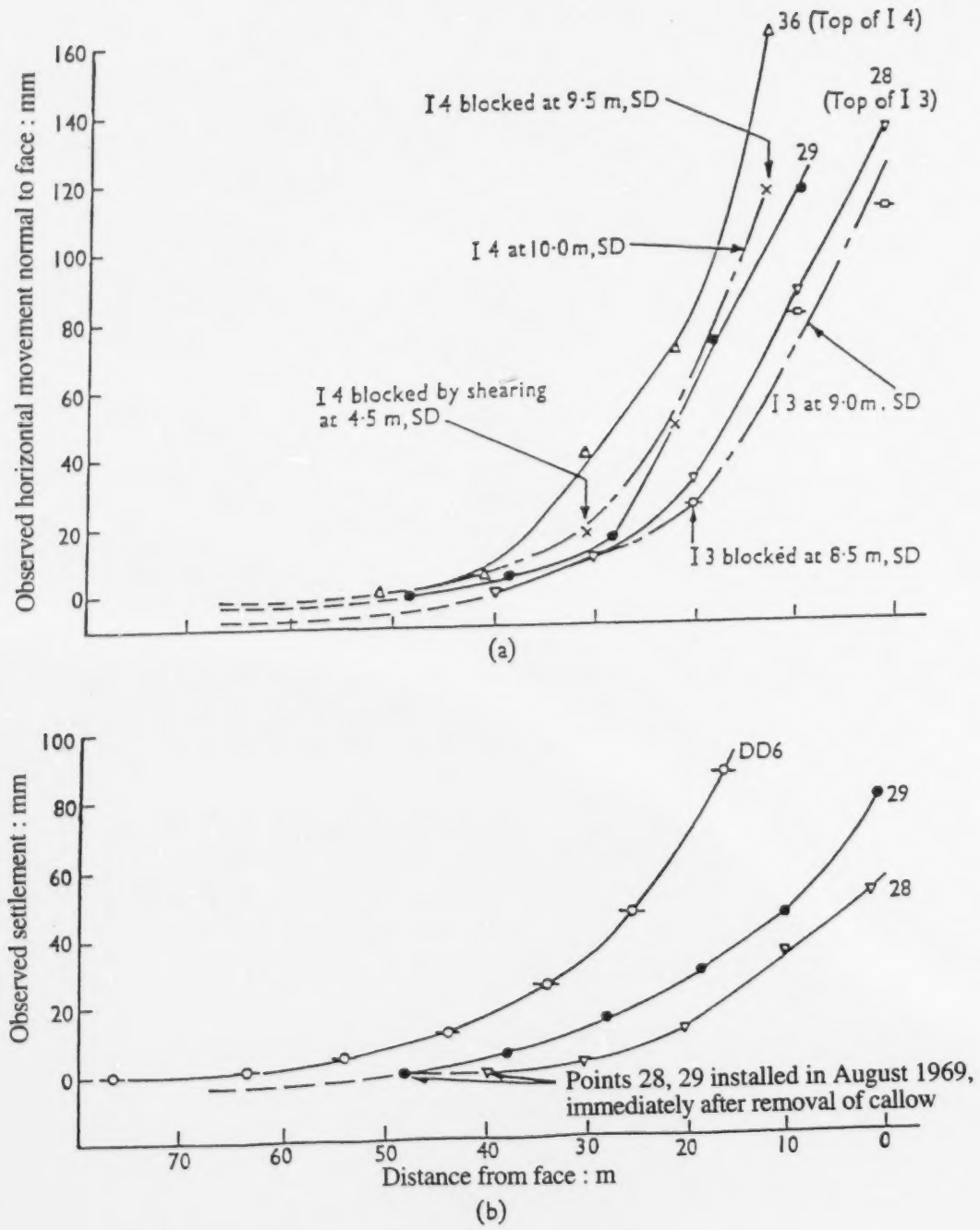

Fig 4.7 Summary of surface displacements (modified after Burland et al., 1977)

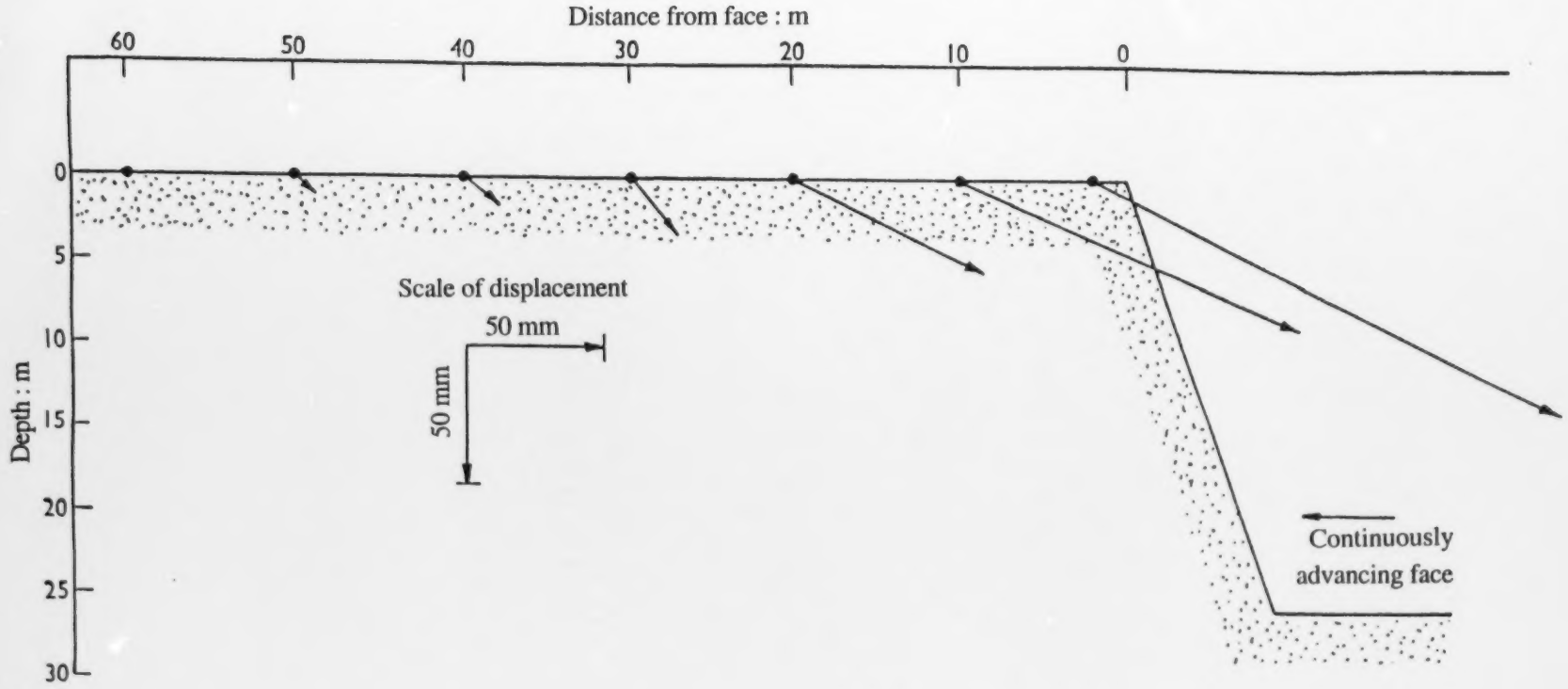

Figure 4.8 Inferred surface displacement trajectories (modified after Burland et al., 1977)

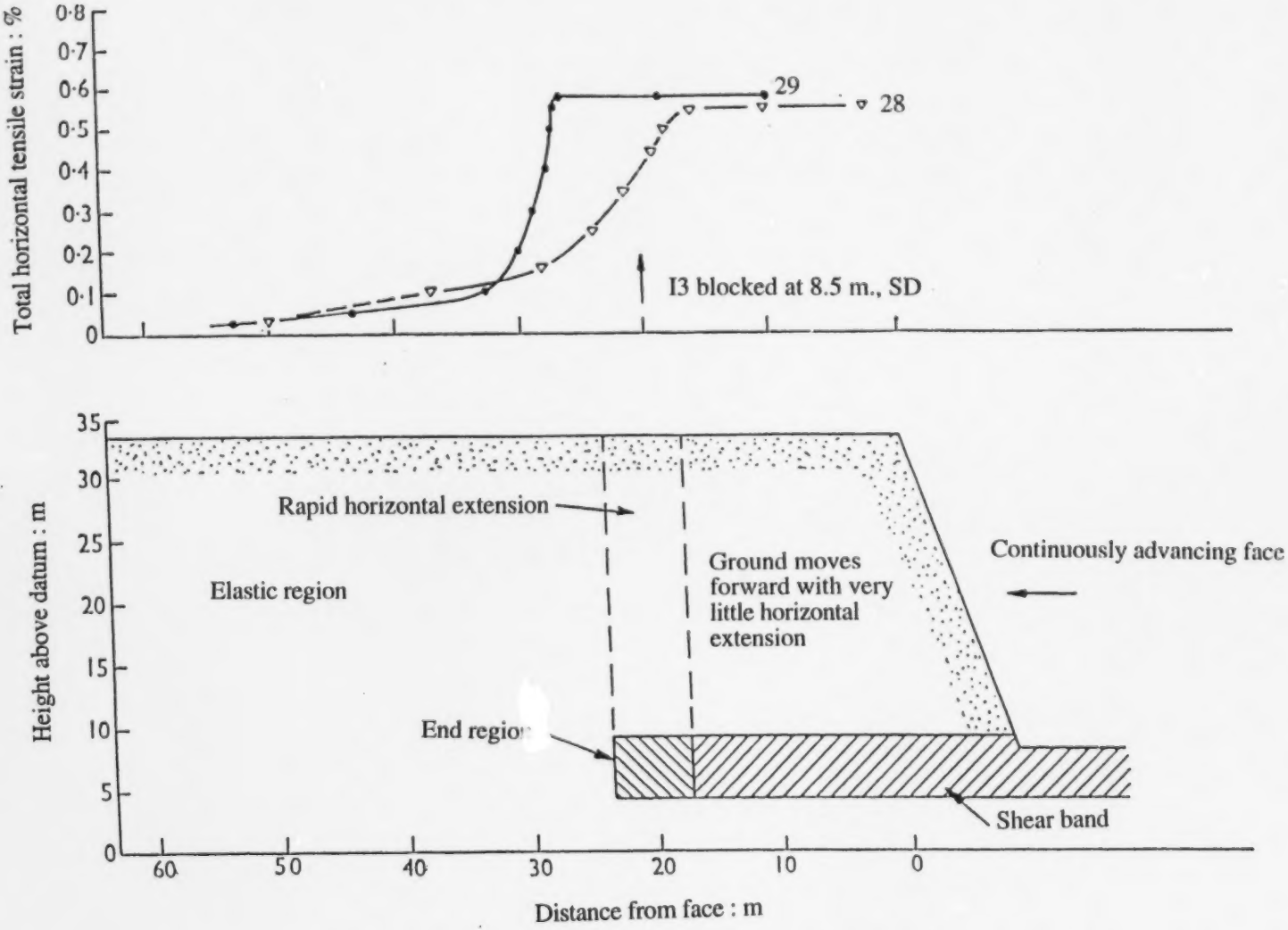

Figure 4.9 Inferred shear band yielding mechanism (modified after Burland et al., 1977)

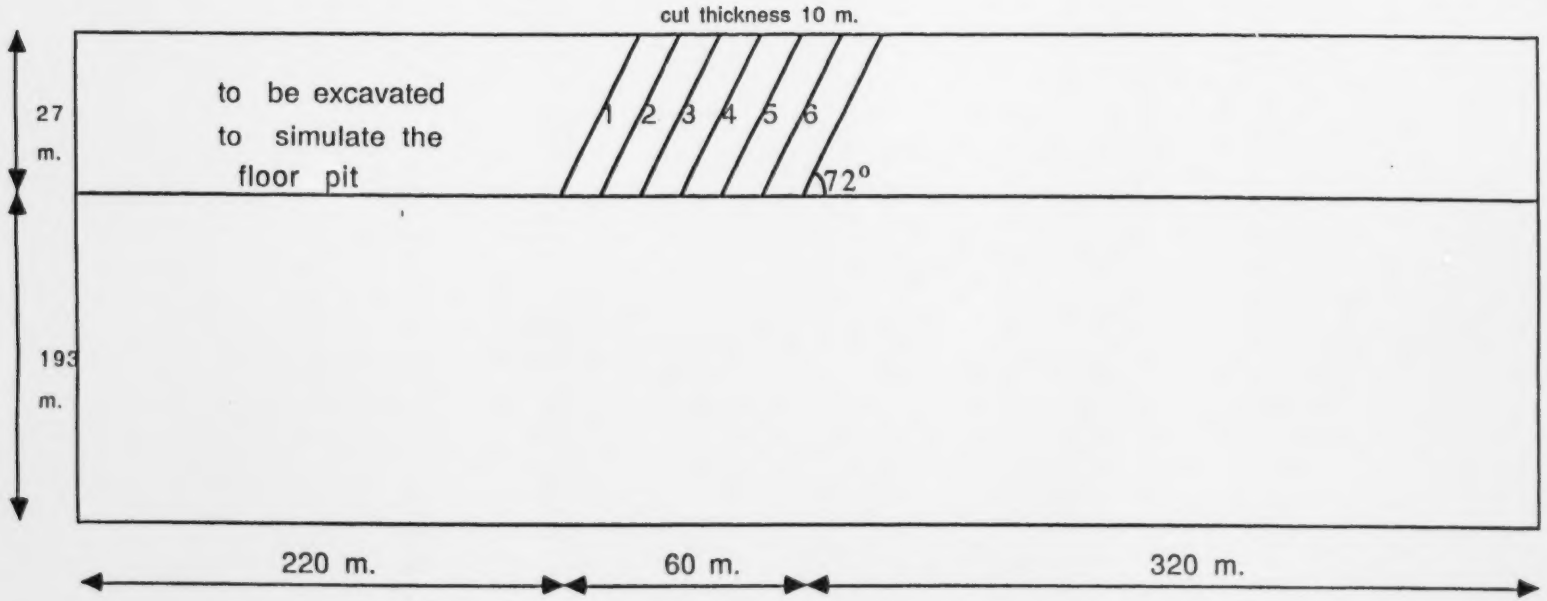

Figure 4.10 Idealized slope for finite element analysis

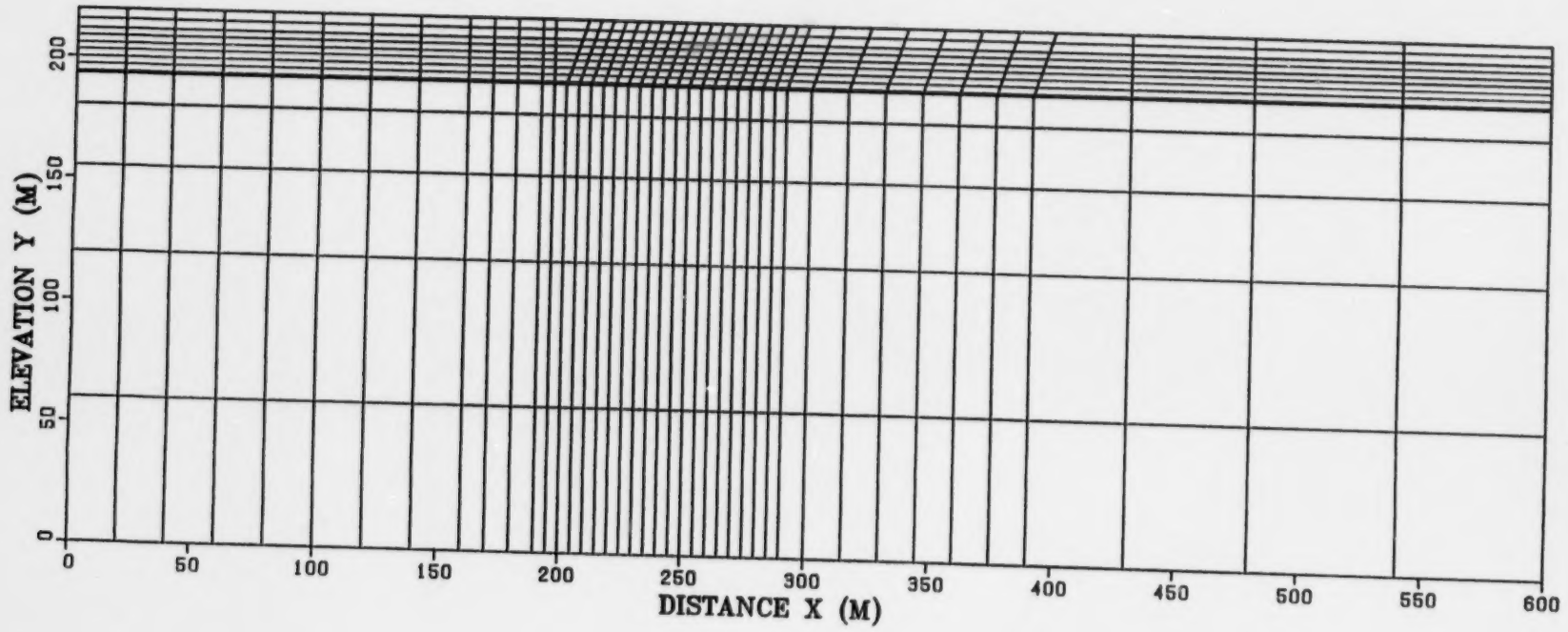

Figure 4.11 Finite element discretization of the idealized domain

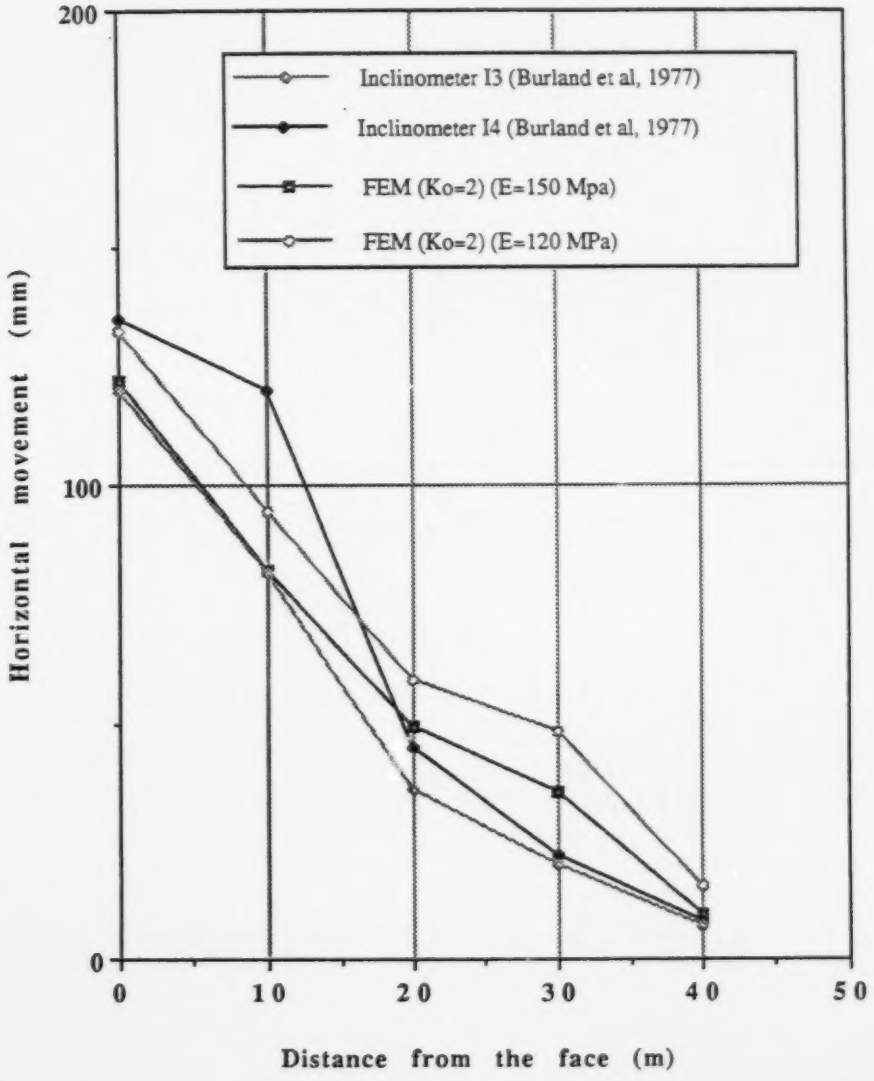

Fig. 4.12 Horizontal displacements of the shear band vs. distance from the advancing excavation face

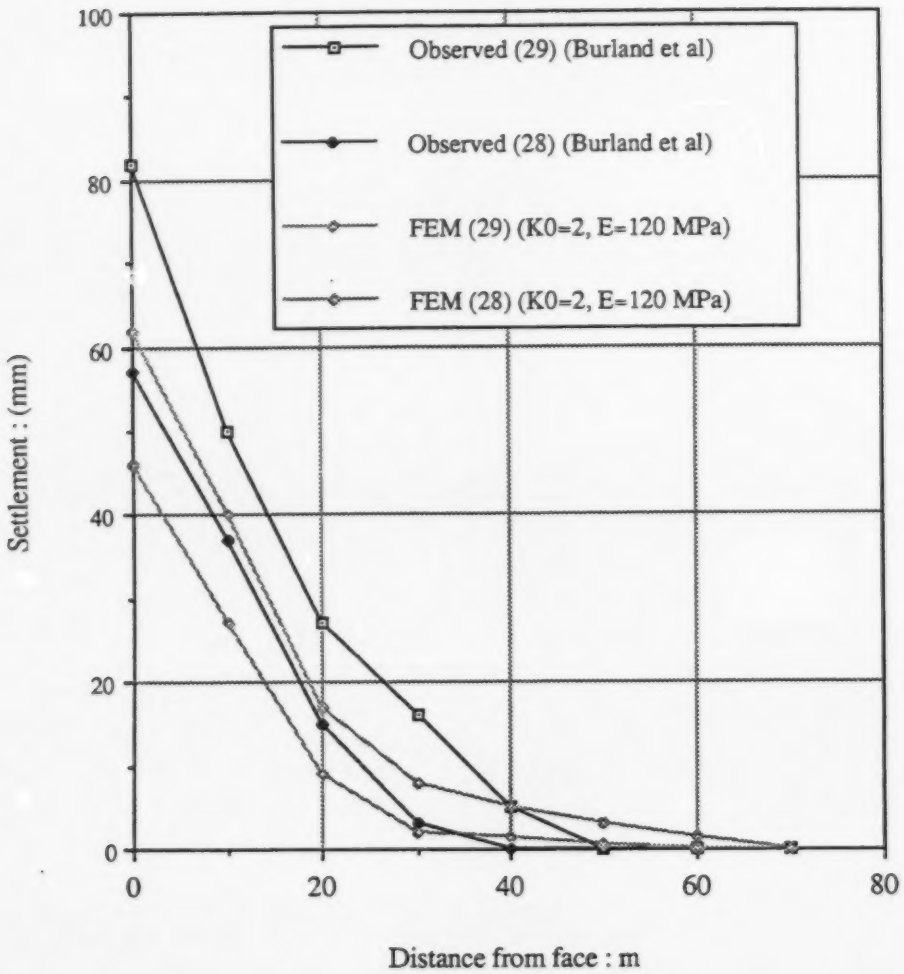

Fig. 4.13 Settlements of surface points on the center line with advancing face

CHAPTER 5

PROGRESSIVE FAILURE ANALYSIS OF WINDROW INDUCED SLOPE MOVEMENTS AT THE SYNCRUDE MINE SITE

5.1 INTRODUCTION

Oil sand mines are among the largest earthmoving operations in the world. A rule of thumb is that it takes approximately 2 tons of oil sand to produce 1 barrel of synthetic crude oil. Adding the handling of tailing material and overburden, the figure reaches 5 tons per barrel produced (Mossop, 1980). Syncrude Canada Limited operates one of the largest open pit mining operations in the world. The mine and plant site are located 40 km north of Fort McMurray in NE Alberta. (Fig. 5.1)

The Syncrude mine produces an average of 160000 m^3 of ore grade oil sand daily (List and McKenna, 1990). The ore is initially exposed by a truck and shovel operation (Fig. 5.2) which removes 15 to 23 m of overburden and then four 70 m^3 draglines

excavate the oil sand from below their operating bench (Fig. 5.3), placing it in a windrow for future handling by bucket wheel reclaimers. The ore is conveyed to the plant site where it yields 165000 barrels of synthetic crude oil daily, which represents approximately 10% of Canada's crude oil production (McKenna and List, 1990).

The oil sand deposits are Early Cretaceous in age, which means that the sands that contain the bitumen were originally laid down about 110 million years ago (Mossop, 1980). Virtually all the reserves are contained within a single continuous reservoir, the Lower Cretaceous McMurray - Wabasca Formation, which was deposited sequentially and conformably in fluvial, estuarine and marine environments. The Base Mine consists primarily of Estuarine sediments. Much of the overlying Marine Sediments have been eroded or are removed during overburden stripping prior to dragline mining. Since 1987, the draglines have advanced into areas where Marine Sediments occur at lower elevation and now constitute approximately 60% of the West Mine operating bench (List and McKenna, 1990).

The presence of Marine Sediments below the operating bench has negatively impacted on the dragline operation in two ways. First, translational failures along thin Marine Clay layers within the Marine Sediments have caused operational delays. Second, the Marine Sands provide poor trafficability and foundation pad performance as evidenced by excessive dragline tub and shoe settlements. The impact of these conditions on the dragline mining operation ranges from limited short-term production restrictions to potential development of highwall failures which may incorporate the dragline.

List and McKenna (1990) present an overview of the behaviour of the Marine Sediments, while McKenna and List (1990) report the impact of the Marine Sediments on Syncrude draglines.

5.2. GEOLOGY OF THE MARINE SEDIMENTS

The geology of the Athabasca Oil Sands has been previously discussed by Mossop (1980). A generalized stratigraphy of the sediments in Syncrude's West Mine is presented in Fig. 5.4 and their depositional geology has been described in detail by List and McKenna (1990). The reservoir rock of the Athabasca deposit, which consists of sands, silts and clays, was deposited in a broad drainage basin that developed on an eroded Devonian limestone surface during an overall inland sea transgression. The McMurray Formation in the Syncrude Mine area has three distinct depositional members: the Lower, Middle and Upper McMurray Members. The McMurray Marine sediments of interest to this study are found in the Upper McMurray member. This member can be further subdivided in two submembers based on depositional environment: estuarine and marine. The Upper McMurray Marine Sediments are further subdivided in three subunits, the Upper, Middle and Lower Shoreface. (Fig. 5.4)

5.3.GEOTECHNICAL PARAMETERS OF MARINE SEDIMENTS

The Marine Sediments are divided into two geotechnical subunits, Marine Sands and Marine Clays. Typical geotechnical properties of these units are summarized by List and McKenna (1990) and are shown in Table T.5.1.

The Marine Sands are composed of dense to very dense, brown, angular sub-horizontally bedded silty sands and generally have low bitumen contents. The Marine Clays are dark gray to black, soft to stiff (typically firm), highly bioturbated silty clays of medium to high plasticity. Borrows and lenses of fine sand make up 5 to 20% of each clay layer which complicates index and strength testing of the clays. Field observations show that failure planes along clay layers do not intersect sand burrows or lenses (McKenna and List, 1990). Marine Clay layers greater than 1 cm thick are generally continuous over tens to hundreds of meters. They are generally flat lying, show fissility along bedding planes, and exhibit a narrow range of material properties as summarized in Table T.5.1 (List and McKenna, 1990).

The residual shear strength curve for the Marine Clays shows an apparent cohesion which suggests a bilinear strength envelope (Cameron and Carr, 1988). Williams (1980) suggests that there is some doubt as to whether the cohesion intercept can be viewed as true cohesion but postulates that the ploughing effect of a sand fraction on the shear planes displaces softer clay and it is this carving of the sand grain into the clay that produces the cohesion intercept. Skempton (1985) gives the residual strength versus the normal effective pressure for most clays as a non-linear relationship and expresses the residual strength as the secant angle of shearing resistance. He also suggests that for design purposes it is often useful to take a "best-fit" linear envelope over the range of pressures involved, using both the effective cohesion and the effective angle of shearing resistance. This approach is used by Syncrude for slope stability analyses involving Marine Clay and is supported by back-analysis of numerous failures. Effective strength parameters of $f'_r=13^o$ and $c'_r=0$ is typical for many design applications, given that the typical average effective vertical stress is about 140 kPa for most designs.

Although Marine Clays are easily polished by hand when inspecting core, pre-sheared failure planes are extremely difficult to detect in the field although evidence of disturbance (upthrust blocks of clay and sand, overhang of Marine Sediments on the highwall and shear planes detected by slope inclinometers) is often seen. Back-analysis of numerous failures including loading and unloading cases indicate that at the time of failure, the Marine Clays are at or close to residual strength (McKenna and List, 1990). Due to the uncertainty of detecting pre-sheared planes in core, designs at the Syncrude Mine site are performed using residual strengths for all significant Marine Clay layers (i.e. greater than 1 cm thick) even if presheared planes are not observed in the core.

In the winter, up to 4 m of frost can penetrate the mining bench which greatly increases the apparent strength of the Marine Sediments. Because the frost penetration depth is extremely variable (mostly due to loading and unloading of windrowed oil sand, but also affected by material anisotropy, variability and water content), quantification of frost effects is difficult but the increase in bench strength is taken into account in a quantitative manner in some designs (McKenna and List, 1990).

5.4. IMPACT OF MARINE SEDIMENTS ON DRAGLINE OPERATIONS

The presence of Marine Sediments on the dragline operating bench has a negative impact on the dragline operation ranging from poor dragline pad performance to unstable slopes along the highwall near the dragline.

5.4.1 OPERATION FOUNDATION PAD PROBLEMS

A dragline requires a reasonably competent foundation soil to support the load of its tub and walking shoes. If the pad is too soft, the dragline will undergo large differential settlements and may not be able to swing. If the pad is too slippery, the dragline tub may rotate counter to the boom rotation and in some cases may slide along a sloping bench. If problems are encountered with the pad, the dragline must be walked off and the pad must be reconstructed. This procedure generally takes approximately 3 hours and has a detrimental impact on the mining operation.

5.4.2 HIGHWALL FAILURES NEAR OPERATING DRAGLINES

It has been long recognized that several highwall failure mechanisms can affect the safety of the draglines. Morgenstern et al (1988) have identified four distinct modes of highwall instability at the Syncrude mine (Fig. 5.5). Out of those four modes of failure only shallow block slides can represent a significant threat to dragline safety. Shallow block failures are controlled by dipping clay beds and require clay bed continuity as well as low shear strength of the interbedded clay layers. They can be triggered by the dragline shoe, by the dragline tub or by the ore windrow. Although all three triggering mechanisms can lead to a highwall failure and potential loss of the dragline, there are no instability incidents that can be attributed to the dragline shoe, while there has been only one dragline tub-driven high wall failure in the Marine Sediments. However, there have been over 250 windrow-driven failures along Marine Clay layers over the past seven years, out of which 5% caused highwall failures. There have been no highwall failures in the absence of windrow or dragline loads (McKenna and List, 1990).

List and McKenna (1990) showed that the windrow location in areas of Marine sediments is important in controlling the risk of a windrow driven bench failure heaving up and under the conveyor system. Placement of the ore windrow further from the conveyors is less optimal for the mining operation and has a negative effect on dragline production rates.

5.5. STATEMENT OF THE PROBLEM

Since Marine Clays exhibit strain weakening behaviour and numerous windrow induced failures have occurred along these layers, the possibility of progressive failure of an idealized highwall due to external soil loading was justifiably assessed in this study. The assumed slope stratigraphy is composed of 40 m of oilsand with a clay inclusion 0.25 m thick at 4.75 m below the top of the slope and a slope angle of 50°. The windrow has a base width of 100 m, 30 m height and its center line is located 65 m away from the edge of the slope. This leaves a 15 m wide equipment access strip on the operating bench between the windrow edge and the crest of the highwall. The ground water table is 3 m below the bench level. The magnitude of the vertical pressure applied due to the windrow loading, in combination with the geological conditions indicate that a progressive failure analysis should be carried out.

The assumed slope stratigraphy is similar to conditions encountered at the Syncrude mining site, where 40-50 m high oil sand slopes with interbedded continuous and/or discontinuous clay layers are overlying the bedrock. Because of its strength (Dusseault and Morgenstern, 1978), the oilsand is unlikely to fail under the windrow loading. On the other hand, excess pore water pressures are measured in the Marine clay layers during the windrow construction, which however dissipate quickly. The fast

dissipation rate of the excess pore water pressures supports the observation that failures associated with windrow construction occur within a few days of the waste piles placement. Therefore, the undrained behaviour of the Marine clays during the windrow construction is likely to be a critical design condition.

OILSAND

Agar et al (1984), after a series of triaxial compression tests on undisturbed samples of Athabasca oilsand reported that the curve fitting of the experimental data indicated that the hyperbolic model may be a useful empirical technique for modeling the nonlinear stress-strain behaviour of oilsand up to about 85% of the peak deviatoric stress level. Since no yielding was expected to occur in the oilsand deposit, the use of the hyperbolic model as proposed by Duncan and Chang (1970) was justified. The following parameters, as reported by Agar et al (1984), were used to model the drained behaviour of the oilsand deposit:

K=25000, K_{ur} = 30000, n = 0.9, G=0.2, R_f = 0.55, P_{atm} = 101.4.

MARINE CLAY

List and McKenna (1990) report typical strength parameters of the Marine Clay layers, as obtained from direct shear tests. The Drucker-Prager failure criterion with an associated flow rule was used to model both the drained and the undrained behaviour of the clay layer. Although it is known that the Mohr-Coulomb failure criterion describes better the stress-strain behaviour of soils, preliminary analysis showed that the Drucker-Prager failure criterion underestimates the extent of the yielding zone by about 5%, for the range of the applied pressures. It is also known that the closest point return algorithms for stress integration cannot be easily applied to yield surfaces that possess corners, when

they are plotted on the p - plane. Therefore, by using the Drucker-Prager instead of the Mohr-Coulomb failure criterion, one enjoys all the merits of fast convergence of the solution which is guaranteed by the use of the closest point return algorithm and does not seriously underestimate the extent of the yielding zone for the problem at hand.

It was assumed that the clay layer behaves in a linearly elastic manner up to the peak strength and then displays brittle perfectly plastic behaviour in the post peak range of deformation (strain weakening).It is common knowledge that using an associated flow rule to predict the direction of plastic straining in geomaterials results in excessive rate of dilation. It is also known that dilation occurs mainly during the transition between the peak and residual state of the stress-strain curve. Since the material model used is brittle perfectly plastic in the post peak range of deformation, the use of an associated flow rule is justified. Also, since the difference between the peak and residual friction angles is not that high, the use of an associated flow rule will not result in an erroneous overprediction of the dilative behavior of the clay layer.

The model parameters initially used to describe the material behaviour during the loading history are:
E=50000 kPa, $f^p = 17.5^o$, $c^p = 50$ kPa, $f^r = 11.0^o$, $c^r = 18$ kPa, $A_p = -0.1$ and $B_p = 0.98$ (List and McKenna, 1990).

BEDROCK

It was assumed that the bedrock was encountered at the bottom of the open pit, as is usually the case in most of the areas on the Syncrude site. Since no failure was expected on the pit floor, it was assumed that the bedrock behaved in a linearly elastic manner. A

Poisson's ratio n= 0.3 and a value of E=2000000 kPa for the elastic modulus were used for the Devonian limestone as indicated by Dusseault (1977).

WINDROW

The windrow material is oil sand excavated from below the operating bench and is therefore expected to behave as a loose granular material. Since the purpose of this study is not to model failures that are located within the windrow, but rather to study the response of the Marine Clay layer due to the windrow construction loading, it was assumed that this material behaves in a linearly elastic manner. A Poisson's ratio n = 0.33 and a value of E=20000 kPa for the elastic modulus were used. (Lambe and Whitman, 1978)

IN-SITU STRESS PROFILE

From the early Cretaceous (start of the Formation deposition) to the Tertiary period there has been an extensive loading and subsequent erosion of the overlying sediments in the area. During the Pleistocene Epoch, the region was subjected to repeated glaciations (ice up to 3000 m thick), which produced considerable scour and deposited a variable thickness of glacial drift over the entire area. Tertiary and Pleistocene erosion was the greatest in what is now the surface -mineable area of the deposit. Locally, the entire McMurray Formation was removed. In the southern and western part of the Athabasca Deposit area, there remains up to 500 m of Cretaceous overburden above the McMurray Formation (Mossop, 1980). In view of this complex geological history of the region, one expects that the McMurray Formation consists of heavily overconsolidated sediments and consequently a high horizontal in-situ stress field is locked into the Formation. This is confirmed by the results of various field and analytical studies conducted in the past

(Morgenstern et al, 1988). Therefore a high value of the coefficient of earth pressures at rest, K_O, ($1.5<K_O<2.0$) was adopted for this study.

5.6. FINITE ELEMENT ANALYSIS

Elastoplastic finite element analyses were carried out to investigate the influence of several variables on the stability of the highwall and to develop a better understanding of the progressive failure mechanism. Fig. 5.6 shows the finite element idealization of the domain under consideration. The domain is 350 m deep and 1500 m long in order to minimize any boundary effects on the solution. The upper 40 m is the idealized stratigraphy as described earlier, while bedrock is encountered from elevation +310 m and below.

Two finite element meshes were employed in the analyses to investigate among others the influence of the windrow construction scheme on the extent of the yielding process. The first mesh consists of 515, 8- and 6-noded isoparametric two dimensional elements with a total of 1642 nodes. The second mesh consists of 525, 8- and 6-noded isoparametric two dimensional elements with a total of 1652 nodes. A 3*3 Gauss integration scheme was used with the modified Newton-Raphson solution algorithm for equilibrium iteration. A "closest point integration algorithm" (Borja et al, 1989) was employed for the stress integration, which preserves the asymptotic rate of convergence of the Newton-Raphson method (Simo and Taylor, 1985). The excavation algorithm scheme as proposed by Ghaboussi and Pecknold (1984) was employed to simulate the open pit excavation as well as the windrow construction. Although some site specific cases may require a three-dimensional simulation, a plane strain case was considered for purposes of illustration. One of the challenges undertaken in this simulation was to generate an in-situ

stress field with K_O higher than 1.0. This was accomplished in two steps by invoking the principle of superposition, which is justified since no yielding occurs at the end of the first step.

In the first phase of the analysis an in-situ stress field with K_O=1.0 was generated. All soil layers were considered to behave as a linear elastic material with values of Poisson ratio of 0.499. The values of the unit weight used in this step were 50% higher than the real values for the respective layers. This procedure results in an in-situ stress field with vertical stresses 50% higher than the desired ones. In the second step of the analysis, all soils were again treated as linear elastic materials with values of Poisson ratio of 0.0. The values of the unit weight used in this stage were 50% less than the real ones, i.e 66% less than those used in the previous step and of opposite sign. This procedure results in a stress field with no horizontal stresses, a 0.0 value for the Poisson ratio was used, while the resulting vertical stresses are 66% less than those of the previous step and of opposite sign. The superposition of this two stress fields results in a stress field with a uniform K_O value of 1.5.

In the second phase of the analysis (steps 3 to 7), the real material properties were assigned to the respective soil layers and the excavation of the open pit was simulated. Since there is no significant pore water pressure response due to the slope excavation (List and McKenna, 1990), all soil layers can be considered for practical purposes that they behave in a drained manner during this stage of the simulation. The hyperbolic and the Drucker-Prager model with an associated flow rule were used to simulate the behaviour of the oilsand and the Marine Clay layer respectively. Linear elastic behaviour was assumed for the bedrock.

In the third phase of the analysis (steps 10 to 22), the stage construction process of the windrow was simulated and its effect on the extent of yielding and the pore pressure response of the clay layer was closely monitored. Again, the hyperbolic and the Drucker-Prager models were used to simulate the behaviour of the oilsand and the Marine Clay layer. Since during the windrow construction no significant excess pore water pressures are recorded in the oilsand deposit, it was assumed to behave in a drained manner during this stage of the simulation. However, significant windrow induced excess pore water pressure are recorded along the Marine Clay layers (List and McKenna, 1990). These construction induced excess pore water pressures, show a rapid rate of dissipation which can be attributed to sand burrows and lenses within and/or adjacent to the Marine Clay layer and/or pore water movement along pre-existing shear planes, but may have also been affected by the neighbouring piezometer installation trench. The length of the drainage path through these burrows and lenses is unknown but is likely critical to the ability of the clay to transport moisture to and from failure planes (List and McKenna, 1990). Values of A_p =-0.1 and B_p =0.98 were initially thought to be appropriate for the pore water pressure coefficients, considering the nature of the clay (stiff, heavily overconsolidated) and that it lies below the groundwater table (saturated). It was assumed that the bedrock and the windrow material behave in a linear elastic manner.

5.7. DISCUSSION OF THE RESULTS

5.7.1 IN-SITU STRESS FIELD GENERATION

By switching on gravity and generating the desirable in-situ stress field, all nodes move vertically downwards only, with all nodes at the same elevation settling by the same amount. As a result, no shear stresses are generated during this step and all vertical force

components on each Gaussian point are compressive and of equal magnitude for points lying on the same elevation.

5.7.2 OPEN-PIT EXCAVATION

This stage of the analysis was carried out in eight loading steps. In each step a row of elements representing the open-pit floor was removed from the mesh to create the new pit floor. During each unloading step, all nodes lying on the new floor of the pit heaved as expected. Nodes lying on the upper half face of the high wall were moving down and in to the pit, while nodes lying on the lower half were moving up and in, creating a compressive stress state in the vicinity of the highwall face. Insignificant tensile stresses were developed locally on the operating bench as a result of the unloading process and they caused no tensile yielding to the respective elements. No yielding along the clay layer occurred during this stage of the analysis, due mainly to the high shear strength of the clay layer and the stiffness of the surrounding oilsand.

5.7.3 WINDROW CONSTRUCTION STEP

The stage-construction of the windrow was simulated in 12 loading steps and its influence on the extent of yielding along the clay layer was assessed. By activating elements representing layers of the windrow material, the incremental displacements of nodes lying along the clay layer and symmetrical around the windrow center line are of equal magnitude but of opposite direction as expected. This results in a net increase of the horizontal displacements of the nodes lying between the windrow center line and the face of the highwall, while the opposite holds true for the nodes lying beyond the windrow center line. Also, the generated excess pore water pressures are increasing after every loading increment, which results in an effective stress state along the clay layer closer to

yielding. At the end of this stage of the simulation, minimal yielding was observed along the clay layer and the calculated construction induced pore pressures were much higher (by 3 times) than those measured in the field. This led us to believe that one or a combination of the following was occurring:

(1) The assumed shear strength parameters of the clay layer were overestimated.

(2) The assumed stiffness of the surrounding oilsand material was overestimated.

(3) The clay layer was not fully saturated.

A series of analyses were carried out, where the stiffness of the oilsand, the shear strength of the clay layer and Skempton's parameters (A_p, B_p) were reduced until the numerically calculated pore pressures matched those measured in the field and reported by List and McKenna (1990). The series of these analyses revealed the following:

(1) As long as the clay layer possesses a value of peak cohesion c^p = 50 kPa and a value of peak friction angle f^p= 17.5°, even a 30 m windrow height will cause no yielding of the clay layer for a value of K_o= 1.5.

(2) A combination of 25% reduction of the oilsand stiffness and an 80% reduction in the value of the peak cohesion of the clay layer will cause some yielding along the clay layer (K_0 =1.5).

(3) In order to match the measured field pore water pressures due to the windrow loading, a value of B_p =0.65 has to be assumed, while A_p can vary between 0.0 and -0.25.

The above conclusions led us to revise the initially assumed "proper" values of the stiffness, strength and pore water pressure parameters of the various soil layers to:

Oilsand K=18500, K_{ur} = 22500, n = 0.9, G=0.2, R_f = 0.55, P_{atm} = 101.4.

Clay E=50000 kPa, $f^p = 17.5^o$, $c^p = 5$ kPa, $f^r = 11.0^o$, $c^r = 5$ kPa, $A_p = -0.1$ and $B_p = 0.65$

Note that the initially assumed strength and stiffness parameters for the limestone remained unchanged. The revised set of parameters resulted in a 140 m long yielding zone along the clay layer and a pore pressure response within 3% of the observed in the field. The revised set of parameters was also considered to be the "benchmark set" for the sensitivity analysis that was carried out.

5.8. SENSITIVITY ANALYSIS

The influence of the following variables on the extent of yielding and the measured construction induced excess pore water pressures has been investigated:

1. Stiffness of the surrounding oilsand material.
2. Shear strength parameters of the clay layer.
3. Pore water pressure parameters.
4. Depth of embedment of the clay layer.
5. Insitu stress field.
6. Construction process of the windrow.

5.8.1 STIFFNESS OF THE SURROUNDING OILSAND MATERIAL

The influence of the stiffness of the surrounding oilsand material on the extent of the yielding along the clay layer was investigated. Three series of analyses were carried out. The first one was the "benchmark", while in the second one the stiffness of the

oilsand was increased by 33% and that resulted in a reduction of the yielding zone by almost 50%, when the windrow reached full height (30 m). In the third set, the stiffness of the oilsand was decreased by 33% and resulted in the yielding of the entire clay layer (~1000 m) and subsequent failure when the windrow reached the height of 22 m, i.e. 8 m before full height. The results of the analysis are illustrated in Fig. 5.7. and confirm the findings reported by Chan and Morgenstern (1988), that the stiffness of the surrounding materials can have a significant effect on the yielding behaviour of the weak layers.

5.8.2 STRENGTH PARAMETERS OF THE CLAY LAYER

The influence of the shear strength of the clay layer on the extent of yielding was investigated. By varying the value of the peak cohesion, c^P, from 5 to 12.5 and 25 kPa, the length of the yielding zone was reduced from 140 m, to 6 m and 4 m respectively after the application of the full windrow height. Hence a small decrease to the value of the peak cohesion, from 12.5 to 5 kPa, results in a dramatic rate of increase in the total length of the yielding zone along the clay layer. The rate of extent of yielding is even more dramatic for higher values of Ko. Therefore, if for any reason softening of an already weakened clay layer will occur, that can cause extensive yielding, which in turn can lead to the development of a shallow block slide failure mechanism along the clay layer with serious consequences for dragline safety. The results of the analysis are illustrated in Fig. 5.8.

Note, that even the value of 25 kPa is 50% less than the value of the peak cohesion reported by List and McKenna (1990) for the clay layer. This led us to believe that the clay layers have experienced a considerable degree of softening prior to the windrow construction, due to a mechanism not necessarily related to the excavation of the pit. List and McKenna (1990) list some possible mechanisms that can cause softening of the clay

layers. The extent of yielding appeared to be insensitive to the value of the Poisson's ratio of the clay layer.

5.8.3 PORE WATER PRESSURE PARAMETERS

As it was mentioned in section 5.6, it was initially thought that the most appropriate values for Skempton's pore pressure parameters (A,B) for plane strain were A_p =-0.2 and B_p =0.98. These parameters failed to predict the measured pore water pressure response due to the windrow loading. In this section of the sensitivity analysis, the relative influence of A_p and B_p on the calculated pore water pressure response of the clay layer was undertaken.

By definition $\Delta u = B_p [\Delta\sigma_3 + A_p (\Delta\sigma_1 - \Delta\sigma_3)]$ (Skempton, 1954)

where Δu = increment of pore water pressure

$\Delta\sigma_1, \Delta\sigma_3$ = changes of principal stresses s_1 and s_3 respectively

A_p, B_p = Skempton's pore pressure coefficients for plane strain.

Evaluating the changes of principal stresses σ_1 and σ_3, i.e. $\Delta\sigma_1$ and $\Delta\sigma_3$, along the clay layer for any two consecutive loading steps, one can see that the term $(\Delta\sigma_1 - \Delta\sigma_3)$ is very small. It can then be concluded that regardless of the value of A_p ($-0.25 < A_p < 0.0$, since the clay is heavily overconsolidated), the dominant parameter in the accurate prediction of the pore pressures is B_p.This is confirmed by the sensitivity analysis, where by varying the value of A_p in the above range, insignificant changes occur in the magnitude of the calculated pore water pressures. By varying the value of B_p from 0.98, to 0.7 and to 0.65, the excess pore water pressure is reduced by 2 and 3 times

respectively. The last is in excellent agreement with the excess pore water pressure response measured in the field.

One can argue that a clay layer that lies underneath the water table cannot have an unsaturated response, i.e. the value of B_p ought to be close to 1.0. Branco and Eisenstein (1991) report that the marine sediments respond to undrained loading very similar to partly saturated soils due to the presence of gas, which results in considerably greater compressibility of the fluids. This unsaturated response can also be attributed to sand burrows and lenses within and/or adjacent to the Marine Clay layer and/or pore water movement along pre-existing shear planes, but may have also been affected by the neighbouring piezometer installation trench.(List and McKenna, 1990).

5.8.4 DEPTH OF EMBEDMENT OF THE CLAY LAYER

The influence of the depth of embedment of the clay layer on the extent of yielding was investigated. Three analyses were carried out, varying the depth of embedment from 4.75, to 9.75 and 19.75 m. The results show a decreasing length of the yielded zone with increasing depth of embedment. This can be explained by the fact that the deeper the clay layer is located, the lesser is the influence of the windrow load on the clay layer, which results in a lesser length of the yielded zone along the clay layer. Consequently, the potential for progressive failure decreases with increasing depth of embedment. This is illustrated from the results of the finite element analysis in Fig. 5.9, where the length if the yielded zone along the clay layer versus its depth of embedment is plotted.

5.8.5 IN-SITU STRESS FIELD

Bjerrum (1967) recognized the importance of the magnitude of the in-situ stress field on the extent and the rate of propagation of progressive failure in overconsolidated clays. To assess quantitatively the influence of K_o on the extent of yielding along the clay layer due to the windrow loading, three analyses were carried out. The value of K_o was varied from 1.5 ("benchmark analysis"), to 1.75 and 2.0. By increasing the value of K_o from 1.5 to 1.75, the length of the yielding zone along the clay layer increased from 140 m to 900 m (entire length of the clay layer) at the end of the windrow construction! I.e. increasing the insitu stress field by 15%, results in an increase of the yielding zone by more than 600%! Increasing the value of K_o to 2.0, results as expected in the spread of yielding along the entire length of the clay layer at the end of the windrow construction. For higher values of the peak cohesion C_p, the extent of yielding is much less. The results of the analysis (Fig. 5.10) show how the softening of the clay layer in combination with the high in-situ stress field can result in an uncontrolled rate of the propagation of yielding with possible catastrophic consequences for manpower and equipment working on and around the highwall.

5.8.6 CONSTRUCTION METHOD

The influence of the construction procedure of the windrow on the extent of yielding and the generated pore water pressures was investigated. Two different construction methods were adopted in this sensitivity analysis, which will be called "center line method" and "double pyramid method", which from now on will be called "CLM" and "DPM" respectively. In CLM, see Fig.5.11, the construction proceeds by building up and sideways from the centerline of the windrow until the desirable height is achieved. In DPM, see Fig. 5.12, the construction starts by building two twin pyramids on both sides

of the windrow center line and proceeds by filling up the in-between gap, until again the desirable height of the windrow is reached.

The horizontal weak layer was assumed to be 4.75 m below the working bench. Although the number of elements employed in the simulation of the two construction modes was not the same, equal number of steps was employed in each simulation. Since it was thought that the weight of the windrow material per construction step would dominate the extent and the propagation of yielding, a considerable effort was made to keep this variable almost equal per corresponding step of the two analyses.

Although it was expected that the construction procedure would have an effect on the extent and the propagation of yielding along the clay layer, the analysis showed that for all practical purposes the total length of the yielding zone along the clay layer is the same for the two modes of construction investigated in the sensitivity analysis.

5.9. CONCLUSIONS

From the results of the analysis, the following conclusions can be drawn:

1. The windrow construction is an undrained loading for the clay layer and can induce progressive failure along the brittle marine clay layers.

2. This process is amenable to analysis by the finite element method.

3. The extent of progressive failure is primarily a function of the shear strength of the clay layer and the insitu stress field. Combinations of softened shear strengths of the clay layer and high insitu stress fields can lead to dramatic rates of propagation of yielding.

4. The extent of progressive failure is also a function of the depth of embedment of the clay layer and the stiffness of the surrounding oilsand material.

5. The progressive failure process is not much influenced by the windrow construction method for the two modes examined in this study.

6. The construction induced pore pressures along the clay layer can be predicted accurately using the finite element method. However, an accurate knowledge of the insitu value of the B_p parameter, rather than both A_p and B_p, is crucial for any reliable prediction.

Once more, the analysis carried out indicated the importance of identifying the location and the strength properties of any weak inclusion in an otherwise strong material. A great deal of effort should be spent during the site investigation phase in order to locate materials that can lead to a progressive mode of failure.

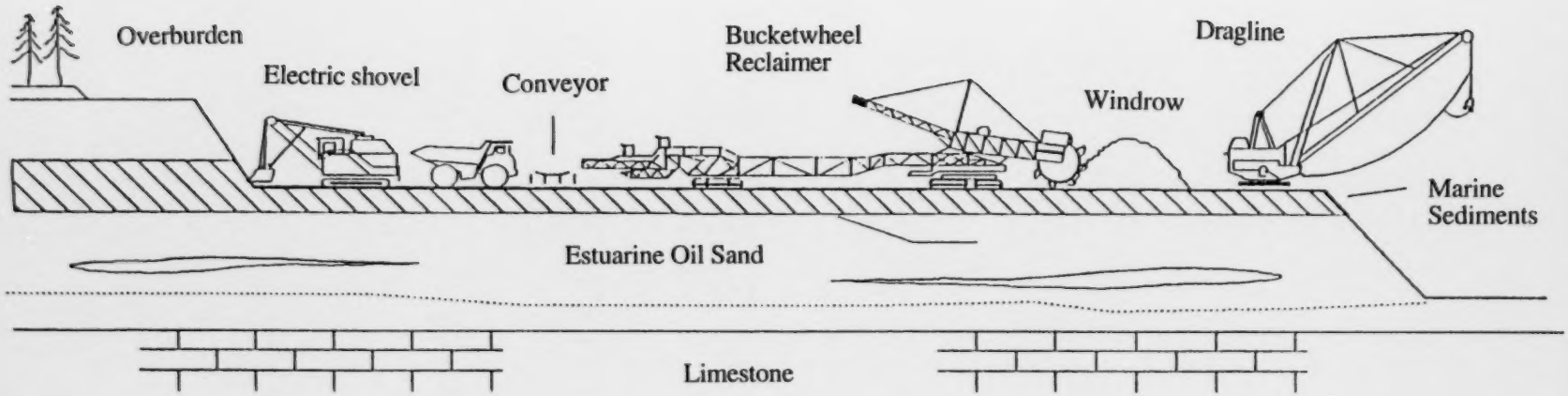

Fig. 5.1 Schematic of Syncrude Mining Operation (modified after McKenna and List, 1990)

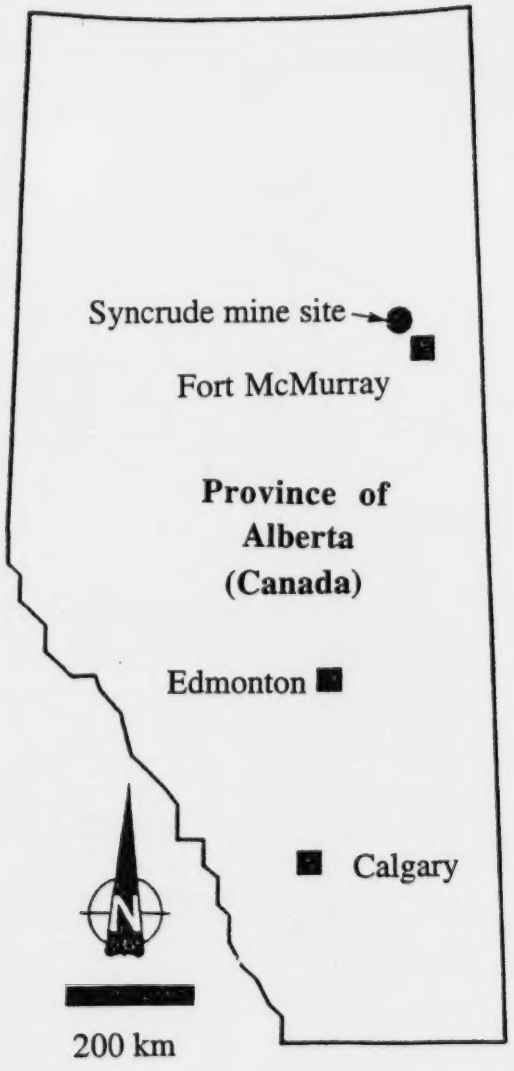

Fig 5.2 Location Map (modified after McKenna and List, 1990)

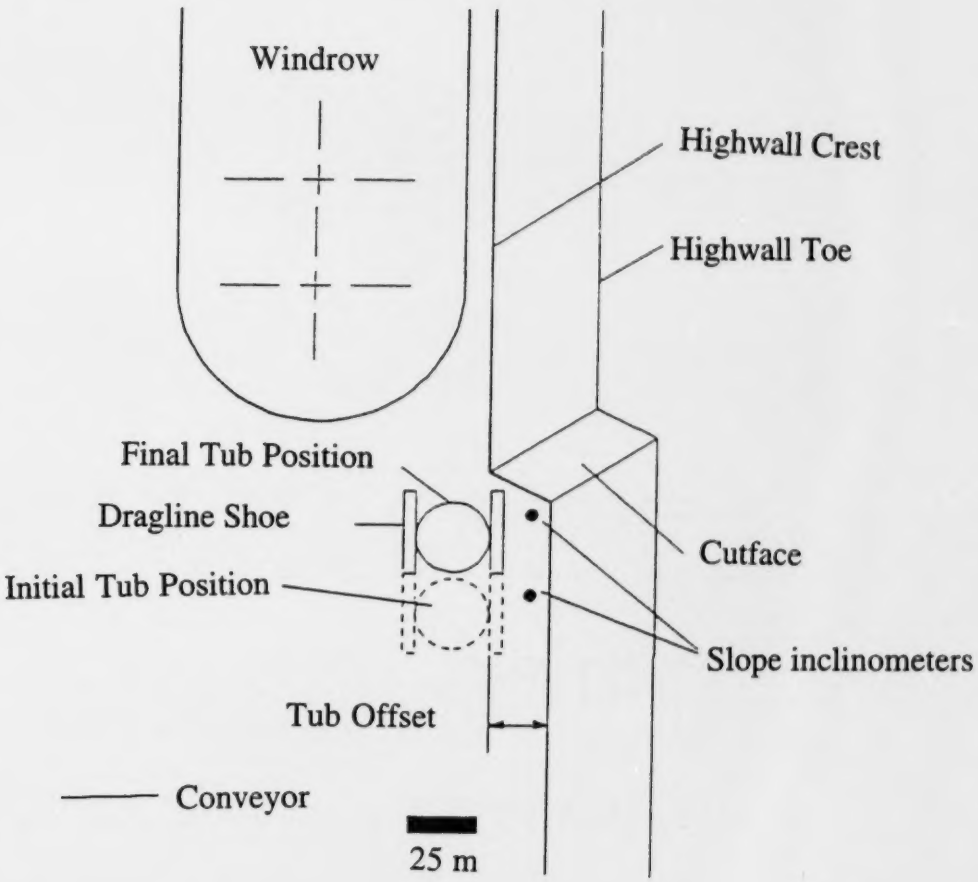

Fig. 5.3 Syncrude Dragline Mining Scheme (modified after McKenna and List, 1990)

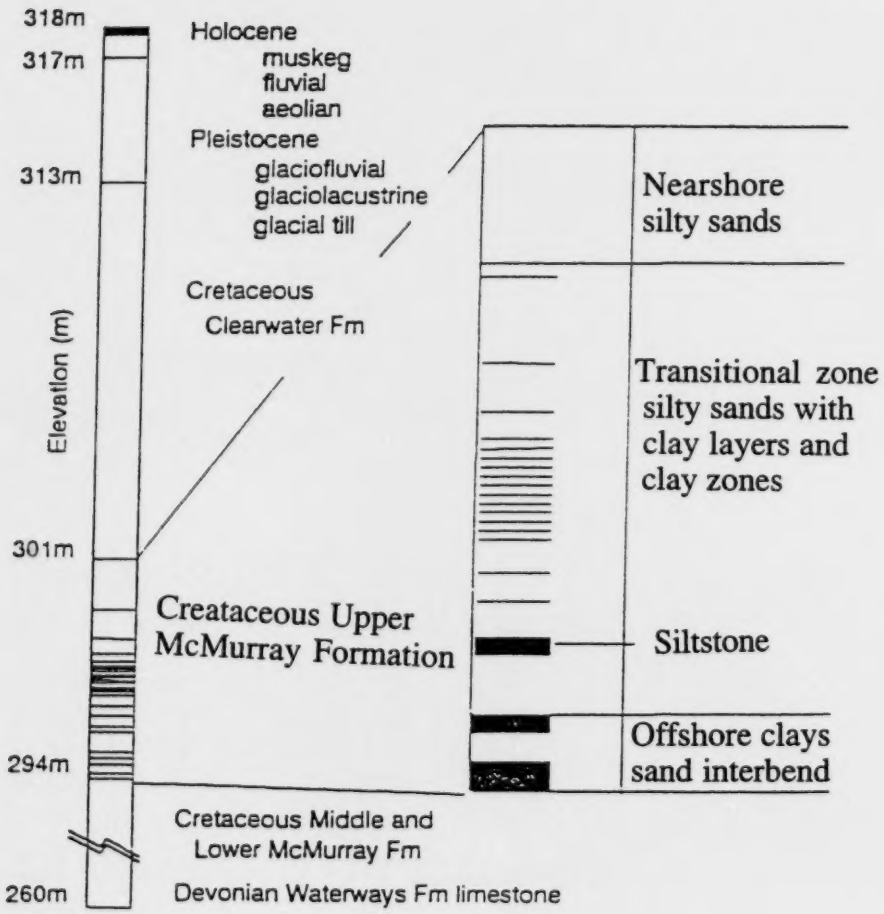

Fig. 5.4. Typical Marine Sediments Geology (modified after McKenna and List, 1990)

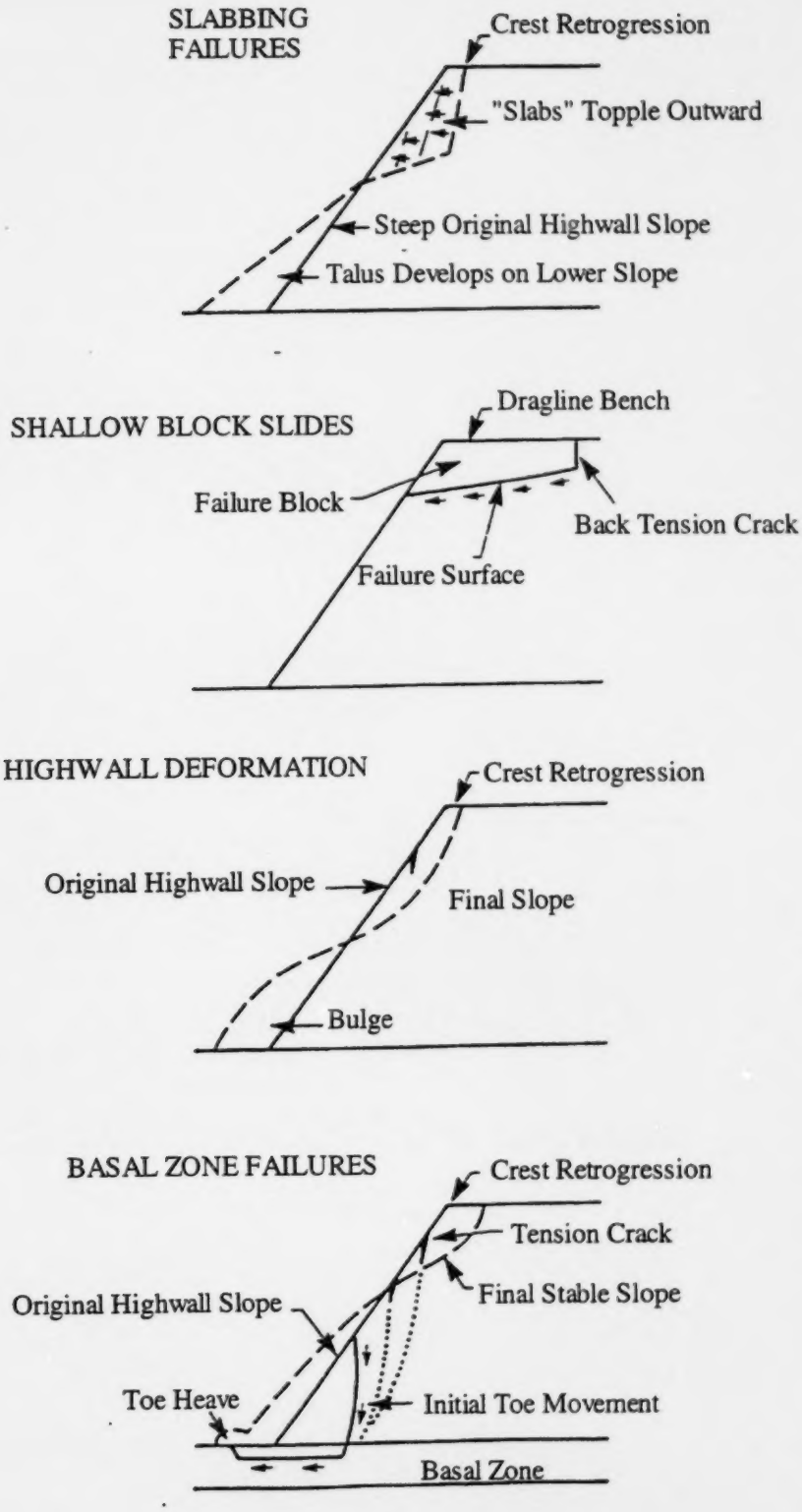

Fig. 5.5 Highwall Failure Modes (modified after Morgenstern et al., 1988)

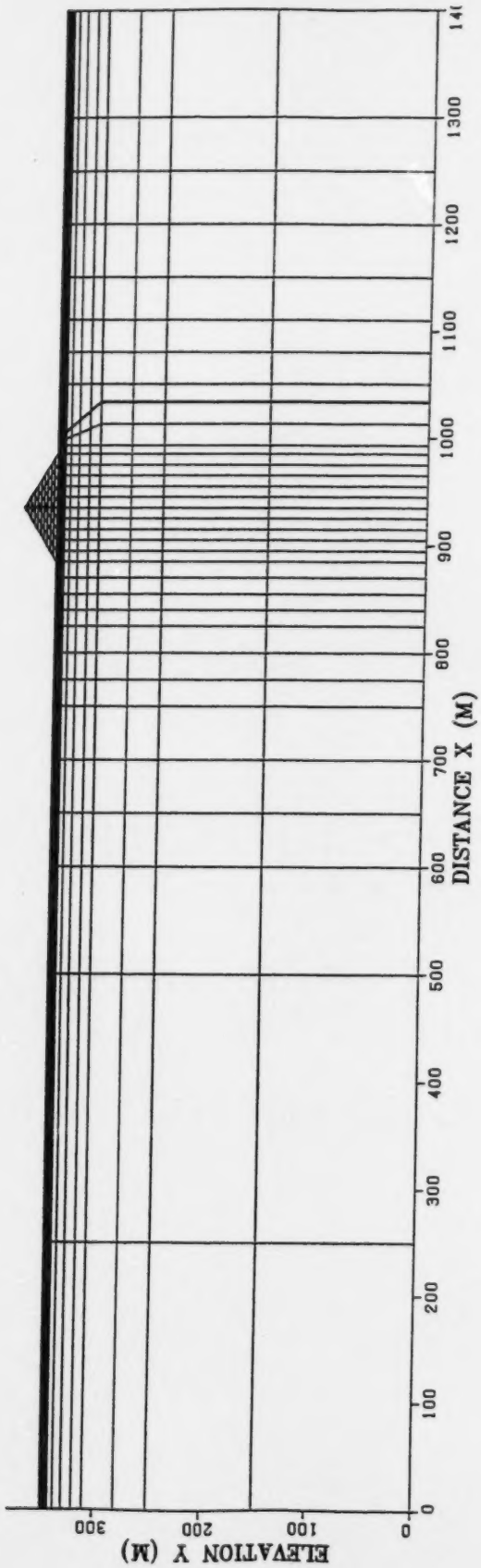

Fig. 5.6 Finite Element Idealization

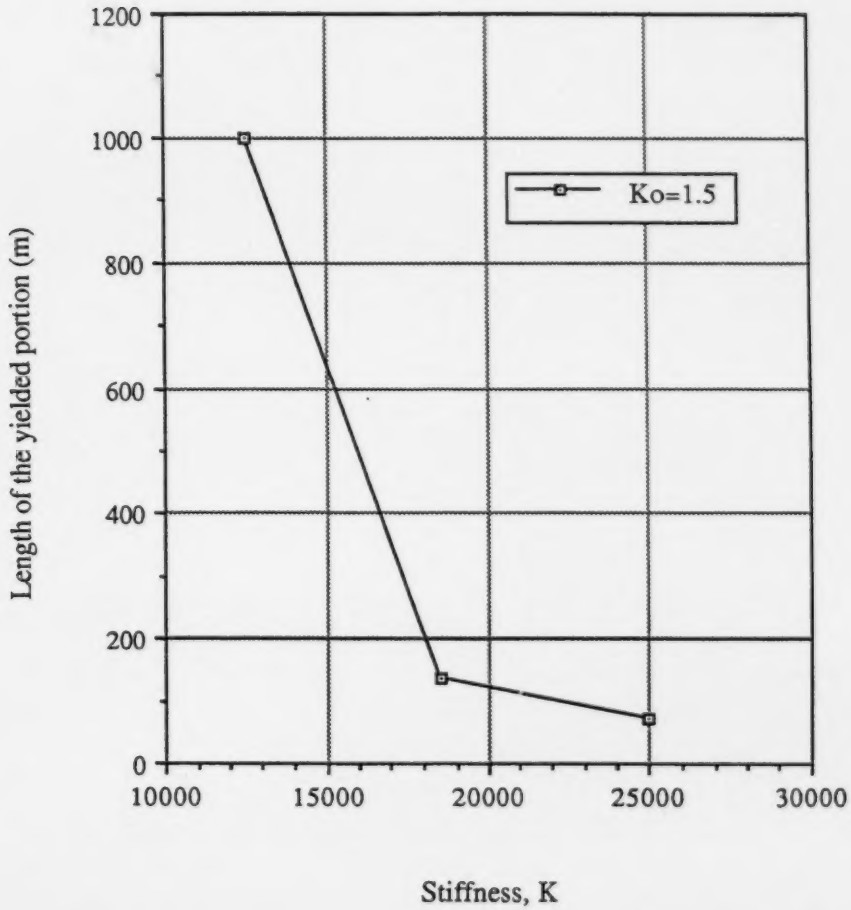

Fig. 5.7 Influence of the stiffness of the oilsand on the length of the yielded portion of the clay layer

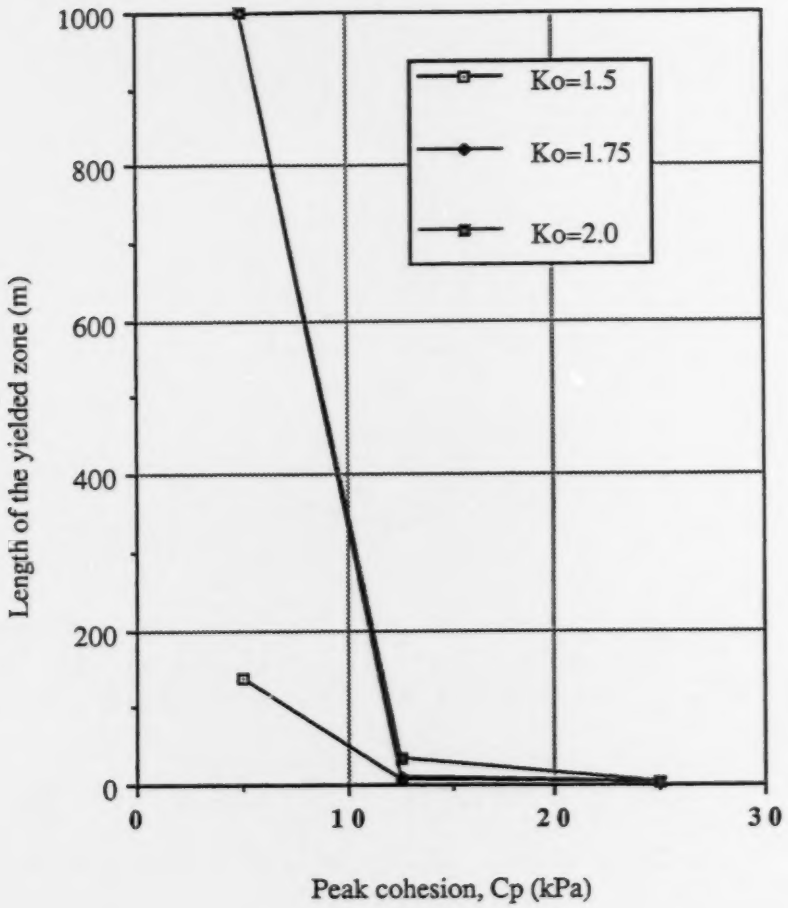

Fig. 5.8 Influence of the value of the peak cohesion on the extend of yielding

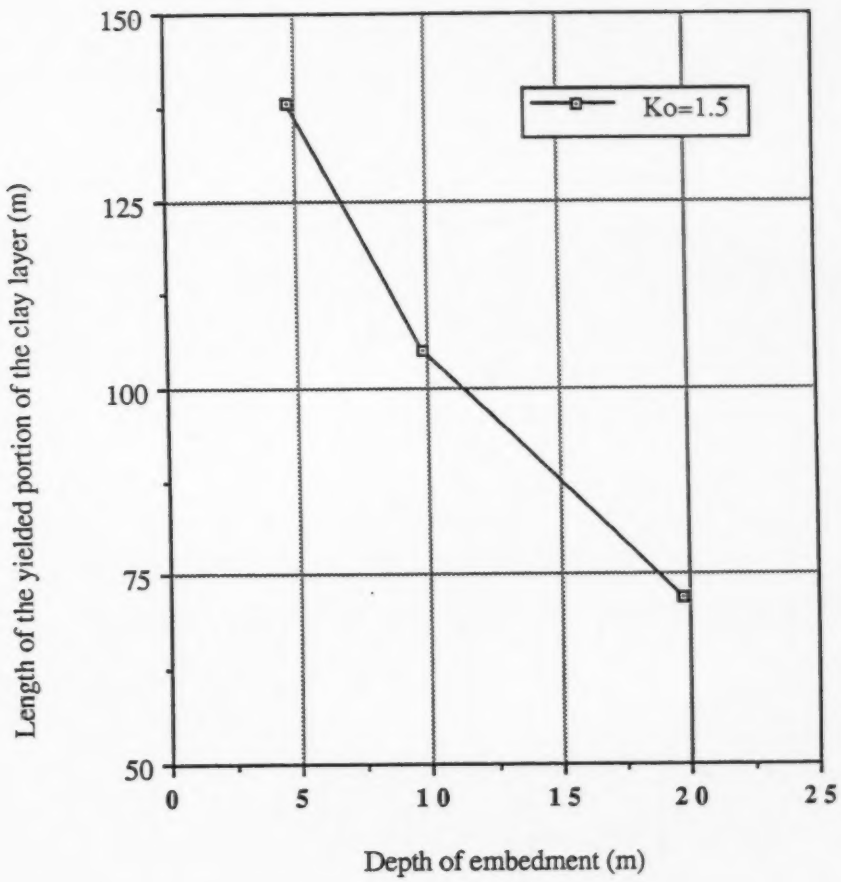

Fig. 5.9 Influence of the depth of embedment on the length of the yielded portion of the clay layer

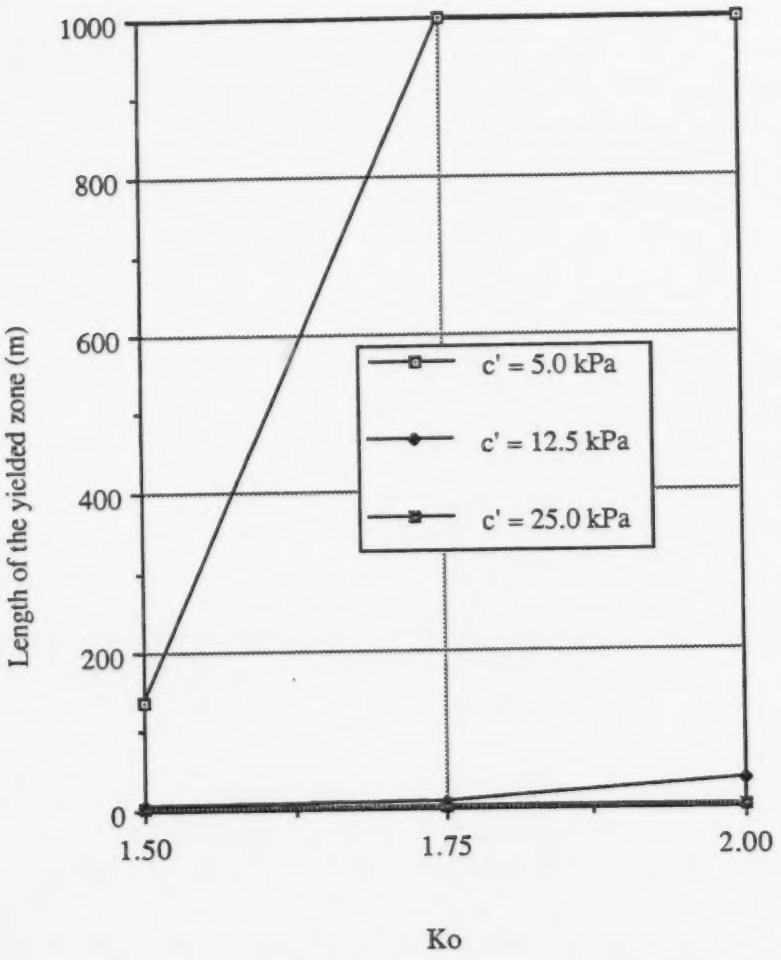

Fig. 5.10 Influence of Ko on the length of the yielded portion of the clay layer

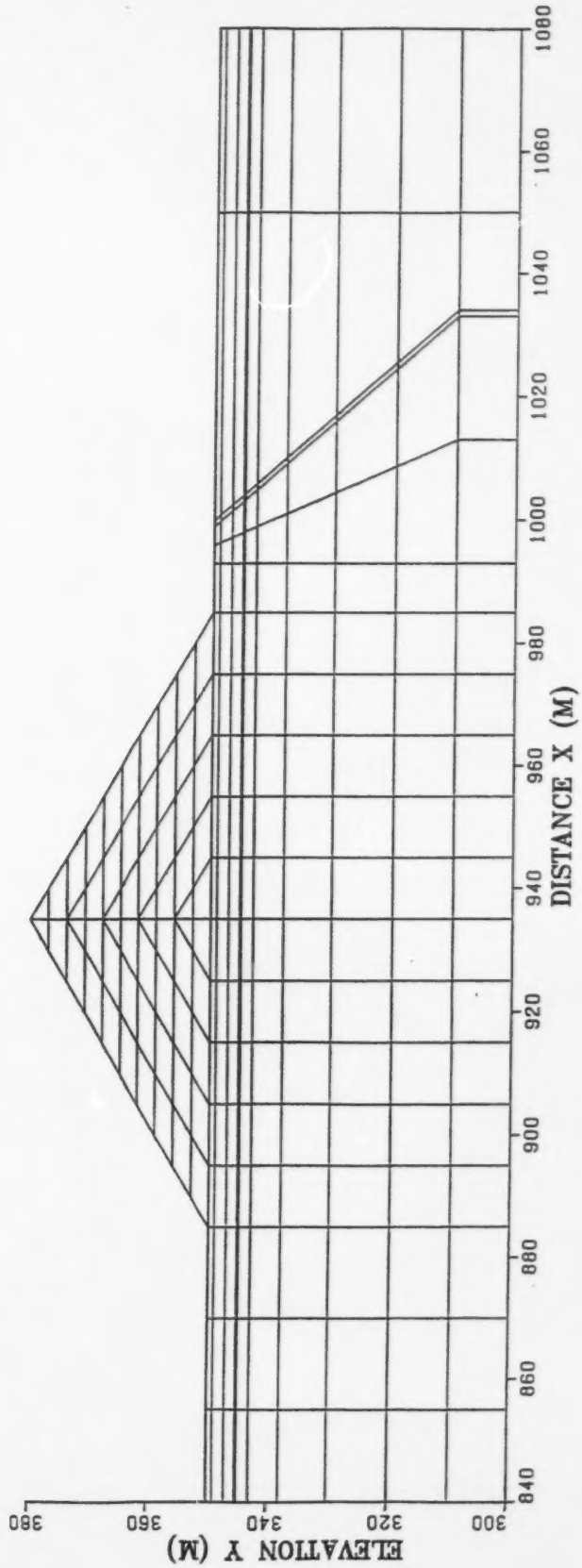

Fig. 5.11 CLM (Center Line Method) of construction

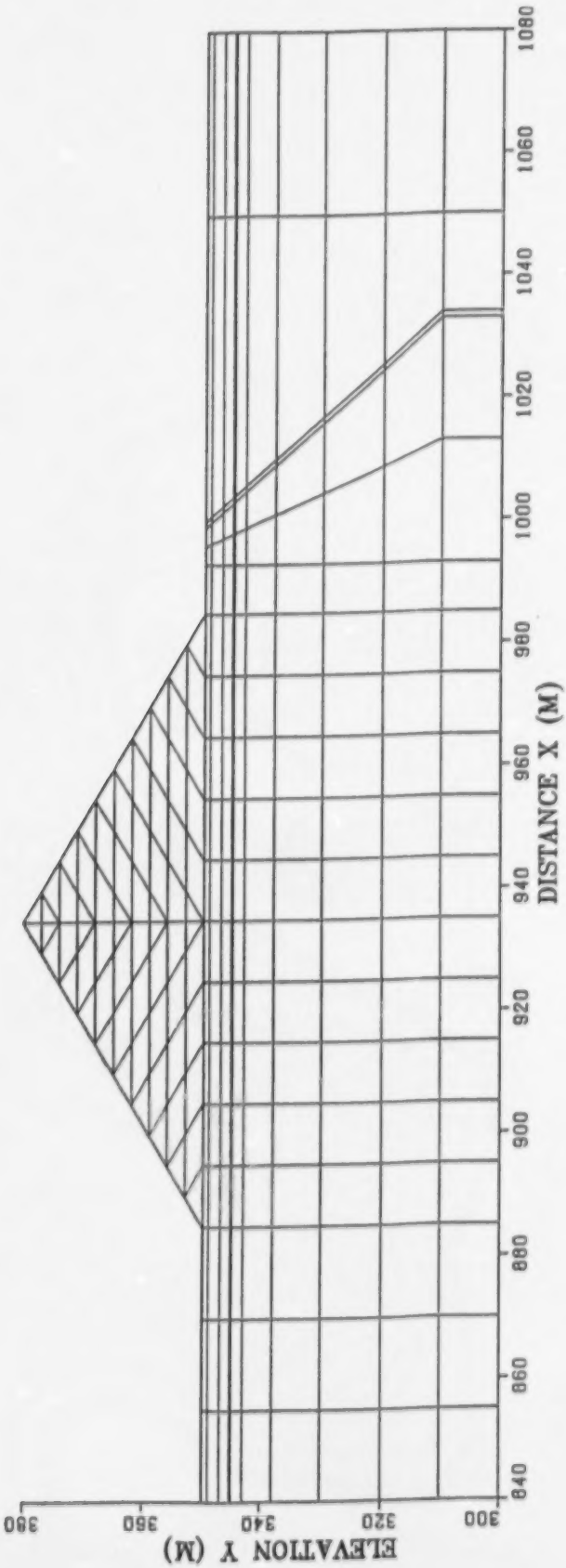

Fig 5.12 DPM (Double Pyramid Method) of construction

GEOTECHNICAL PARAMETERS (List and McKenna, 1990)		
	Marine Sand	Marine Clay
Unit weight (kN/m^3)	19.6	20.2
Peak cohesion (kPa)	0	50
Peak friction angle (degrees)	50	17.5
Residual cohesion (kPa)	0	10
Residual friction angle (degrees)	34	9.5

STRENGTH PARAMETERS ASSIGNED TO THE MATERIALS OF THE STRATIGRAPHY

OILSAND (Hyperbolic model)

K=25000, Kur=30000, n=0.9, G=0.2, Rf=0.55, Patm=101.4

CLAY (Elastic-brittle perfectly plastic Drucker-Prager with an associated flow rule)

E=50000 kPa, Fp=17.5, Cp=50 kPa, Fr=10, Cr=5 kPa, Ap=-0.1, Bp=0.98

BEDROCK (Linear Elastic)

E=2000000 kPa, v=0.3

WINDROW MATERIAL (Linear Elastic)

E=20000 kPa, v=0.33

CHAPTER 6

PROGRESSIVE FAILURE ANALYSIS OF OFFSHORE GRAVITY BASE STRUCTURES[1]

6.1 INTRODUCTION

Gravity Base Structures (GBS), used as production platforms and/or storage tanks at sea, are built at a deep water coastal site and then towed to the immersion point. The stability of these structures is achieved primarily by self-weight as a result of the dimensions and the weight of the reinforced concrete base. Therefore they do not require any anchoring to the sea bottom (Le Tirant, 1979). The advantage of such an installation procedure is that the installation time is reduced to a minimum (1 or 2 days), compared to fixed platforms on piles. This is very beneficial in hostile environments such as that often encountered off the NE Atlantic Canadian coast.

The foundation behaviour of a GBS is similar to a surface foundation structure consisting of a concrete mat and differs only in the sense that there is no excavation prior

---

[1] A version of this chapter was presented at the 2nd ISOPE Conference (San Francisco, USA, June 1992) as : Mathioudakis, M., Morgenstern, N.R., Chan, D.H. : "Progressive Failure Analysis of Offshore Gravity Base Structures".

to the laying of the concrete mat. The analysis of the foundation behaviour of a GBS involves the estimation of the risk of complete shear failure, and of deformations under conditions of self-weight and any other environmental loads (wave or ice). Therefore, stability analysis is one of the most important aspects to be considered in studies of actual platform locations.

Most GBS require detailed analyses of foundation bearing capacity and resistance to sliding and overturning. Where the base dimensions of the structure are controlled by foundation conditions (i.e weak layers), the Commentary to the Canadian Code for the Design Construction and Installation of Fixed Offshore Structures, CSA S 472.1-M1989, recommends that "comprehensive analyses of foundation failure modes using numerical and physical modelling will likely be necessary". It is also clearly stated in the Canadian Code that "the methods of analysis shall be compatible with all the anticipated deformation modes and potential mechanisms of failure and shall be appropriate for the intended structure, foundation materials and loading conditions." It is required that, "geotechnical parameters for stability and deformational analyses shall be based on the results of a site investigation" and in their selection consideration should be given to, among other factors "post-peak strength reduction and the possibility of progressive failure". Therefore, a progressive failure analysis should be carried out whenever the structure is founded on soils with distinct post peak softening behaviour.

Any material that exhibits strain softening behaviour is prone to progressive failure. Strain softening is defined as the loss in strength after the material reaches a clearly defined peak at a lower strain level. The mechanisms of progressive failure and the conditions for progressive failure to occur have been well studied and understood (Chan, 1985). Progressive failure is a process by which the soil mass fails without mobilizing throughout the maximum available strength. The degree of softening is not

necessarily a characteristic of the material since it depends on the stress path and the drainage conditions. For example in a triaxial compression test, dense sands and overconsolidated clays under drained conditions and loose sands and normally consolidated clays under undrained conditions exhibit a strain-softening stress strain curve. However, loose sands tested under drained conditions exhibit lesser or no softening behaviour. Whenever strain weakening materials are found in the seabed soil profile, a progressive failure analysis of a GBS founded on such stratigraphy is not only justified but also recommended by the Canadian Code. To study progressive failure problems, stress analysis is necessary and the use of plasticity based constitutive relations to describe the complex material response, in combination with the finite element analysis, provides an appropriate basis for conducting such a study.

6.2 STATEMENT OF THE PROBLEM

The possibility of progressive failure of the foundation of a GBS sitting on an idealized soil profile was assessed. The assumed foundation strata are composed of 100 m of very dense granular soil with a cohesive soil inclusion 0.5 m thick at 9.5 m below the mudline (BML), resting on top of the bedrock (Fig. 6.1). The GBS is placed on top of the very dense sand deposit and its assumed structural configuration is a cylindrical tank of 100 m diameter and 100 m height. The assumed submerged weight of the full platform is approximately 5200 MN, including iron ore ballast placed offshore. The magnitude of both the vertical pressure and the horizontal environmental forces in combination with the geological conditions indicate that a progressive failure analysis should be carried out.

6.3 GEOLOGICAL PROFILE

The assumed soil profile of the seabed floor is similar to conditions off the NE Atlantic coast of Canada and consists of approximately 100 m of very dense sand with interbedded continuous and/or discontinuous clay layers overlying the bedrock. Because of their density, the sands are unlikely to fail in shear under the loading conditions. On the other hand, the clay layers, depending on their thickness, remain substantially undrained during the critical design loadings, and thus the undrained behaviour of clays is likely to be a critical design condition.

Sand layer

In this study, the drained peak friction angle of the sand , ϕ^p, which might vary from 37^o to 43^o, was taken to have an average value of 38^o. These values are believed to be typical measurements from laboratory tests of soils that can be found off the NE Atlantic Canadian coast (Thompson and Long, 1989). An average value for the drained residual friction angle ϕ^r of 35^o was assumed. It was also assumed that this material shows brittle failure at axial strains of 5%. Such material generally exhibits a very prominent non-linear pre-peak deformation with moderate strain softening effects. Therefore modelling accurately the pre-peak deformation of the material behaviour is very important in order to capture the correct deformation pattern. In view of the influence of the confining pressure on the material behaviour, the hyperbolic model as proposed by Duncan and Chang (1970) was adopted to model the behaviour of the sand in this study.

Clay layer

Data from the literature for clay samples recovered off the NE Atlantic Canadian coast, indicate that the unconfined compression strength C_u, determined from UU tests, generally ranges from about 120 to 630 kPa (Thompson and Long, 1989). Also, results from CIU tests indicate that the effective peak friction angle has an average value of approximately 22° with corresponding average effective cohesion of 80 to 150 kPa. Atterberg limit tests performed on clay samples recovered from depths of 10 to 15 m BML, showed that the material can be characterized as a medium to low plasticity clay (PI=21- 23). One therefore does not anticipate a dramatic strain weakening behaviour in the friction of this material and a value of 18° was chosen as the residual friction angle. A value of 120 kPa was reported as representative of the undrained shear strength of the clay samples recovered from 9.5 m. depth BML. It was assumed in this study that the clay layer was continuous at a depth of 9.5 m as shown in Figure 6. 1. The effect of the depth of embedment of this weaker layer on the progressive failure mechanism was investigated.

Following set-down, the clay layer will tend to consolidate under the weight of the GBS. It was assumed that when the full design wave load would be applied, the consolidation of the clay layer would be complete. As a result of the reconsolidation of the clay layer, an increase of the undrained shear strength is anticipated before the wave load is applied. The effect of the GBS weight diminishes with depth and distance away from the structure and it was calculated using stresses obtained from the set-down step of the analysis. At some distance away from the GBS, which depends on the assumed depth of embedment of the clay layer, the effect is minimal and no reconsolidation of the clay layer occurs. Changes less than 3% were ignored. As a result, beyond this distance away from the GBS and for a given depth of embedment, the undrained shear strength of the

clay remains unchanged. It was assumed that the clay was initially overconsolidated with an OCR value of approximately 4.5 at a depth of 9.5 m. The application of the full gravity pressure might change a portion of the clay underneath the GBS from an overconsolidated to a normally consolidated state.

Bedrock

It was assumed that the bedrock was encountered at a depth of 100 m BML, just beneath the bottom of the sand layer. Since no significant movement is expected in this stratum, it was assumed that the bedrock behaved in a linearly elastic manner. A high value of elastic modulus of 600,000 MPa was used for the bedrock together with a Poisson's ratio of 0.3.

6.4 IN - SITU STRESS PROFILE

Consolidation data from samples recovered off the NE Atlantic Canadian coast (Thompson and Long, 1989), showed evidence of preconsolidation. An overconsolidation ratio (OCR) versus depth profile was assumed where the OCR varies from values greater than 6 near sea-floor level to approximately 1 (a normally consolidated state - NC) at 100 m depth BML. The OCR versus depth profile can be used to estimate the coefficient of earth pressure at rest (K_o) versus depth profile, using the relationship proposed for sands, by Mayne and Kulhawy (1982) as follows:

$$K_o = (1\text{-}\sin\phi') * OCR^{\sin\phi'}$$

The resulting Ko versus depth profile from 0.0 to 100.0 m. depth BML for $\phi'=38^o$ (effective peak friction angle of the soil) is shown in Figure 6. 2. The Ko versus depth profile is needed to establish the appropriate in-situ stress field in the finite element

analysis.

6.5 FINITE ELEMENT ANALYSIS

Elastoplastic finite element analyses were carried out to investigate the influence of several variables on the stability of the GBS and to develop a better understanding of the progressive failure mechanism. Figure 6. 3 shows the finite element idealization of the domain under consideration. The domain is 800 m deep and 1500 m long in order to minimize any boundary effects on the solution. The upper 100 m BML is the idealized stratigraphy as described earlier, while bedrock is encountered from 100 m to 800 m BML.

The finite element mesh used in all the analyses consisted of 816, 8-noded isoparametric two-dimensional elements with a total of 2579 nodes. A 3*3 Gauss integration scheme was used with the modified Newton-Raphson solution algorithm for equilibrium iteration. A "closest point integration algorithm" (Borja et al, 1989) was employed for the stress integration, which preserves the asymptotic rate of convergence of the Newton-Raphson method (Simo and Taylor, 1985). For purposes of illustration, a plane strain case is considered with a rigid platform resting at mudline. Site specific studies may require a three-dimensional simulation. An equivalent elastic modulus for the GBS of 600,000 MPa was used in the analysis.

In the first step of the analysis, an insitu stress field was generated. All soil layers were considered to behave as a linear elastic material with values of Poisson's ratio decreasing with depth. The values of the Poisson's ratio were chosen in a way that the desired K_O versus depth profile could be obtained at the end of the "switch on gravity" step. A fully drained condition was assumed.

In the second step of the analysis, the GBS was placed with full tank pressure applied on the mudline. All nodes along the tank-mudline interface were free, so that minimum shear stresses develop at the GBS-mudline interface. Note that the values of the Poisson's ratio were changed from those of the first step, to values more realistically representing the respective materials.Various constitutive models were utilized to describe the different layers behaviour in this part of the analysis. The hyperbolic model (Duncan and Chang, 1970) was used to model the drained behaviour of the sand layer with the following parameters: K= 1250, K_{ur}=1750, n=0.5, R_f= 0.90, P_{atm}=101.4 and G=0.33.

The Tresca model with an associated flow rule was used to model the undrained behaviour of the clay layer. It was assumed that the material behaves linearly elastic up to the peak strength and then displays brittle perfectly plastic behaviour in the post peak range of deformation (strain weakening). The model parameters used to describe the material behaviour during this loading stage are: c_u^p =120 kPa and c_u^r = 70 kPa., i.e there is a 40% decrease in the value of the undrained strength from peak to residual, which agrees with experimental results reported by Thompson and Long (1989) for similar material. Although the platform pressure was applied in a very short period of time (1 to 2 days) and therefore the loading is undrained, i.e excess pore water pressures will be generated, it was assumed that when the wave loading was applied on the structure, all the excess pore water pressures in the clay layer had dissipated. This is justified by the fact that the probability that immediately following installation the platform will experience the 100 year period storm is minimal . Linear elastic behaviour was assumed for the bedrock.

In the third step, the design wave load was applied as a horizontal force in the upper left corner of the structure. The magnitude of the wave forces was estimated using

diffraction theory for a vertical circular cylinder (Sarpkaya and Isaacson, 1987, Instanes, 1991) and assumed the following characteristics for the 100 year return period wave. The height of the wave was taken to be 30 m with a period of 15 sec. Then for deep water conditions (70 m), the resulting maximum force was calculated to be 1636 MN following the procedure given by Sarpkaya and Isaacson (1981).

The forces exerted on the GBS as a result of an iceberg impact were calculated based on a simplified design procedure proposed by Sanderson, (1988). An iceberg of mass $6*10^6$ tonnes, radius of 120 m, moving at an extreme velocity of 1.0 m/s was assumed and the resulting peak iceberg impact load was 565 MN (Instanes, 1991).

Since the resulting maximum wave forces are higher than the ice forces, the wave loading is considered as critical in this study. Before applying the critical design storm forces, all nodes along the base-mudline interface are now forced to move together in both the horizontal and vertical directions. The constitutive models utilized to describe the various material behaviour in this step of the analysis are the same as those used in the previous step.

The increase of the undrained shear strength in the clay was calculated from the relationship

$$C_u = \frac{c * \cos\phi + p' [K_0 + A_f * (1 - K_0)]}{1 + (2 * A_f - 1) * \sin\phi}$$

which can be derived by examining the Mohr circles (total and effective) at failure of a soil element that is being subjected to an undrained triaxial test. For the yielded part of the clay layer, $c'=0$, $\phi=\phi^r$, p' is the effective vertical pressure and $A_f = 0.3$.

For the non-yielded part of the clay layer, the increase of the undrained shear strength can be calculated from the correlation

$$C_u = p' * 0.38 * OCR^{0.8}$$

which describes the best - fit line to CIU data obtained from testing clays sampled off the NE Atlantic coast of Canada. The resulting undrained shear strength and OCR profiles along the clay layer after set-down are shown in Figs. 6.4 and 6.5 respectively. Due to the short nature of the loading event and the low permeability of the clay, it was assumed that the clay layer behaves in an undrained manner. The clay material is assumed to behave in a perfectly plastic manner in the presheared area but in a brittle plastic manner in the unsheared area, as before.

6.6 DISCUSSION OF THE RESULTS

6.6.1 SWITCH ON GRAVITY STEP

By switching on the gravity and generating the desirable in situ stress field, all nodes move vertically downwards only, with all nodes at the same elevation settling by the same amount. As a result, no shear stresses are generated during this step and all vertical force components on each Gaussian point are compressive and of equal magnitude for points lying on the same elevation.

6.6.2 FULL GBS PRESSURE

After the GBS pressure has been applied, the nodes lying on the mesh centerline move again only vertically downwards, due both to the symmetry of the applied loading and of the mesh (see Figure 6. 6).

A contour plot of the maximum shear stresses t_{max} is shown in Figure 6. 7 The

shear stresses tmax generated at the end of this loading step are symmetrical along the centerline axis of the GBS, which coincides with the centerline of the mesh. This is due to the fact that nodes that are symmetrical around the mesh centerline settle equally and displace equally horizontally but in opposite directions. It can also be observed that the contours of maximum tmax develop close to the edges of the GBS, sink and then turn away from the GBS at about the depth of 100 m BML. There is also a bulb of high shear stresses that starts near the corner of the GBS, sinks and turns upwards all the way up to the opposite corner of the GBS. The clay layer starts to yield during this loading step, with the yielding starting from the part of the clay layer in the vicinity of the corner of the GBS and propagates both towards the centerline and the edges of the mesh. After the end of this loading step, the clay layer has yielded 30 m underneath the corners of the GBS.

6.6.3 CRITICAL STORM LOAD

The calculated maximum storm force of 1636 MN was applied incrementally on the structure in four equal loading steps of 409 MN each. This procedure was adopted for two reasons. It is unrealistic that the wave loading will reach its maximum magnitude instantaneously and also it is of interest to study the propagation of yielding with the increasing magnitude of the storm load.

By applying the storm load on the GBS, the wave-stricken side of the structure tends to lift up, while the other side tends to sink. Although there is a lift-off tendency, the structure always remains in contact with the mudline. All nodes along the mudline and on the wave-stricken side of the structure and all nodes along the GBS-mudline interface move in the direction of the wave force. As expected, the magnitude of the horizontal displacements of the nodes lying on the mudline and on the wave-stricken

side of the GBS are higher than those calculated from the switch-on-gravity step of the analysis, while smaller horizontal displacements are calculated for those nodes lying on the other side of the GBS. The opposite holds true for the magnitude of the vertical displacements (see Figure 6. 8).

The magnitude of the generated maximum shear stresses, tmax, increases after each increment of the applied storm load, but the material possesses higher undrained shear strength as a result of the reconsolidation process due to the GBS pressure. This reconsolidation process dominates and there is no increase in the length of the yielded zone along the clay layer.

6.7 SENSITIVITY ANALYSIS

The influence of the following variables on the foundation behaviour has been investigated:

a. Depth of the clay layer.

b. Stiffness of the granular material above the clay layer.

c. Undrained stiffness of the clay layer.

d. Undrained strength parameters of the clay layer.

6.7.1 EMBEDMENT DEPTH OF THE CLAY LAYER

The influence of the depth of embedment of the clay layer on the extent of yielding was investigated. Three analyses were carried out, varying the depth of embedment from 9.5 to 14.5 and 29.5 m. The results show a decreasing length of the yielded zone with increasing depth of embedment and this can be attributed to:

(1) The deeper the clay layer is located, the lesser is the influence of the gravity stresses of the GBS on the yielding of the clay layer.

(2) The deeper the clay layer is located, the higher is the in-situ confining pressure. As a result the peak value of the existing undrained shear strength is higher even before the GBS pressure is applied.

Consequently, the deeper the clay layer is located, the lesser is the extent of the yielded zone along the clay layer and therefore the potential for progressive failure will decrease. This is illustrated from the results of the finite element analysis in Figure 6. 9, where the length of the yielded zone along the clay layer versus its depth of embedment is plotted.

6.7.2 STIFFNESS OF THE GRANULAR MATERIAL

The influence of the stiffness of the granular material was investigated by varying the values of the loading and unloading moduli K and K_{ur} respectively. The clay layer was assumed to be at a depth of 9.5 m. Two analyses were carried out, where the values of K were varied from 1250, to 1000 and 750 while the corresponding values of K_{ur} were 1750, 1500 and 1250. It can be readily observed from the analyses that the stiffness of the granular material has no significant effect on the yielding behaviour of the clay layer, since by reducing the stiffness of the granular material by 50%, there was no significant increase in the yielded zone along the clay layer (<20%) within the range of K and K_{ur} investigated. However, in other geotechnical settings (Chan and Morgenstern , 1987), the stiffness of the overburden materials can have a significant effect on the behaviour of the weak layer.

6.7.3 STIFFNESS OF THE UPPER MOST GRANULAR LAYER

It was concluded from laboratory studies that the upper 5 m of the granular material has a much higher stiffness than the underlying material (Thompson and Long, 1989). In this section, the influence of the stiffness of the upper 5 m of the granular material on the extent of yielding of the clay layer is investigated. Three analyses were carried out, where the value of the elastic modulus E of the upper 5 m layer is taken as 150000, 125000 and 75000 kPa respectively, while the stiffness of the underlying granular material was varied as in the previous section. Again, no significant change in the extent of the yielding zone can be observed, which indicates that even a 50% reduction of the overall stiffness of the granular material does not significantly influence the propagation of yielding along the clay layer. As expected, the calculated displacements increase in magnitude with decreasing stiffness of the granular material.

6.7.4 UNDRAINED STIFFNESS OF THE CLAY LAYER

The influence of the undrained stiffness of the clay layer on the extent of the yielding zone was investigated. Two analyses were carried out. In the first one, an undrained elastic modulus E of 15000 MPa was used, while in the second, E was decreased to 7500 MPa, with all other material properties kept constant. The extent of the yielding zone is almost identical in both cases, which indicates that the value of the undrained elastic modulus of the clay layer does not significantly influence the propagation of yielding.

6.7.5 UNDRAINED SHEAR STRENGTH OF THE CLAY LAYER

To assess the influence of the undrained shear strength of the clay layer on the

propagation of yielding, the estimated undrained shear strength profile used in previous analyses was reduced by 50% . The calculation show that a total length of 180 m along the clay layer yielded after the application of the full GBS pressure. Hence a reduction of the undrained shear strength by 50%, results in a 300% increase of the total length of the yield zone along the clay layer.

6.8 CONCLUSIONS

From the results of the analysis, the following conclusions can be drawn:

1. The GBS set down is an undrained loading for the clay layers and can induce progressive failure of the brittle clay layers in the foundation.

2. This process is amenable to analysis by the finite element method.

3. The extent of progressive failure is a function of the depth of embedment and the undrained peak and residual strength of the clay layer.

4. The progressive failure process is not much influenced by the stiffness of the adjacent dense sands in this particular geological profile.

5. Reconsolidation following set down can lead to sufficient strength increase to avert further progressive failure under wave and/or ice loading. However, this will depend upon the residual friction angle of the previously sheared material.

The analysis carried out in this study indicated the importance of identifying the location and strength properties of any weak inclusion in an otherwise strong material. A great deal of effort should be spent during the site investigation phase in order to locate materials that can lead to a progressive mode of failure. The importance of obtaining a

detailed stratigraphy of the upper foundation layers was demonstrated from the results of the sensitivity analysis.

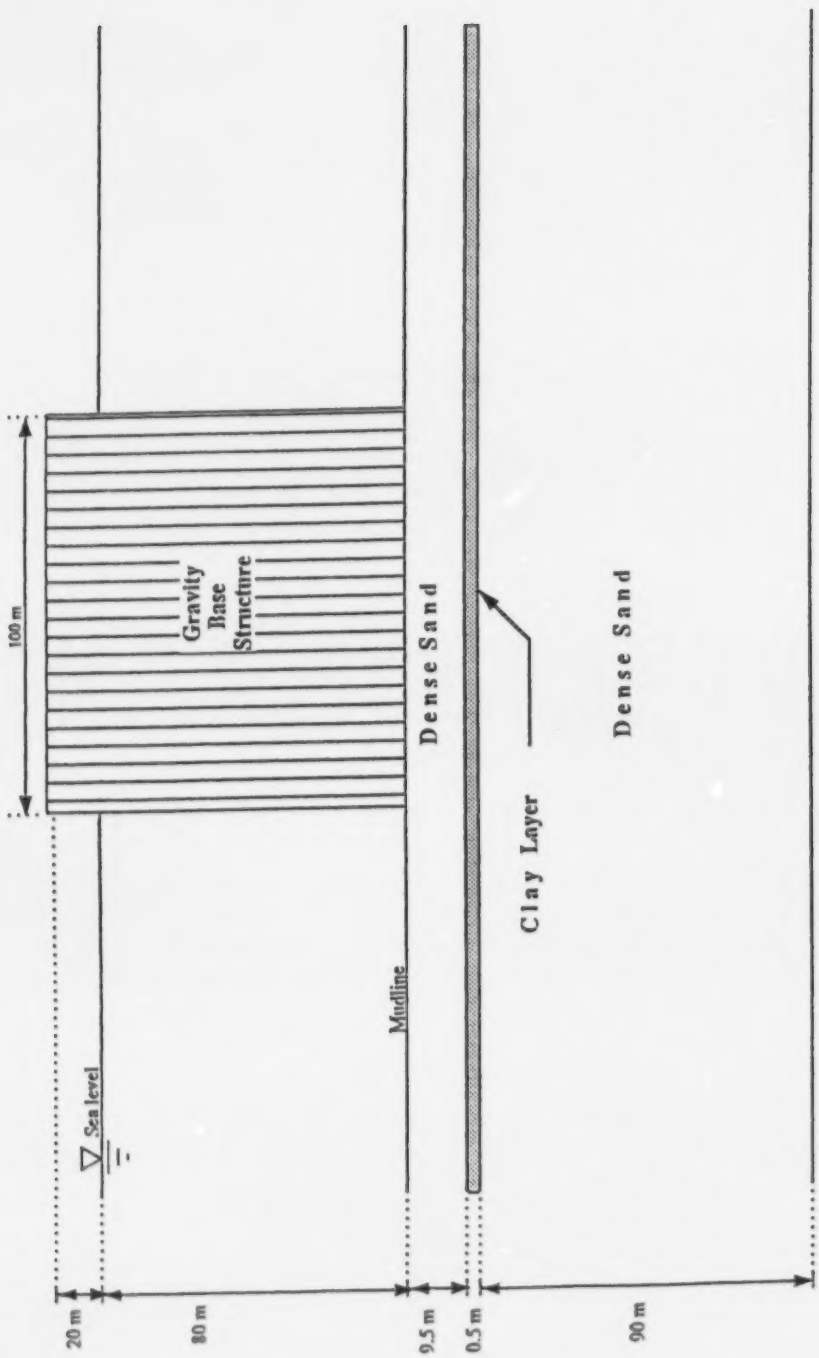

Fig. 6.1 Assumed foundation profile for the GBS

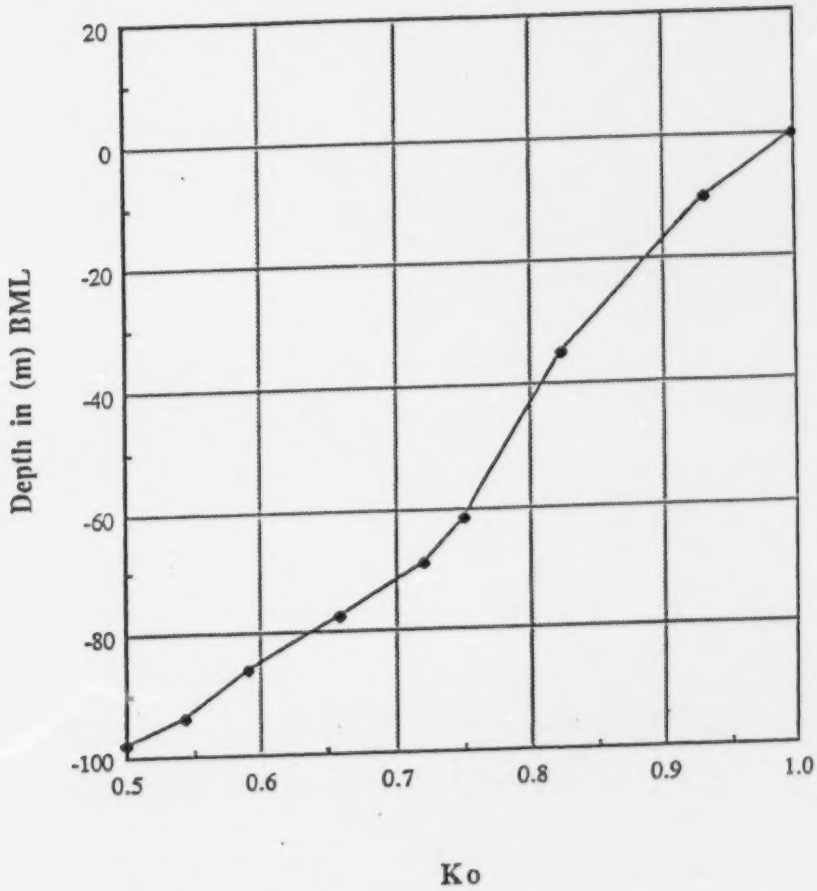

Fig. 6.2 Ko versus depth profile

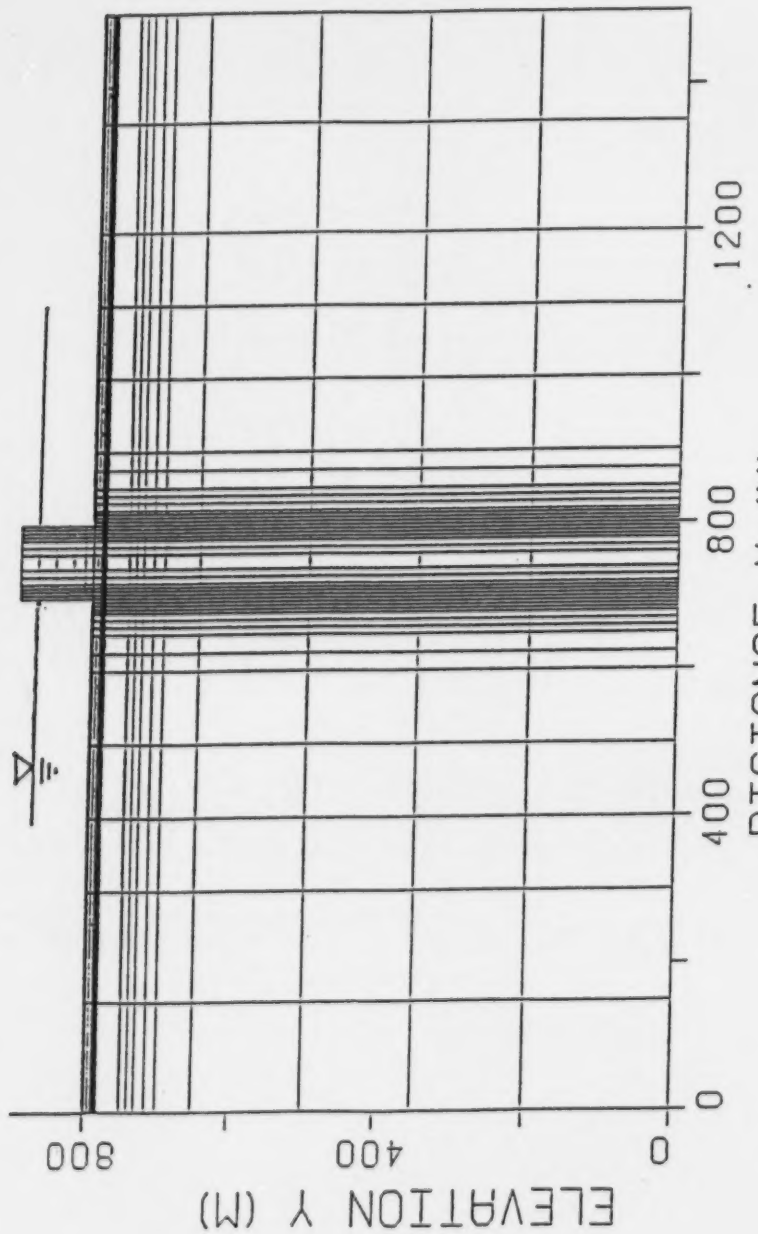

Fig. 6.3. Finite element idealization

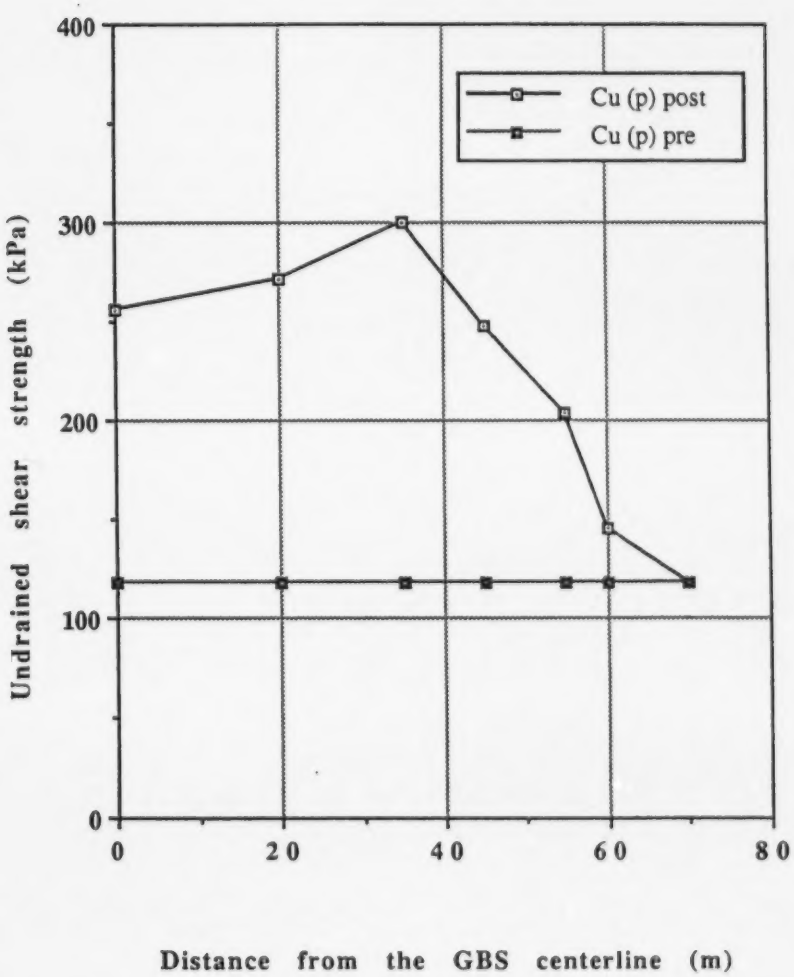

Fig. 6.4 Variation of undrained shear strength along the clay layer after GBS set down

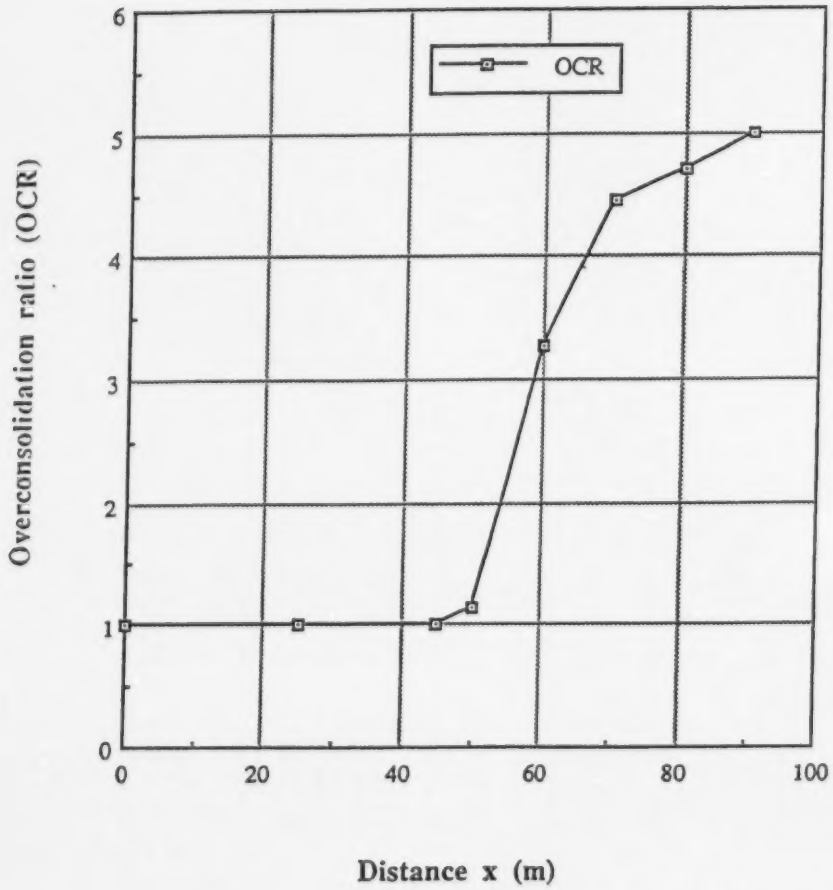

Fig. 6.5. Variation of the OCR from the GBS centerline along the clay layer after the full tank pressure

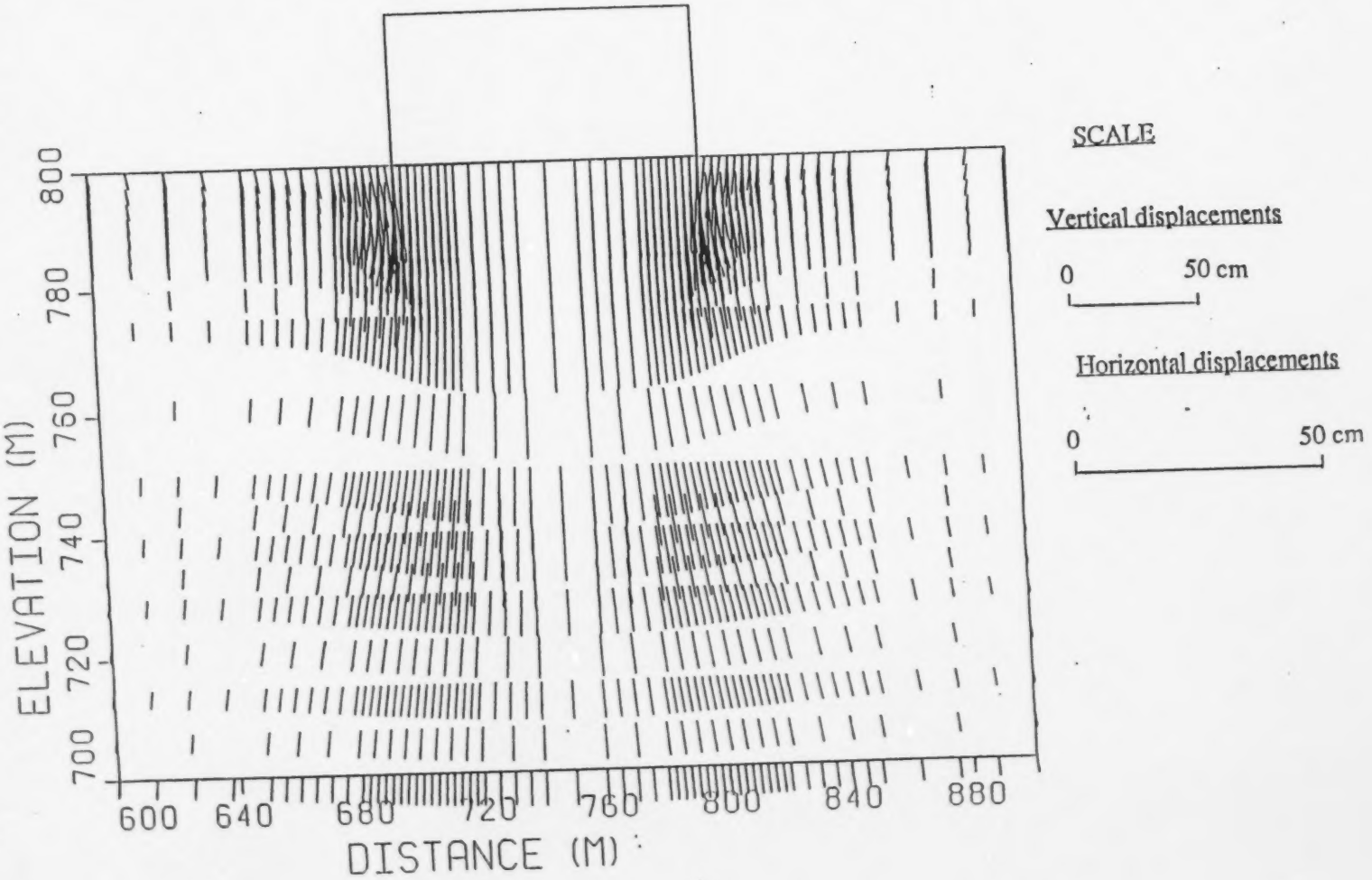

Fig. 6.6. Displacement field under full GBS pressure.

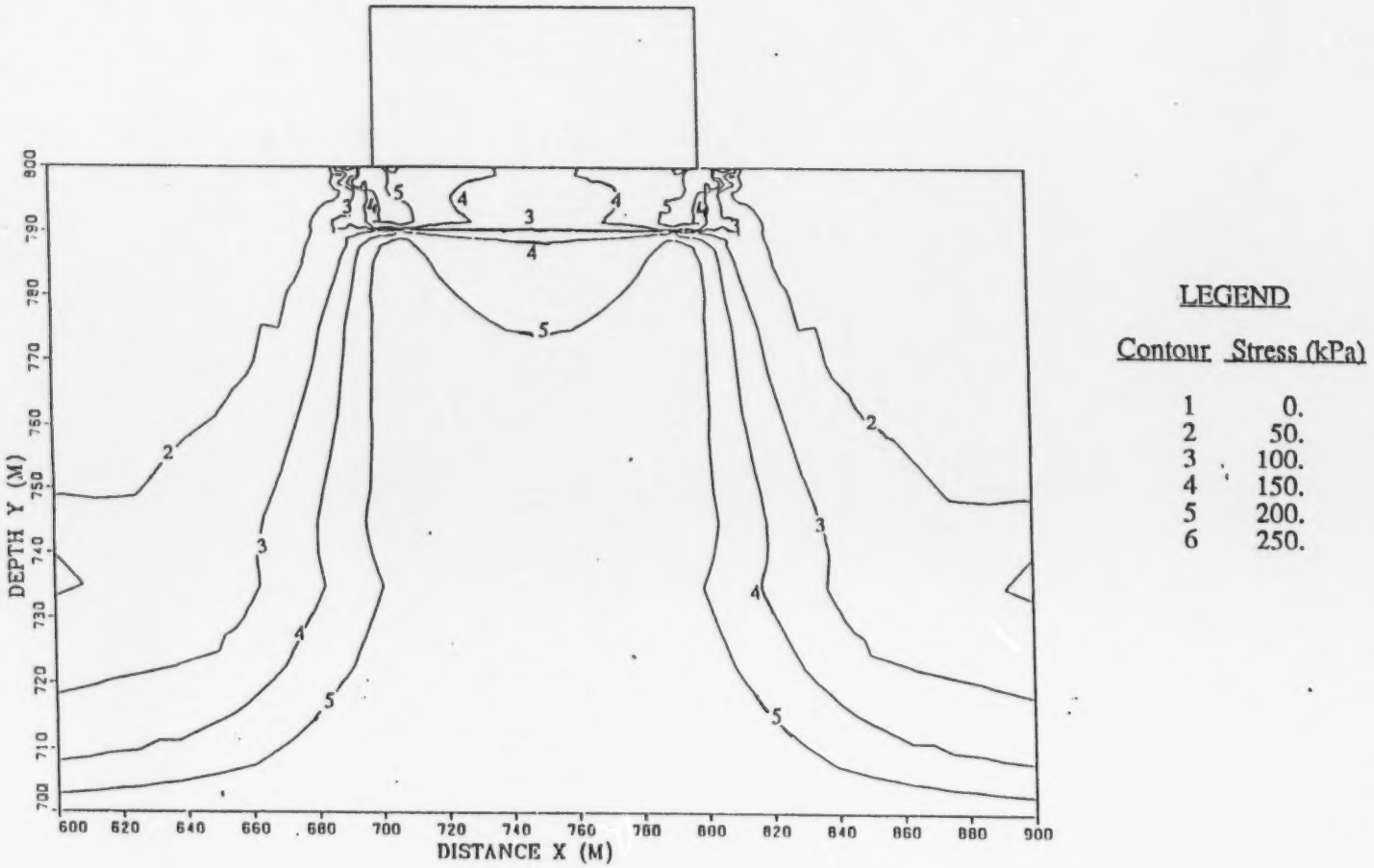

GBS FOUNDATION – WEAK LAYER AT 9.5 M. – FULL GBS PRESSURE

Fig. 6.7. Plot of the maximun shear stress τ_{max} under full GBS pressure.

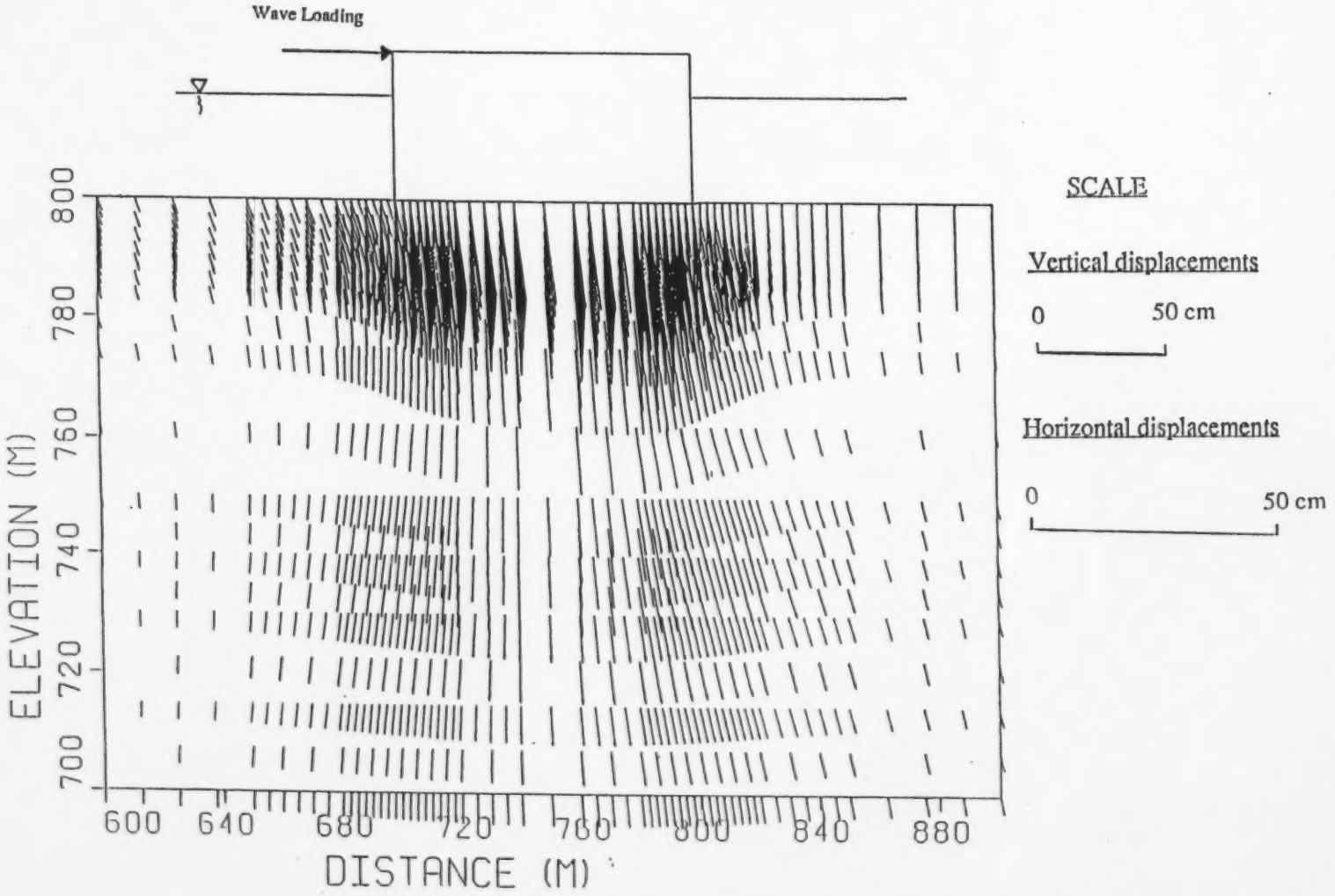

Fig. 6.8. Displacement field of the foundation under full wave load.

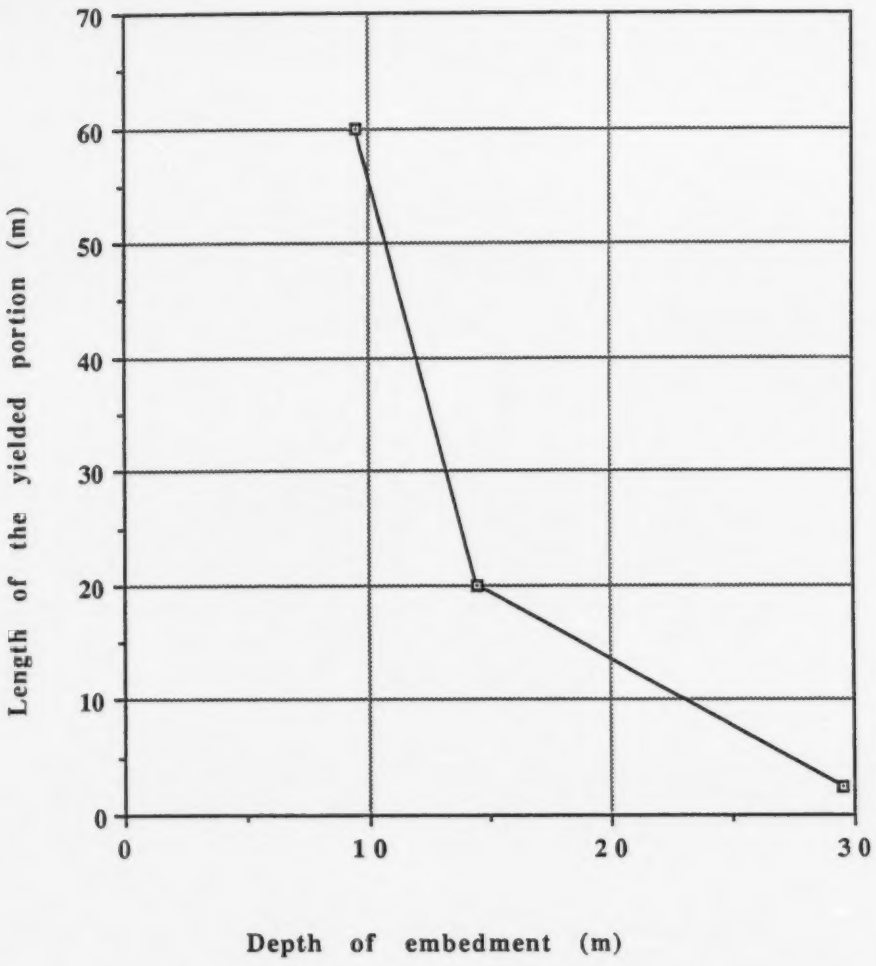

Fig. 6.9 Influence of the depth of embedment on the length of the yielded portion of the clay layer

CHAPTER 7

CONCLUSIONS AND RECOMMENDATIONS

7.1 INTRODUCTION

The mechanism of progressive failure in brittle soils has been known for some time, but there has been limited field evidence to show its magnitude. However, several general analytical procedures to model the presence of discontinuity surfaces (shear bands) in a soil mass have been presented in the last few years. The difficulties associated with obtaining a convergent numerical solution when shearband yielding commences and the associated high cost of the finite element analysis during the equilibrium iteration procedure has not been an attraction for the practicing geotechnical engineer. Finite element analysis is a science and like any other science demands patience, skill and experience. Practicing geotechnical engineering is usually far removed from the realms of finite element analysis and unfortunately this leads to too great an emphasis on results rather than what is involved in getting the results.

Nevertheless, several decisive steps have been made during the last decade in bridging the gap between analysis and practice.

7.2 GENERAL CONCLUSIONS

The applicability of a general numerical solution to perform quantitative analyses and calculations on the extent and amount of progressive failure in real engineering structures has been demonstrated. The adopted finite element solution for problems involving a geometrically altering domain (excavation and/or fill) was based on a variational formulation (Ghaboussi and Pecknold, 1984) which explicitly treats excavation and/or fill as a process where the contributions of the external and internal forces acting on the excavated/filled elements were removed/added directly from/onto the global matrix equations. The resulting equations were solved by Newton-Raphson iteration algorithm using the notion of consistent tangent operator for rate-independent elastoplasticity which results in an asymptotically quadratic rate of convergence (Simo and Taylor, 1985). The derived formulations were implemented in the finite element program PISA to demonstrate the theoretical validity of the modeling technique and to demonstrate its application to full scale problems which involve simulation of actual field conditions.

The following conclusions can be derived from the results of the simple numerical examples of this study:

1. The excavation/fill simulation technique is theoretically sound and computationally efficient. It was shown that in elastic analyses, the solutions to problems

involving geometrically altered domain and boundaries are superimposable and do not depend on the number of construction stages, thus satisfying Ishihara's (1970) uniqueness postulate for the elastic case.

2. It was demonstrated that for the case of an elastoplastic excavation analysis in a non-softening medium, an asymptotically "numerically unique" solution can be achieved with these adopted analytical methods. The convergence of the elastoplastic solution is shown to be exponentially asymptotic, demonstrating the computational efficiency engendered by the consistent linearization scheme employed.

3. The modeling technique provides a framework for incorporating relatively complex elastoplastic constitutive models to describe soil behavior permitting a more realistic and computationally efficient modeling of soil behavior than earlier analyses. The evaluation of certain quantities like the gradients of the flow direction, the normal to the yield surface, the plastic moduli etc. may prove to be laborious for complicated plasticity models.

4. The modeling technique can be used for predicting or backanalysing the behavior of excavations and fills in a soil mass and the effects of such construction activities on nearby structures, machinery and utilities.

The application of this modeling technique on real engineering structures provided us not only with a deeper understanding of the effect of progressive failure and the behavior of strain weakening inclusions on the deformation response of soil masses but also with a powerful arsenal of analytical tools to tackle efficiently problems of this nature. As already mentioned, the library of the consistent elastoplastic stress-strain

tensors can be further enriched by applying the same consistent linearization principle to any convex yield surface.

Some general conclusions can also be drawn from the application of the proposed modeling scheme on the three case studies:

1. Construction activities (excavation/fill) induced displacements and natural loading events can induce progressive failure along brittle soil layers.

2. These processes are amenable to analysis by the finite element method.

3. The extent of progressive failure is primarily a function of the shear strength of the brittle layer and the in-situ stress field.

4. It is also a function of the depth of embedment of the brittle layer and the stiffness of the surrounding soil mass for most cases.

5. If reconsolidation of the brittle layers at the end of a loading event occurs, it can lead to sufficient strength increase to avert further progressive failure. However, this will depend upon the residual friction angle of the previously sheared material.

6. The identification of the location and the strength properties of any weak inclusion in an otherwise strong material is extremely important during the site investigation phase.

7. The modified modeling scheme enables us to adopt a computationally efficient approach in the design or backanalysis of geotechnical structures where progressive failure can pose a threat to their safety.

It is common knowledge that the validity of the results obtained by the use of any model are depended on the accuracy of the input information coming out of the site investigation and the laboratory testing program. Therefore, this modeling effort does not intend to replace the judgment required in any engineering design but rather to enhance it. Referring to the problems which involve yielding of shear bands, the case histories analyzed in this thesis illustrate the unique value of the adopted modeling scheme in evaluating or backanalysing field performance.

7.3 RECOMMENDATIONS FOR FUTURE RESEARCH

It is generally accepted that modeling in geotechnical engineering has been enjoying its "golden era" in the last decade. Nevertheless, the uncertainty of the input parameters, that affect directly the quality of the modeling predictions, rather than the cost/inefficiency of the solution algorithms prevents the nonlinear finite element analysis from finding wider application in practice.

Robust algorithms for the search of equilibrium states guarantee a convergent numerical solution and advanced constitutive models can describe adequately the behavior of the soil mass undergoing complex loading histories. But none of the above will answer categorically the questions of the practicing engineer when the model input parameters are not known to the desired degree of accuracy. Therefore, techniques of

site investigation to locate brittle layers as well as laboratory and/or in-situ testing should be improved so that material parameters related to deformation analysis (deformation moduli, and in-situ stress field primarily) can be measured with confidence. The cost associated with these testing procedures remains still a factor, but it can not outweigh the benefits of predicting the behavior of a soil mass with the desired degree of accuracy.

In order to have a complete model, another problem should be addressed. It is necessary to include in the analysis a formulation for modeling hydrodynamic lag (consolidation) problems. Full implementation of these consolidation (pore pressure dissipation) phenomena is a vital key to the development of a complete overall solution.

Finally, although this work shows promising results in further understanding the progressive failure mechanism as well as giving us the confidence that the analytical tools are available to tackle problems of this nature (at least where there is evidence for geologically controlled failure), more case histories need to be analyzed to obtain more comprehensive knowledge. Argilaceous sediments, clays, shales and mudstones are by far the commonest rocks on the surface of the earth. Thus, they are of great importance in many aspects of human activity and therefore problems arising from their mechanical behavior demand a practically oriented numerical analysis.

REFERENCES

ADINA [1981], "A Finite Element Program for Automatic Dynamic Incremental Nonlinear Analysis", ADINA Engineering, Report AE81-1, September, Cambridge, MA.

Agar, J. G., [1984], "Geotechnical Behaviour of Oil Sands at Elevated Temperatures and Pressures", unpublished Ph.D thesis, University of Alberta, Edmonton, Alberta, Canada.

Alencar de, J. A., [1988], "Deformation of Dams on Sheared Foundations", unpublished Ph.D thesis, Department of Civil Engineering, University of Alberta, Edmonton, Alberta, Canada.

Bjerrum, L., [1967], "Progressive failure in slopes of overconsolidated plastic clay and clay shales", *Journal of the Soil Mechanics and Foundations Division*, A.S.C.E, vol. 93, SM5, pp. 3-49.

Bishop, A.W., [1967], "Progressive failure - with special reference to the mechanism causing it", Proceedings of the Geotechnical Conference, Oslo, Norwegian Geotechnical Institute, Volume II, pp. 143-149.

Borja, RI, Lee, SR, and Seed, RB [1989]. "Numerical Simulation of Excavation in Elastoplastic Soils," *Int J for Num and Anal Meth in Geomechanics*, Vol 13, pp 231-249.

Branco, P. J. and Eisenstein, Z., [1991], "Numerical Modelling of the Transient Isothermal Response of Gassy Soils", *Proc. 44th Can. Geotech. Conf.*, Calgary, Alberta.

Brown, P. T. and Booker, J. R., [1986], "Finite Element Analysis of Excavations", *School of Civil and Mining Engineering Research Report,* No. 532, The University of Sidney, Sidney, Australia.

Burland, J. B., Longworth, T. I. and Moore, J. F. A., [1977], "A study of ground movement and progressive failure caused by a deep excavation in Oxford Clay", *Geotechnique*, volume 27, number 4, pp. 557 - 591.

Cameron, R. and Carr, C. A., [1988], "The Influence of thin Clay Layers on the design and performance of a flexible cantilever retaining wall", *Proc. 2nd Intl Conf on Case Histories in Geotech Engng*, St. Louis, Missouri.

Canadian Standards Association [1989]. "Canadian Code for the Design Construction and Installation of Fixed Offshore Structures, CSA S 472-M1989," Toronto, Ontario.

Canadian Standards Association [1989]. "Special Publication S 472.1 - M1989. Commentary to the CSA Preliminary Standards S 472- M1989. Foundations. Offshore Structures," Toronto, Ontario.

Chan, DH [1985]. "Finite Element Analysis of Strain Softening Material," unpublished Ph.D thesis, University of Alberta, Edmonton, Alberta, Canada.

Chan, D H [1986]. "PISA (Program for Incremental Stress Analysis)", Department of Civil Engineering, University of Alberta, Edmonton, Alberta, Canada.

Chan, DH, and Morgenstern, NR [1987]. "Progressive Deformation of the Edmonton Convention Center," *Can. Geotech. J.*, vol. 24, pp 430-440.

Chandrasekaran, V. S and King, G. J. W., [1974], "Simulation of Excavation Using Finite Elements", J. of Geotech Eng Division, ASCE, Vol. 100, No. GT9, pp. 1086 - 1089.

Chang, C. Y., [1969], "Finite Element Analysis of Soil Movements Caused by Deep Excavation and Dewatering", *Ph. D Dissertation*, University of California, Berkeley, California.

Chen, Z, [1990], "Analysis of Progressive Failure of Carsington Dam", unpublished Ph.D thesis, Department of Civil Engineering, University of Alberta, Edmonton, Alberta, Canada.

Christian, J. T. and Whitman, R. V., [1969], "A one-dimensional model for progressive failure", Proceedings, 7th International Conference on Soil Mechanics and Foundation Engineering, Mexico City, volume 2, pp. 541-545.

Christian, J. T. and Wong, I. H., [1973], "Errors in Simulating Excavation in Elastic Media by Finite Elements", Soils and Foundations, Japanese Society of Soil Mechanics and Foundation Engineering, Vol. 13, No. 1, March, pp. 1-10.

Cleary, M. P. and Bathe, K.-J. and Dong, J. L., [1979], "On tractable constitutive relations and numerical procedures for structural analysis in masses of geological materials", Proc. of the 3rd Int. Conf. on Num. Meth. in Geomechanics, Aachen, Germany, volume 1, pp. 15-29.

Clough, G.W., [1969], "Finite Element Analysis of Soil-Structure Interaction in U-Frame Locks", *Ph. D Dissertation*, University of California, Berkeley, California.

Clough, G.W. and Duncan, J. M. [1969], "Finite Element Analyses of Port Allen and Old River Locks", Contract Report, No S-69-6, U.S. Army Engineer Waterways Experiment Station, Corps of Engineers, Vicksburg, Mississippi, September.

Clough, G. W. and Mana, A. I., [1976], "Lessons Learned in Finite Element Analyses of Temporary Excavations", Numerical Methods in Geomechanics, 2nd Intl Conf on Num Methods in Geomechanics, C. S. Desai (Ed.), Blacksburg, Virginia, U.S.A, Vol. 1, pp. 243 - 265.

Cramer, H., Wunderlich, W., Kutter, H. K. and Rahn, W., [1979], "Finite element analysis of stress distribution, induced fracture, and post-failure behaviour along a shearzone in rock", Proc. of the 3rd Int. Conf. on Num. Meth. in Geomechanics, Aachen, Germany, volume 2, pp. 505-513.

Desai, C. S. and Sargand, S., [1984], "Hybrid Finite Element Procedure for Soil - Structure Interaction", *J of Geotech Engng*, ASCE, Vol. 110, No. GT4, pp. 473 - 486.

Dong, J. L., [1980], " Analyses of deformation and failure in geological materials", M. Sc. dissertation, Department of Mechanical Engineering, Massachusetts Institute of Technology, Cambridge, Massachusetts.

Drucker, D. C. and Prager, W., [1952], "Soil Mechanics and Plastic Analysis of Limit Design", *Quart. of Appl. Mechanics*, Vol. 10, pp. 157 - 165.

Duncan, J. M. and Dunlop, P., [1969], "Slopes in Stiff-Fissured Clays and Shales", *J of the Soil Mechanics and Foundations Division,* ASCE, Vol. 95, No. SM3, March, pp. 467 - 492.

Duncan, JM, and Chang, CY [1970]. "Nonlinear Analysis of Stress and Strain in Soils," *J of the Soil Mechanics and Foundations Division, ASCE*, Vol 95, No SM5, pp 1629-1653.

Dunlop, P., Duncan, J. M. and Seed, H. B., [1968], "Finite Element Analyses of Slopes in Soil", Contract Report, No S-68-6, U.S. Army Engineer Waterways Experiment Station, Corps of Engineers, VIcksburg, Mississippi, May.

Dunlop, P. and Duncan, J. M., [1969], "Development of Failure around Excavated Slopes", *J of the Soil Mechanics and Foundations Division,* ASCE, Vol. 96, No. SM3, March, pp. 471 - 493.

Dusseault, M. B., [1977], "Geotechnical Characteristics of the Athabasca Oil Sands", unpublished Ph.D thesis, University of Alberta, Edmonton, Alberta, Canada.

Dusseault, M. B. and Morgenstern, N. R., [1978], " Shear Strength of Athabasca Oil Sands", *Can. Geotech. J.*, Vol. 15, No. 2, pp. 216 - 238.

Ghaboussi, J. and Pecknold, D. A. , [1984], "Incremental Finite Element Analysis of Geometrically Altered Structures", *Int. J. for Num. Meth. in Engineering,* Vol. 20, pp. 2051 - 2064.

Hoeg, K., [1972], "Finite element analysis of strain softening clay", *Journal of the Soil Mechanics and Foundation Engineering Division,* ASCE, volume 98, SM1, pp. 43-58.

Instanes, A [1991]. "Personal communication".

Ishihara, K., [1970], "Relations between Process of Cutting and Uniqueness of Solutions", *Soils and Foundations*, Vol. 10, No. 3, pp. 50 - 65.

James, P.M., [1970], "Times Effects and Progressive Failure in Clay Slopes", unpublished Ph.D thesis, Department of Civil Engineering, Imperial College, University of London, U.K.

Kawamoto, T. and Takeda, N., [1979], "An analysis of progressive failure in rock slopes", Proc. of the 3rd Int. Conf. on Num. Meth. in Geomechanics, Aachen, Germany, volume 2, pp. 797-808.

Krieg, R. D. and Krieg, D. B., [1976], "Accuracies of Numerical Solution Methods for the Elastic-Perfectly Plastic Model", *J. Pressure Vessel Tech.*, ASME, 99.

Lambe, T. W. and Whitman, R. V., [1978], "Soil Mechanics - SI Version", *Series in Soil Engineering*, John WIley & Sons, NY.

Lauritzen, R, and Schjetne, K [1976]. "Stability Calculations for Offshore Gravity Structures," *Proccedings of the 8th Offshore Technology Conference*, Dallas, Texas, Vol 1, Paper No OTC 2431, pp 75-82.

Le Tirant, P [1979]. "Seabed Reconnaissance and Offshore Soil Mechanics for the Installation of Petroleum Structures," Institut Francais du Petrole Publications, Paris.

Lee, S. R., [1989], "Nonlinear Elastoplastic Finite Element Analysis of Braced Excavations in Clay", *Ph. D Dissertation*, Stanford University, Stanford, California.

List, B. R. and McKenna, G. T., [1990], "Shallow Translational Failure along thin Marine Clay Layers at the Syncrude Canada Ltd Open Pit Mine", *Proc. 43rd Can. Geotech. Conf.*, Quebec City, P.Q, Canada.

Lo, K. Y. and Lee, C. F., [1973a], "Stress analysis and slope stability in strain-softening materials", *Geotechnique*, volume 2, pp. 1-11.

Lo, K. Y. and Lee, C . F., [1973b], "Analysis of Progressive Failure in Clay Slopes", Proc. 8th Intl. Conf. on Soil Mech. and Foundns Engng., Moscow, USSR, pp. 251 - 258.

Mana, A. I., [1978], "Finite Element Analyses of Deep Excavation Behaviour in Soft Clays", *Ph. D Dissertation*, Stanford University, Stanford, California.

Mayne PW, and Kulhawy, FH [1982]. "K_o - OCR relationships in Soils," *Journal of the Geotechnical Engineering Division*, ASCE, Vol. 108, pp 851-872.

McKenna, G. T. and List, B. R., [1990], "Impact of Upper McMurray Formation Marine Oil Sands on Dragline Mining at the Syncrude Canada Limited Open Pit Mine", *2nd Intl Symposium on Mine Planning*, Calgary, Alberta.

Morgenstern, N.R. and Tchalenko, J.S, [1967], "Microscopic structures in kaolin subjected to direct shear", *Geotechnique*, Volume 17, No. , pp. 309-328.

Morgenstern, N.R., [1977], "Slopes and excavations in heavily over-consolidated clays", Section 3 of "Slopes and Excavations - State of the Art", with co-reporters G. Blight, N. Janbu and D. Resendiz., Proceedings of the 9th International Conference on Soil Mechanics and Foundation Engineering, Tokyo, Japan.

Morgenstern, N. R., Fair, A. E. and McRoberts, E. C., [1988], "Geotechnical Engineering beyond Soil Mechanics - A Case Study", Can. Geotech. J., Vol. 25, pp. 637 - 661.

Mossop G. D., [1980], "Geology of the Athabasca Oil Sands", *Science*, Vol. 207, pp. 145 - 152.

Nagtegaal, J. C., [1982], "On the Implementation of Inelastic Constitutive Equations with Special Reference to Large Deformation Problems", *Comp. Meths. Appl. Mech. Engrg.*, Vol. 33, pp. 463 - 484.

Nayak, G. C. and Zienkiewicz, O. C., [1972], "Elasto-plastic stress analysis: A generalization of various constitutive relations inducing strain-softening", *Int. J. Num. Meth. Engng.*, volume 5, pp. 113-135.

Ortiz, M. and Pinsky, P. M., [1981], "Global Analysis Methods for the Solution of Elastoplastic and Viscoplastic Dynamic Problems", *Report UCB/SESM*, No 81/08, Department of Civil Engineering, University of California, Berkeley, California.

Ortiz, M. and Popov, E., [1985], "Accuracy and Stability of Integration Algorithms for Elastoplastic Constitutive Equations", *Int. J. for Num. Meth. in Engineering,* Vol. 21, pp. 1561 - 1576.

Owen, D. R. J. and Hinton, E., [1980], "Finite Elements in Plasticity: Theory and Practice", Pineridge Press Limited, Swansea, U.K.

Peck, R. B., [1973], " Influence of Nontechnical Factors on the Quality of Embankment Dams", *Embankment - Dam Engineering, Casagrande Volume*, Willey, New York, pp. 201-208.

Pinsky, P. M., Ortiz, M. and Pister, K. S., [1983], "Numerical Integration of Rate Constitutive Equations in Finite Deformation Analysis", *Computer Meth in Appl Mech and Eng,* Vol. 40, pp. 137 - 150.

Prevost, J. H. and Hoeg, K., [1975], "Soil mechanics and plasticity analysis of strain softening", *Geotechnique*, volume 25, No. 2, pp. 279-297.

Prevost, J. H. , [1987], "Modelling the Behaviour of Geomaterials", *Geotechnical Modelling and Applications*, S. M. Sayed (Ed.), Gulf Publishing Company, Houston, Chapter 2.

Sanderson, TJO [1988] "Ice mechanics - Risk to Offshore Structures," Graham & Trotman, London, UK.

Sarpkaya, T, and Isaacson, M [1981]. "Mechanics of Wave Forces on Offshore Structures," Van Nostrand Reinhold Company, New York.

Simo, JC and Taylor, RL [1985]. "Consistent Tangent Operators for Rate-Independent Elastoplasticity," *Computer Meth in Appl Mech and Eng,* Vol 48, pp 101-118.

Skempton, A.W., [1964], "Long-term stability of clay slopes", *Geotechnique*, 14, No. 2, pp. 77-101.

Skempton, A. W. and Hutchinson, J. [1969], "Stability of Natural Slopes and Embankment Foundations", *7th Int. Conf. Soil Mech. and Foundn Engng.*, Mexico City, Mexico, State-of-the-art volume, pp. 291 - 340.

Sture, S., [1976], "Strain softening behaviour of geologic materials and its effect on structural response", Ph.D thesis, University of Colorado at Boulder.

Sture, S. and Ko, H.-Y., [1978], "Strain-softening of brittle geologic materials", *Int. J. Num. and Anal. Meth. in Geomechanics*, volume 2, pp. 237-253.

Thompson, G. R. and Long, L. G., [1989]. "Hibernia Geotechnical Investigation and Site Characterization," *Can. Geotech. J.*, Vol 26, pp 653-678.

Wan, R. G., [1990], "Numerical modelling of shearbands in geomaterials", unpublished Ph.D thesis, Department of Civil Engineering, University of Alberta, Edmonton, Alberta, Canada.

Wilkins, M. L., [1964], "Calculation of Elastic - Plastic Flow", *Methods of Computational Physics*, Academic Press, Vol. 3, New York.

Williams, A. A. B., [1980], "Shear Testing of some Fissured Clays", 7th Reg. Conf. for Africa on Soil Mech. and Foundn. Engng., Accra, pp. 133 - 139.

Wong, I. H. [1971], "Analysis of Braced Excavations", *Ph. D. Dissertation*, Massachusetts Institute of Technology, Cambridge, Massachusetts.